

PEER-REVIEW OF THE MANUSCRIPT:

Breakup of nocturnal low-level stratiform clouds during southern West African Monsoon Season (acp-2020-602)

RESPONSES TO THE REVIEWER

Interactive comment on “Breakup of nocturnal low-level stratiform clouds during southern West African Monsoon Season”

Dear reviewer 1,

We thank the reviewer for his/her helpful suggestions, which led to significant improvements of our paper. Below we detailed how his/her comments are addressed in the revised version of the paper. The major corrections of the paper are cited here in *italic*. We refer to specific pages by “P” and lines by “L”. For example, “P1, L1” refers to page 1, line 1.

General comment: I got confused at times, even after reading this twice, keeping track of the large number of acronyms made throughout this text. I see and acknowledge their importance for keeping the paper at an appropriate length, however, I think the authors should take care to re-state some acronyms through the text to clarify what is being discussed.

We fully understand this difficulty and we tried to re-state the different acronyms through the text and figure captions.

Section 1: Since this paper describes in great detail many processes responsible for nocturnal cloud maintenance and subsequent breakup, this section (and paper in general) would benefit greatly with some discussion about the land-surface types of the 3 supersites. The a priori knowledge of the typical land surface over this part of the continent may be unknown to several readers, and is especially worth noting since boundary layer heights depend somewhat on the land-surface.

We thank the reviewer for this remark. We added the climatic zones of West Africa affected by the LLSC in the introduction P2, L12-15: “During the West Africa monsoon season, the LLSC form frequently at night over a region extending from Guinean coast to several hundred kilometres inland (van der Linden et al., 2015), which includes the coastal, Sudanian and Sudanian-Sahelian climatic zones (Emetere, 2016).”

In addition, this statement in section 3: “The ground sites were located at roughly the same distance from the Guinean coast (200 km in land) but with different topography (Kalthoff et al., 2018)”, has been modified as follow, P6, L25: “The DACCIWA supersites were located at roughly the same distance from the Guinean coast (200 km in land, Fig. 1), between the coastal and the Sudanian areas, but with a different topography (Kalthoff et al., 2018). The supersites are part of the savannah ecosystem, where grassland is intercut with crops and degraded forest.”

P2, First Paragraph: In this section, you state “However, the diurnal cycle of those clouds is still poorly represented in numerical models” and cite Hannak et al. (2017). This is definitely a strong motivation, but I do not think this point is expanded upon enough in this paragraph. Furthermore, I had some trouble reading through this paragraph as this text seemed is jointed and unclear as to the main motivation. I recommend re-writing this paragraph focusing on the

importance of stratiform cloud cover in a global context (e.g. earth's radiation budget, difficulty representing these clouds in climate models; I included a reference that may be of interest and relevant here) and expand upon the processes that make this difficult. Move Fig. 1, the discussion of Fig. 1, and the discussion about “scarce weather monitoring over West Africa” to elsewhere in the text.

We thank the reviewer for this comment. The paragraph was modified:

1/ The comment on figure 1 was moved in the next paragraph.

2/ We improved the first paragraph of section 1, as follow, **P2**:

“The low-level stratiform clouds (LLSC) are Earth’s most common cloud type (Wood, 2012). During the West Africa monsoon season (WAM), the LLSC form frequently at night over a region extending from Guinean coast to several hundred kilometres inland (van der Linden et al., 2015), which includes the coastal, Sudanian and Sudanian-Sahelian climatic zones (Emetere, 2016). The LLSC coverage persists for many hours during the following day, reducing the incoming solar radiation, impacting the surface energy budget and related processes such as the diurnal cycle of the atmospheric boundary layer (ABL) (Schuster et al., 2013; Adler et al., 2017; Knippertz et al., 2017). However, the diurnal cycle of those clouds is still poorly represented in numerical weather and climate models, especially over West Africa (Hannak et al., 2017). Indeed, their lifetime is generally underestimated in the numerical simulations, causing high incoming solar radiation at the surface in this region where the meteorological conditions are governed by convection activities and by surface thermal and moisture gradients (Knippertz et al., 2011). That could be an important factor for which the forecasts of WAM features still have a poor skill (Hannak et al., 2017). Therefore, a better understanding of the processes behind LLSC over SWA is useful to improve the numerical weather prediction and climate projection quality. Due to the scarce weather monitoring network over West Africa, the first studies addressing the LLSC over this region were mostly conducted with satellite images and traditional synoptic observations (Schrage and Fink, 2012; van der Linden et al., 2015), as well as with numerical simulations at regional scale (Schuster et al., 2013; Adler et al., 2017; Deetz et al., 2018). They emphasized that the physical processes, spanning from local to synoptic scale such as, horizontal advection of cold air associated to WAM, lifting induced by topography, gravity waves or shear-driven turbulence, are relevant for the LLSC formation during the night. However, the LLSC evolution after the sunrise received little attention.”

P3, L9: I recommend adding a short description of what a “supersite” is.

The sentence has been modified to define a supersite as a site gathering a comprehensive set of instrumentation, **P3, L8-10**: *“To this end, three so-called “supersites”, which gather a large set of complementary instruments, were installed at Kumasi (6.68° N, 1.56° E) in Ghana, Savè (8.00° N, 2.40° W) in Benin, and Ile-Ife (7.55° N, 4.56° W) in Nigeria (Fig. 1).”*

P4, L23: “... due to the cooling...” at what level of the atmosphere does this cooling occur? Also, change “their formation” to “cloud formation”.

The sentence has been corrected and completed as follow **P4, L26-28**: *“The increase of relative humidity (Rh) within the ABL leading to saturation and LLSC formation is due to the cooling which mainly occurs during the stable and the jet phases in the monsoon layer, up to around 1.5 km above ground level (a.g.l.).”*

Section 4: I really liked this section and found the intricate level of analysis excellent, though I have to admit – again – I needed to read this multiple times to understand it due mostly to the authors’ writing style.

We thank the reviewer for this comment. The section 4 was deeply modified and, we hope, improved. We added a section (4.3, **P26**) in order to discuss the different processes possibly responsible for the LLSC coupling with the surface during the stratus phase.

Section 4: I will leave it up to the authors to proceed with this next comment as they see fit. Have you looked into the role of nocturnal cloud thickness as a possible reason why coupling sometimes does (or does not) occur (e.g. Fig. 5)? This is an interesting hypothesis that can (I think) be easily tested using your data. I would expect thicker cloud cover to inhibit surface warming enough to delay or possibly prohibit coupling if other meteorological factors cannot enable the transition. Likewise, could entrainment or precipitation – two sink terms for nocturnal cloud fraction under most conditions – correlate to a delayed coupling? These are questions bred from pure scientific curiosity based on the results you have shared.

We had the same questions as the reviewer and all the reviewer suggestions were tested. We know that it is a bit frustrating but no clear reason explaining the cloud coupling during the stratus phase was highlighted and so only hypotheses were suggested. Concerning the cloud thickness, we showed in Figure 6 that there are no obvious differences between coupled and decoupled LLSC thickness. We were not able to compare the liquid water path of coupled and decoupled LLSC, which could also play an important role.

However it is not a question of convection at that time of the day, since section 4 shows that the stratus phase ends more or less when the convection starts.

The entrainment at the end of the stratus phase is small and very similar in coupled and decoupled cases, but we were not able to check if it was also the case before the coupling. The estimation of the entrainment term along the stratus phase was not possible either.

At last, the precipitation hypothesis could be excluded since only LLSC without precipitation recorded at surface are considered. Of course, precipitation above the LLSC from higher clouds could not be investigated but is one of the hypotheses.

P4, L20: This is an unusual title for a section in a manuscript. Did you mean “State of Art”? Maybe call this section “Review”?

We actually meant “State of Art”. *“Review”* is now the title.

P5, paragraph beginning at L19: There are several recent studies from the Cloud System Evolution over the Trades (CSET) experiment that, I believe, can really strengthen this

paragraph and provide additional interesting results to compare & contrast your own results with. I believe intertwining principle results from these works will make your paper more interesting and accessible to research groups studying stratiform cloud breakup elsewhere across the globe, especially since the topic of stratocumulus-to-cumulus (or stratiform cloud breakup) has received increasing attention over the past several years.

We thank the reviewer for these recent studies based on CSET field experiment. They are now cited as many others previous studies addressing the stratocumulus-to-cumulus transition in marine conditions. These studies focused on aerosol microphysical role in the scenario of transition from stratocumulus-to-cumulus. Assessing the impact of low-troposphere aerosol loading on the LLSC diurnal cycle is not among the objectives of our study. But, this aspect will be addressed in future research work based on DACCIWA dataset. Thus, this perspective was added in section 6, **P36, L25**: *“The aerosol loading in the low-troposphere is a potential factor controlling the LLSC evolution and lifetime (Deetz et al., 2018; Mohrmann et al., 2019). The airborne measurements of low-cloud properties over SWA during DACCIWA (Flamant et al., 2017) could be used to assess the microphysical role for aerosol in the LLSC evolution scenario. This may help to differentiate the scenarios DC and DD.”*

End of P5: Again, this is an overall well-written section. This section seems to come to an abrupt end, however, with no suggestions or links as to how the described relevant dynamical processes relate to the observation studies presented in the remainder of the work.

We thank the reviewer for this comment. A sentence was added at the end of the paragraph to better link the LES study with the present observational work. **P6, L7**: *“Since the LES made by Pedruzo-Bagazgoitia et al. (2020) are set with atmospheric and surface conditions measured at Savè during the DACCIWA campaign, some simplifying assumptions used in our study are based on their results, and the simulated and observational results are compared.”*

Section 3.1 Header: I recommend renaming this section as “Instrumentation” instead of “Observational Data Used”

We thank the reviewer for this suggestion. The modification has been done; *“Instrumentation”* is now the title.

P7, L2: Are missing CTH data from the ceilometer the result of attenuation from optically thick daytime cumulus cloud, or were there frequent instrument malfunctions? This would be useful to know.

Section 3.1: What measurements did the radiosondes collect? And what versions/ types of radiosondes were used? This section in general is also lacking descriptions of measurement uncertainties for each instrument. For example, how accurate are the cloud base and cloud top height estimates from the ceilometer? What uncertainty is expected with radiosonde temperature and humidity measurements? I noted some statements of measurement uncertainty and accuracy elsewhere in the text, but these need to be stated here. Finally,

presuming meteorological conditions are estimated from the radiosondes, I would put paragraph 2 after the current 3rd paragraph since its unclear at that point in the paper how the authors estimate SHF, LHF, etc.

We agree with the reviewer that some indications were missing in this section. The paragraph has been deeply modified and includes now:

1/ The reason why some CTHs are missing, P7, L24: “Unfortunately, several values of CTHs are missing, particularly during daytime for many selected cases, due to the retrieval technique limitation.”

2/ Radiosondes sensors measurements accuracy, P7, L26: “The thermodynamical and dynamical characteristics of the low troposphere are retrieved from the radiosondes of the MODEM radiosounding system. The MODEM radiosonde collects, every second (which corresponds to a vertical resolution of 4-5 m), the air temperature and relative humidity, and the probe GPS localization from which horizontal wind speed components, altitude and pressure are deduced (Derrien et al., 2016). The sensors accuracy is 0.2 °C, 2 % and 0.01 m for temperature, relative humidity and GPS localization respectively.”

3/ Information on the data acquired by the surface station, P8, L5: “The meteorological conditions at the surface (temperature, relative humidity and pressure of the air at 2 m a.g.l), and some terms of the surface energy budget (net radiative flux (R_{n0}), sensible heat (SHF_0) and latent heat (LHF_0) fluxes at 4 m a.g.l) were continuously acquired. SHF_0 and LHF_0 are deduced from high-frequency (20 Hz) measurements processed with Eddy-covariance methods by using the TK3.11 software (Mauder et al., 2013).”

P11, L11: “Therefore, it has a spatio-temporal variability” this is true but is out of place at this point in the text.

We meant to say that despite the spatial and temporal variability of A, this parameter is very often considered as a constant. The sentences were modified, P12, L8: “A varies with $\Delta\theta_1$, Δq_t , wind shear at the cloud top, surface turbulent fluxes and cloud microphysical processes via the buoyancy flux vertical profile (Stevens et al., 2005; Stevens, 2006). Despite the spatial and temporal variability of A, its value is generally fixed and treated as a constant parameter in several research studies (e.g. van Zanten et al., 1999; van der Dussen et al., 2014).”

P20, L7: What do you mean by “help us to depart the cases”? Do you mean “differentiate” instead of “depart”? This is confusing and needs clarified since this is obviously a key science question motivating subsection 4.2.

We apologize for this word which was misleading. The sentence was modified as follow, P21, L7: *“Does the LWP budget analysis help us to differentiate the cases C and D?”*

P20, L12: “Indeed, the crossing of the cloud wets the probe” this sounds very flowery. I recommend rewriting this entire sentence. Suggestion: “Liquid water buildup on the radiosonde’s sensors possibly renders some measurements suspect, especially near cloud top.”

We thank the reviewer for this suggestion. *The correction was made accordingly, P21, L13.*

P20, L23: Again, it is critical to know what the instrument uncertainties (or accuracy) are, such that these over/underestimations have context. This will elucidate the magnitude and seriousness of liquid water condensation on the sensors and subsequent computations using these measurements.

The accuracy of the radiosonde sensors is now introduced in section 3. See response to previous comment.

P28, L18-19: “... for which the hydrometeors radar reflectivity from the cloud radar reveals light precipitations above the LLSC layer” The way this sentence is written implies that precipitation is occurring above the cloud layer, which is physically not possible. Did you mean to say that there is precipitation occurring inside the cloud layer? I have a stylistic comment here too: its fine to simply say “collocated cloud radar data revealed precipitation inside the LLSC layer” or something to that effect. “hydrometeors radar reflectivity” is confusing and does not make much sense.

We thank the reviewer for this suggestion. The paragraph is certainly unclear. There are sometimes higher clouds above the LLSC. In that case, the radar reveals light precipitation between the higher clouds and the LLSC which was not recorded at surface. The sentence was modified, P31, L23:

“The latest breakup time occurring at 16:00 UTC corresponds to the 02-03 July 2016 case for which the collocated radar reveals light precipitations from higher clouds, above the LLSC layer, during the first hours of the convective phase (not shown) while nothing was recorded by the surface rain gauge.”

P29, L17: "30% lower" what exactly is 30% lower? the cloud base height? Also, the beginning of this sentence should be "The latter..."

We thank the reviewer for this comment. The sentence was clarified, P32, L21: *“The LLSC breakup time impacts the radiative budget at surface over the day, then the surface fluxes, and consequently, the vertical development of the ABL, as shown by Lohou et al., 2020. They estimated that the ABL height is about 900 m when the LLSC*

breaks up at 09:00 UTC and is 30% lower when the LLSC breaks up at 12:00 UTC. Consequently, one can expect a quite different vertical development of the ABL in C/DC cases than in DD cases.”

P31, L26: “This could favour the convection in the cloud...” just state “This favours convection which...”

We thank the reviewer for this suggestion. The sentence was corrected, **P34, L25**: *“This favours convection in the LLSC which enhances the entrainment, at the expense of the cloud moistening by the underlying turbulent mixing.”*

P34, L11: “more significantly impact” is this because the coupled cases generally result in longer lasting cloud cover and therefore decrease the total amount of solar insolation received at the surface? I would be much more specific here since and this statement as written is pretty bold yet a bit hand-wavy.

We fully agree with this comment. The discussion concerning the LLSC impact on surface energy budget is now, **P36, L15**: *“It determines the LLSC lifetime and the way by which the transition towards shallow convective clouds occurs. The coupled LLSC last longer (breakup time at 12:00 in average) than decoupled cases (breakup time at 10:00 UTC in average). According to Lohou et al. (2020), such a difference in breakup time leads to a reduction of about 15% of net radiation at surface and of ABL vertical development during the day, for coupled cases compared to decoupled one.”*

Figure captions (general comment): It would be helpful to the reader to re-state or spell out acronyms. I found it tough at times to try to dig variable abbreviations from the text while also trying to follow and learn from the figures.

We modified the legends and we hope they are clearer.

Finally, all the minor comments suggested by the reviewer were taken into account in the new version.

Adler, B., Kalthoff, N. and Gantner, L.: Nocturnal low-level clouds over southern West Africa analysed using high-resolution simulations, *Atmospheric Chemistry and Physics*, 17(2), 899–910, doi:10.5194/acp-17-899-2017, 2017.

Deetz, K., Vogel, H., Knippertz, P., Adler, B., Taylor, J., Coe, H., Bower, K., Haslett, S., Flynn, M., Dorsey, J., Crawford, I., Kottmeier, C. and Vogel, B.: Cloud and aerosol radiative effects as key players for anthropogenic changes in atmospheric dynamics over southern West Africa, *Atmos. Chem. Phys. Discuss.*, 1–36, doi:10.5194/acp-2018-186, 2018.

van der Dussen, J. J., de Roode, S. R. and Siebesma, A. P.: Factors Controlling Rapid Stratocumulus Cloud Thinning, *J. Atmos. Sci.*, 71(2), 655–664, doi:10.1175/JAS-D-13-0114.1, 2014.

Emetere, M. E.: Investigations on aerosols transport over micro- and macro-scale settings of West Africa, *Environmental Engineering Research*, 22(1), 75–86, doi:10.4491/eer.2016.080, 2016.

Flamant, C., Knippertz, P., Fink, A. H., Akpo, A., Brooks, B., Chiu, C. J., Coe, H., Danuor, S., Evans, M., Jegede, O., Kalthoff, N., Konaré, A., Lioussé, C., Lohou, F., Mari, C., Schlager, H., Schwarzenboeck, A., Adler, B., Amekudzi, L., Aryee, J., Ayoola, M., Batenburg, A. M., Bessardon, G., Borrmann, S., Brito, J., Bower, K., Burnet, F., Catoire, V., Colomb, A., Denjean, C., Fosu-Amankwah, K., Hill, P. G., Lee, J., Lothon, M., Maranan, M., Marsham, J., Meynadier, R., Ngamini, J.-B., Rosenberg, P., Sauer, D., Smith, V., Stratmann, G., Taylor, J. W., Voigt, C. and Yoboué, V.: The Dynamics-Aerosol-Chemistry-Cloud Interactions in West Africa field campaign: Overview and research highlights, *Bull. Amer. Meteor. Soc.*, doi:10.1175/BAMS-D-16-0256.1, 2017.

Hannak, L., Knippertz, P., Fink, A. H., Kniffka, A. and Pante, G.: Why Do Global Climate Models Struggle to Represent Low-Level Clouds in the West African Summer Monsoon?, *J. Climate*, 30(5), 1665–1687, doi:10.1175/JCLI-D-16-0451.1, 2017.

Kalthoff, N., Lohou, F., Brooks, B., Jegede, G., Adler, B., Babić, K., Dione, C., Ajao, A., Amekudzi, L. K., Aryee, J. N. A., Ayoola, M., Bessardon, G., Danuor, S. K., Handwerker, J., Kohler, M., Lothon, M., Pedruzo-Bagazgoitia, X., Smith, V., Sunmonu, L., Wieser, A., Fink, A. H. and Knippertz, P.: An overview of the diurnal cycle of the atmospheric boundary layer during the West African monsoon season: results from the 2016 observational campaign, *Atmospheric Chemistry and Physics*, 18(4), 2913–2928, doi:10.5194/acp-18-2913-2018, 2018.

Knippertz, P., Fink, A. H., Schuster, R., Trentmann, J., Schrage, J. M. and Yorke, C.: Ultra-low clouds over the southern West African monsoon region, *Geophysical Research Letters*, 38(21), doi:10.1029/2011GL049278, 2011.

Knippertz, P., Fink, A. H., Deroubaix, A., Morris, E., Tocquer, F., Evans, M. J., Flamant, C., Gaetani, M., Lavaysse, C., Mari, C., Marsham, J. H., Meynadier, R., Affo-Dogo, A., Bahaga, T., Brosse, F., Deetz, K., Guebsi, R., Latifou, I., Maranan, M., Rosenberg, P. D. and Schlueter, A.: A meteorological and chemical overview of the DACCIWA field campaign in West Africa in June–July 2016, *Atmospheric Chemistry and Physics*, 17(17), 10893–10918, doi:10.5194/acp-17-10893-2017, 2017.

van der Linden, R., Fink, A. H. and Redl, R.: Satellite-based climatology of low-level continental clouds in southern West Africa during the summer monsoon season: Low-level clouds in southern West Africa, *Journal of Geophysical Research: Atmospheres*, 120(3), 1186–1201, doi:10.1002/2014JD022614, 2015.

Lohou, F., Kalthoff, N., Adler, B., Babić, K., Dione, C., Lothon, M., Pedruzo-Bagazgoitia, X. and Zouzoua, M.: Conceptual model of diurnal cycle of low-level stratiform clouds over southern West Africa, *Atmospheric Chemistry and Physics*, 20(4), 2263–2275, doi:https://doi.org/10.5194/acp-20-2263-2020, 2020.

Mauder, M., Cuntz, M., Drüe, C., Graf, A., Rebmann, C., Schmid, H. P., Schmidt, M. and Steinbrecher, R.: A strategy for quality and uncertainty assessment of long-term eddy-covariance measurements, *Agricultural and Forest Meteorology*, 169, 122–135, doi:10.1016/j.agrformet.2012.09.006, 2013.

Mohrmann, J., Bretherton, C. S., McCoy, I. L., McGibbon, J., Wood, R., Ghate, V., Albrecht, B., Sarkar, M., Zuidema, P. and Palikonda, R.: Lagrangian Evolution of the Northeast Pacific Marine Boundary Layer Structure and Cloud during CSET, *Monthly Weather Review*, 147(12), 4681–4700, doi:10.1175/MWR-D-19-0053.1, 2019.

S. Derrien, Y. Bezombes, G. Bret, O. Gabella, C. Jarnot, P. Medina, E. Piques, C. Delon, C. Dione, B. Campistron, P. Durand, C. Jambert, F. Lohou, M. Lothon, F. Pacifico and Y. Meyerfeld: DACCIWA field campaign, Savè super-site, UPS instrumentation, 2016.

Schrage, J. M. and Fink, A. H.: Nocturnal Continental Low-Level Stratus over Tropical West Africa: Observations and Possible Mechanisms Controlling Its Onset, *Monthly Weather Review*, 140(6), 1794–1809, doi:10.1175/MWR-D-11-00172.1, 2012.

Schuster, R., Fink, A. H. and Knippertz, P.: Formation and Maintenance of Nocturnal Low-Level Stratus over the Southern West African Monsoon Region during AMMA 2006, *Journal of the Atmospheric Sciences*, 70(8), 2337–2355, doi:10.1175/JAS-D-12-0241.1, 2013.

Stevens, B.: Bulk boundary-layer concepts for simplified models of tropical dynamics, *Theor. Comput. Fluid Dyn.*, 20(5–6), 279–304, doi:10.1007/s00162-006-0032-z, 2006.

Stevens, B., Moeng, C.-H., Ackerman, A. S., Bretherton, C. S., Chlond, A., de Roode, S., Edwards, J., Golaz, J.-C., Jiang, H., Khairoutdinov, M., Kirkpatrick, M. P., Lewellen, D. C., Lock, A., Müller, F., Stevens, D. E., Whelan, E. and Zhu, P.: Evaluation of Large-Eddy Simulations via Observations of Nocturnal Marine Stratocumulus, *Mon. Wea. Rev.*, 133(6), 1443–1462, doi:10.1175/MWR2930.1, 2005.

vanZanten, M. C., Duynkerke, P. G. and Cuijpers, J. W. M.: Entrainment Parameterization in Convective Boundary Layers, *J. Atmos. Sci.*, 56(6), 813–828, doi:10.1175/1520-0469(1999)056<0813:EPICBL>2.0.CO;2, 1999.

Wood, R.: Stratocumulus Clouds, *Mon. Wea. Rev.*, 140(8), 2373–2423, doi:10.1175/MWR-D-11-00121.1, 2012.

Interactive comment on “Breakup of nocturnal low-level stratiform clouds during southern West African Monsoon Season”

Dear reviewer 2,

We thank the reviewer for his/her helpful suggestions, which led to significant improvements of our paper. Below we detailed how his/her comments are addressed in the revised version of the paper. The major corrections of the paper are cited here in *italic*. We refer to specific pages by “P” and lines by “L”. For example, “P1, L1” refers to page 1, line 1.

(1) Insufficient treatment of radiative cooling term (RAD) quantification RAD is the dominant term controlling the convective overturning before the early morning, as also recognized by the authors. However, the equations (Eq. 2 and 3) used to quantify RAD in this study are too rough. As shown by Zheng et al. (2019), the RAD is most sensitive to two parameters: cloud optical thickness and moisture loading in the free atmosphere. If high clouds are present, the RAD will weaken significantly (e.g. Christensen et al., 2013). Even though the free-tropospheric moisture loading can be somewhat accounted for in Eq. (2) (the IWP), the cloud optical thickness and higher clouds can also modulate the RAD considerably. The blackbody assumption is only always valid for not-too-thick stratiform clouds (Zheng et al., 2019). The authors show that the RAD varies very little ($\sim 5 \text{ Wm}^{-2}$), which could be artificial consequence of the two assumptions behind the equations (i.e. blackbody and no high clouds). Thus, given the significant role of RAD, it should be worthwhile to use a radiative transfer model instead. All inputs for the model are available from the observations: cloud-base and -top heights and soundings. Running it is computationally cheap.

We thank the reviewer for this valuable suggestion to use a radiative transfer code. However, the water or ice content, the base and the summit of each cloud layers is needed in the radiative transfer code in order to take into account the higher clouds effect. This information is missing for the DACCIWA campaign, since only integrated LWP, the LLSC base and top heights are available. So the use of the radiative code does not fully answer the reviewer comment. Despite this, the SBDART (Santa Barbara DISORT Atmospheric Radiative Transfer; Ricchiazzi et al., 1998) model is now used in our study to estimate the radiative cooling over the LLSC layer at the end of the stratus phase, based on radiosonde, ceilometer and cloud-radar measurements. The LLSC optical thickness is determined by a parameterized LWP. The higher clouds impact is partly taken into account through vertical profiles of temperature and relative humidity given by the radiosonde but an emissivity of clear air is applied to these thermodynamical characteristics. This limitation is further discussed in the paper. We obtain higher values ($+ 15 \text{ W m}^{-2}$ in average) of cloud-top radiative cooling than previously, but the standard deviation among the cases is still of 5 W m^{-2} and no difference can be noticed between coupled and decoupled LLSC.

The text was modified in several places to include the SBDART radiative code description, and the discussion of the results:

P11-12: *“The term RAD (Eq. 1.d) is retrieved from the vertical profiles of upwelling and downwelling radiative fluxes which are computed by using the Santa Barbara DISORT Atmospheric Radiative Transfer (SBDART) model (Ricchiazzi et al., 1998). This software tool, which solves the radiative transfer equation for a plane-parallel atmosphere in clear and cloudy conditions, was used in the studies of Babić et al. (2019a) and Adler et al. (2019) to estimate the temperature tendency due to radiative interactions during the LLSC diurnal cycle. For our simulations, the model configuration was very similar to that used in these studies. We prescribed 65 vertical input levels with a vertical resolution of 50 m below 2 km a.g.l, 200 m between 2 and 5 km a.g.l, and, 1 km above 5 km a.g.l. The vertical profiles of air pressure, temperature and water vapour density as well as the integrated water vapour are based on 05:00 UTC standard radiosounding data. The cloud optical thickness, which varies with its water and ice content, is required to describe a cloud layer in the SBDART model. Yet, the LWP provided by the microwave radiometer deployed at Savè supersite (Wieser et al., 2016) includes all the existing cloudy layers, and also is not available for five of our selected cases. Therefore, the LLSC optical thickness is determined from a parameterized LWP (Eq. 2), by assuming an adiabatic cloudy layer in which the liquid water mixing ratio (q_l) increases linearly (van der Dussen et al., 2014; Pedruzo-Bagazgoitia et al., 2020). The downwelling longwave radiations from potential mid-level and high-level clouds may reduce the radiative cooling at the stratocumulus top (e.g. Christensen et al., 2013). However, the cloud layers above the LLSC (base, top and water content) cannot be precisely described in the SBDART model from the available data set. Thus, the higher clouds radiative effect is not directly included in our estimate of downwelling radiative fluxes, but it is partially taken into account through vertical profiles of temperature and relative humidity given by the radiosonde. As the shortwave radiations are zero before the sunrise, only the longwave range, 4.5-42 μm with spectral resolution of 0.1 μm (Babić et al., 2019a), was selected for radiative fluxes calculations. For all the cases, the vertical optical depth of ABL aerosol is fixed to 0.38, which corresponds to the average value of the measurements performed with a sun photometer in June and July 2016 at Savè.”*

(2) Inappropriate classification of the scenario of DD I am very reluctant to consider the clouds in Fig.10 c as "decoupled throughout the day". There are three possibilities for this case: (1) initially decoupled clouds remain decoupled and surface-heating driven cumulus clouds start to form underneath it. If they don't interact, the upper-layer clouds are decoupled and the bottom clouds are coupled; (2) if they interact, they form the cumulus-coupled stratocumulus-topped boundary layer such as those in downstream subtropical oceans; (3) If the initially decoupled clouds dissipate rapidly after decoupling, with only the underlying cumulus clouds left, this case is simply regular continental shallow cumulus that are, by definition, coupled.

All the above-stated cloud regimes are possible. Thus, it is a little bit misleading to call all of them "decoupled throughout". I would suggest either renaming it or adding additional discussions to clarify the definition of the decoupling.

We thank the reviewer for this comment. We fully agree that the three possibilities for scenario DD may occur. However, as stated in the paper, the scenario description is based on temporal changes of surface-based LCL and cloud base height measured by the ceilometer. From this point of view, in the scenario DD, the LLSC remains decoupled from the surface and thermally-driven (and coupled) shallow cumulus forms below it at the beginning of the convective phase. We are not able to test if the top of this underlying shallow cumulus interacts or not with the LLSC. So we kept the same name (DD) for this case. However, we completed the discussion about it.

The previous sentence *"In such conditions, the underlying cumulus clouds act to intermittently and locally couple the stratocumulus layer with the surface (Wood, 2012)."* was replaced by a more complete comment as suggested by the reviewer, **P29, L24**: *"In the case where the two cloud layers are superimposed, two possibilities may occur: (i) the underlying surface-convection driven cumulus cloud do not interact with the LLSC which remains decoupled from the surface, (ii) the underlying cumulus clouds develop vertically, reach the LLSC layer, and act to intermittently and locally couple it with the surface (Wood, 2012)."*

We moderated the statement in several sentences like this one, **P30, L3**, *"One can wonder what conditions lead the LLSC to either be coupled to the surface in the scenario DC, or remains POSSIBLY decoupled with the formation of an underlying cumulus layer in the scenario DD."*

The previous sentence, in the Abstract, *"In the eight remaining cases, the stratiform cloud remains decoupled from the surface all along its life cycle."*, is now **P2, L1**: *"In the eight remaining cases, the stratiform cloud remains HYPOTHETICALLY decoupled from the surface all along its life cycle, since the cloud base remains separated from the condensation level."*

(3) Other comments: - Figure 2 and other figures: it should be helpful to use local time as well, which makes the readers easier to think of the problem from a diurnal cycle perspective.

We thank the reviewer for this suggestion. We indicate in the section 3, **P7-L12**, that the local time at Savè, Benin is UTC +1 hour. In the revised version, this local time is repeated in the caption of Figures 2, 10 and 13.

- Page 10-11: some discussions on what determines the RAD is useful (check the work by Zheng et al., 2019).

We thank the reviewer for this comment. The radiative transfer across the stratocumulus layer is discussed in section 2; the text was modified to make it clear as follow, **P5-L15**: *"During night-time, the longwave radiative cooling at the stratocumulus top is the leading process governing its maintenance. This cooling occurs because the cloud droplets emit more infrared radiation towards the free*

troposphere than they receive from the drier air above. It is modulated by cloud-top temperature, cloud optical thickness, thermodynamic and cloudy conditions in the free troposphere (Siems et al., 1993; Wood, 2012; Christensen et al., 2013; Zheng et al., 2019)."

- Page 12, Line1: large-scale subsidence is commonly obtained from reanalysis data. Not very accurate, but better than nothing.

We agree with the reviewer and actually tried to use reanalysis data from the beginning. As mentioned in Pedruzo-Bagazgoitia et al. (2020), the large scale vertical velocity from reanalysis products present strong temporal and vertical variability, especially on early morning hours. We observed the same behaviour when we tried to use the ERA5 reanalysis products. Beside this, we observed a steady LLSC top at the end of the stratus phase in many cases. Consequently, we decided to use the Lilly (1968) assumption that implies the same order of magnitude between parameterized entrainment and subsidence velocities at the LLSC top.

The text is now, **P12, L25**: *"For the term SUBS (Eq. 1.e), we have no possibility of estimating precisely the large scale subsidence at the LLSC top. One possibility is to consider evaluations from models or re-analyses. However, we decided to discard this approach, because the subsidence profiles from regional simulations with Consortium for Small-Scale Modelling (COSMO) or from ERA-interim and ERA-5 reanalyses showed a very high temporal variability and a strong lack of coherence among the different cases. According to the cloud-radar CTH estimates, the LLSC top is often stationary at the end of the stratus phases during DACCIWA. This feature has been observed (Adler et al., 2019; Babić et al., 2019a; Dione et al., 2019) but also simulated by Pedruzo-Bagazgoitia et al. (2020). Based on the LLSC top stationarity at the time of our LWP budget analysis, $w_{s,CTH}$ is estimated following Lilly (1968):"*

$$\frac{\partial CTH}{\partial t} = w_{s,CTH} + w_e \approx 0 \quad (6)$$

"

- Section 4.1 as a whole: this section is centered on the difference between coupling and decoupling, however, what may cause the decoupling/coupling in the first place is not discussed in detail. There are several influential factors: cloud-top cooling itself (Nicholl 1984), precipitation (this is not important in your case), "deepening warming" decoupling (Bretherton and Wyant, 1997), and warm thermal advection (Zheng and Li, 2019). It may be more enlightening to discuss your results in the context of these potential influential controllers.

We thank the reviewer for this suggestion, and we hope to have improved the text. The section 4 has been deeply modified; a section 4.3 has been added, **P26-27**, to discuss the results presented in section 4.1 and 4.2 about the relevant processes which are able to couple the LLSC during the stratus phase. In summary, none of these processes was clearly pointed out as responsible for the coupling during this phase and a combination of several of them, each with a small effect, should be considered.

- Page 22, Line 15: again, it could be due to too simple treatment of RAD.

We do agree with the reviewer. The use of SBDART certainly gives a better treatment of RAD but still not complete, since the higher clouds are not fully taken into account. This is discussed in the revised version P24, L3:

“We find only a 5 W m^{-2} standard deviation for the radiative cooling at the LLSC top and no particular difference between cases C and D. This very low standard deviation may be due to the conditions which remained very steady from one case to the other, but may also be underestimated because the higher clouds impact is not fully included in the radiative fluxes estimate. In order to evaluate the error due to the temperature underestimation above the LLSC top, SBDART is run with the measured and a corrected temperature profile, while the other inputs remain unchanged. The correction of the potential temperature vertical profile consists in a linear tendency between the measured θ plus a 1.2K correction right above the CTH, and the measured θ at 800 m, where we consider that the radiosonde sensor is no more affected by the cloud crossing. The cloud-top radiative cooling estimated by SBDART with this corrected temperature vertical profile is larger by less than 2 W m^{-2} .”

- Figure 13: there are too many symbols, making the readers hard to recognize each of them. This defeats the purpose of using a diagram for illustrations. Try to use process-based cartoons (e.g. the one from Wood 2012).

We thank the reviewer for this valuable suggestion. Process-based cartoons are now used in Figure 13 to illustrate the different scenarios, P37.

Adler, B., Babić, K., Kalthoff, N., Lohou, F., Lothon, M., Dione, C., Pedruzo-Bagazgoitia, X. and Andersen, H.: Nocturnal low-level clouds in the atmospheric boundary layer over southern West Africa: an observation-based analysis of conditions and processes, *Atmospheric Chemistry and Physics*, 19(1), 663–681, doi:10.5194/acp-19-663-2019, 2019.

Babić, K., Adler, B., Kalthoff, N., Andersen, H., Dione, C., Lohou, F., Lothon, M. and Pedruzo-Bagazgoitia, X.: The observed diurnal cycle of low-level stratus clouds over southern West Africa: a case study, *Atmospheric Chemistry and Physics*, 19(2), 1281–1299, doi:10.5194/acp-19-1281-2019, 2019.

Christensen, M. W., Carrió, G. G., Stephens, G. L. and Cotton, W. R.: Radiative Impacts of Free-Tropospheric Clouds on the Properties of Marine Stratocumulus, *Journal of the Atmospheric Sciences*, 70(10), 3102–3118, doi:10.1175/JAS-D-12-0287.1, 2013.

Dione, C., Lohou, F., Lothon, M., Adler, B., Babić, K., Kalthoff, N., Pedruzo-Bagazgoitia, X., Bezombes, Y. and Gabella, O.: Low-level stratiform clouds and dynamical features observed within the southern West African monsoon, *Atmos. Chem. Phys.*, 19(13), 8979–8997, doi:10.5194/acp-19-8979-2019, 2019.

van der Dussen, J. J., de Roode, S. R. and Siebesma, A. P.: Factors Controlling Rapid Stratocumulus Cloud Thinning, *J. Atmos. Sci.*, 71(2), 655–664, doi:10.1175/JAS-D-13-0114.1, 2014.

Lilly, D. K.: Models of cloud-topped mixed layers under a strong inversion, *Q.J.R. Meteorol. Soc.*, 94(401), 292–309, doi:10.1002/qj.49709440106, 1968.

Pedruzo-Bagazgoitia, X., de Roode, S. R., Adler, B., Babić, K., Dione, C., Kalthoff, N., Lohou, F., Lothon, M. and Vilà-Guerau de Arellano, J.: The diurnal stratocumulus-to-cumulus transition over land in southern West Africa, *Atmos. Chem. Phys.*, 20(5), 2735–2754, doi:10.5194/acp-20-2735-2020, 2020.

Ricchiazzi, P., Yang, S., Gautier, C. and Sowle, D.: SBDART: A Research and Teaching Software Tool for Plane-Parallel Radiative Transfer in the Earth's Atmosphere, *Bull. Amer. Meteor. Soc.*, 79(10), 2101–2114, doi:10.1175/1520-0477(1998)079<2101:SARATS>2.0.CO;2, 1998.

Siems, S. T., Lenschow, D. H. and Bretherton, C. S.: A Numerical Study of the Interaction between Stratocumulus and the Air Overlying It, *J. Atmos. Sci.*, 50(21), 3663–3676, doi:10.1175/1520-0469(1993)050<3663:ANSOTI>2.0.CO;2, 1993.

Wieser, A., Adler, B. and Deny, B.: DACCIWA field campaign, Savè super-site, Thermodynamic data sets, , doi:10.6096/dacciwa.1659, 2016.

Wood, R.: Stratocumulus Clouds, *Mon. Wea. Rev.*, 140(8), 2373–2423, doi:10.1175/MWR-D-11-00121.1, 2012.

Zheng, Y., Rosenfeld, D., Zhu, Y. and Li, Z.: Satellite- Based Estimation of Cloud Top Radiative Cooling Rate for Marine Stratocumulus, *Geophys. Res. Lett.*, 46(8), 4485–4494, doi:10.1029/2019GL082094, 2019.

PEER-REVIEW OF THE MANUSCRIPT:

Breakup of nocturnal low-level stratiform clouds during southern West African Monsoon Season (acp-2020-602)

ALL MODIFICATIONS IN THE MANUSCRIPT:

By comparing the original and revised versions

Breakup of nocturnal low-level stratiform clouds during the southern West African Monsoon Season

Maurin ZOUZOUA¹, Fabienne LOHOU², Paul ASSAMOI¹, Marie LOTHON², Véronique YOBOUE¹,
Cheikh DIONE³, Norbert KALTHOFF⁴, Bianca ADLER⁴, Karmen BABIĆ⁴, and Xabier PEDRUZO-
5 BAGAZGOITIA⁵

¹Laboratoire de Physique de l'atmosphère et de Mécanique des fluides-~~(LAPA-MF)~~, Université Félix Houphouët Boigny, Abidjan, Côte d'Ivoire

²Laboratoire d'Aérogologie, Université de Toulouse, CNRS, UPS, Toulouse, France

³African Centre of Meteorological Applications for Development, Niamey, Niger

10 ⁴Institute of Meteorology and Climate Research, Karlsruhe Institute of Technology (KIT), Karlsruhe, Germany

⁵Meteorology and Air Quality Group, Wageningen University and Research, Wageningen, the Netherlands

Correspondence to: Maurin ZOUZOUA (maurin.zouzoua@aero.obs-mip.fr)

Abstract.

15 Within the framework of ~~the~~ DACCIWA (Dynamics-Aerosol-Chemistry-Cloud-Interactions over West Africa) project, and based on a field experiment conducted in June and July 2016, we ~~analyse~~analyze the daytime breakup of the continental low-level stratiform clouds in southern West Africa. We use the observational data gathered during twenty-two precipitation-free occurrences at Savè-~~supersite~~, in Benin. Our analysis, which starts ~~since~~from the stratiform cloud formation usually at night, focuses on the role played by the coupling between the cloud and the surface in the transition towards shallow convective clouds-~~during daytime~~. It is based on several diagnostics, including Richardson number and various cloud
20 macrophysical properties. The distance between lifting condensation level and cloud base height is used as a criterion of coupling. We also make an attempt to estimate the most predominant terms of the liquid water path budget on early morning.

When the nocturnal low-level stratiform cloud forms, it is decoupled from the surface, except in one case. On early morning, the cloud is found coupled with the surface in nine cases and ~~is remained~~remains decoupled in the thirteen other cases. The coupling, which occurs within the four hours after the cloud formation, is accompanied with a cloud base
25 lowering and near-neutral thermal stability in the subcloud layer. Further, at the initial stage of the transition, the stratiform cloud base is slightly cooler, wetter and more homogeneous in the coupled cases. The moisture jump at cloud top is found usually around 2 g kg^{-1} , and the temperature jump within 1-5 K, which is significantly smaller than typical marine stratocumulus, and explained by the monsoon flow environment within which the stratiform cloud develops. No significant difference of liquid water path budget terms was found between the coupled and decoupled cases. In agreement with
30 previous numerical studies, we found that the stratiform cloud maintenance before the sunrise results from the interplay between the predominant radiative cooling, and ~~the~~ entrainment and large scale subsidence at its top.

Three transition scenarios were observed, depending on the state of the coupling at the initial stage. In the coupled cases, the low-level stratiform cloud remains coupled until its ~~break-up~~breakup. In five of the decoupled cases, the cloud couples

with the surface as the LCL is rising. In the eight remaining cases, the stratiform cloud remains hypothetically decoupled from the surface all along its life cycle, since the cloud base height remains separated from the condensation level. In case of coupling during the transition, the stratiform cloud base lifts with the growing convective boundary layer roughly between 06:30 and 08:00 UTC. The cloud deck breakup occurring at 11:00 UTC or later leads to the formation of shallow convective clouds. When the decoupling subsists, shallow cumulus clouds form below the stratiform cloud deck between 06:30 and 09:00 UTC. The breakup time in this scenario has a stronger variability, and occurs before 11:00 UTC in most of the cases. Thus we argue that the coupling with the surface during the daytime hours has a crucial role in the low-level stratiform cloud maintenance and in its transition towards shallow convective clouds.

Keywords: Stratiform cloud breakup, surface coupling, liquid water path budget, DACCIWA experiment.

1 Introduction

The low-level stratiform clouds (LLSC) are Earth's most common cloud type (Wood, 2012). During the West Africa monsoon season (~~WAM~~), the LLSC form frequently at night over a region extending from Guinean coast to several hundred kilometres inland (van der Linden et al., 2015). ~~Figure 1 gives an overview of the horizontal scale of this phenomenon. It shows the low cloud coverage fraction from ECMWF (European Centre for Medium range Weather Forecast) ERA5 re-analyses (Copernicus Climate Change Service, 2019) averaged between 05:00 and 07:00 UTC on 8 July 2016. The expansion of the LLSC over the southern West Africa (SWA) during the night to day transition on 07-08 July 2016 was analyzed by Babić et al. (2019a). One can see that the inland-affected area spans up to around 11°N, which includes the coastal, Sudanian and Sudanian-Sahelian climatic zones (Emetere, 2016).~~ The LLSC coverage persists for many hours during the following day, reducing the incoming solar radiation, and impacting the surface energy budget and related processes such as the diurnal cycle of the atmospheric boundary layer (ABL) (Schuster et al., 2013; Adler et al., 2017; Knippertz et al., 2017). However, the diurnal cycle of those clouds is still poorly represented in numerical weather and climate models, especially over West Africa (Hannak et al., 2017). Indeed, their lifetime is generally underestimated in the numerical simulations, causing high incoming solar radiation at the surface in this region where the meteorological conditions are governed by convection activities and by surface thermal and moisture gradients (Knippertz et al., 2011). ~~That~~This could be an important factor for which the forecasts of ~~WAM~~West African monsoon features still have a poor skill (Hannak et al., 2017). Therefore, a better understanding of the processes behind LLSC ~~is useful for modelling purposes.~~over southern West Africa (SWA) is useful to improve the numerical weather prediction and climate projection quality. Due to the scarce weather monitoring network over West Africa, the first studies addressing the LLSC over this region were mostly conducted with satellite images and traditional synoptic ~~observation~~observations (Schrage and Fink, 2012; van der Linden et al., 2015), as well as with numerical simulations at regional scale (Schuster et al., 2013; Adler et al., 2017; Deetz et al., 2018). They emphasized

that the physical processes, spanning from local to synoptic scale such as; horizontal advection of cold air associated to WAM West African monsoon, lifting induced by topography, gravity waves or shear-driven turbulence, are relevant for the LLSC formation during the night. However, the LLSC evolution after the sunrise received little attention.

5

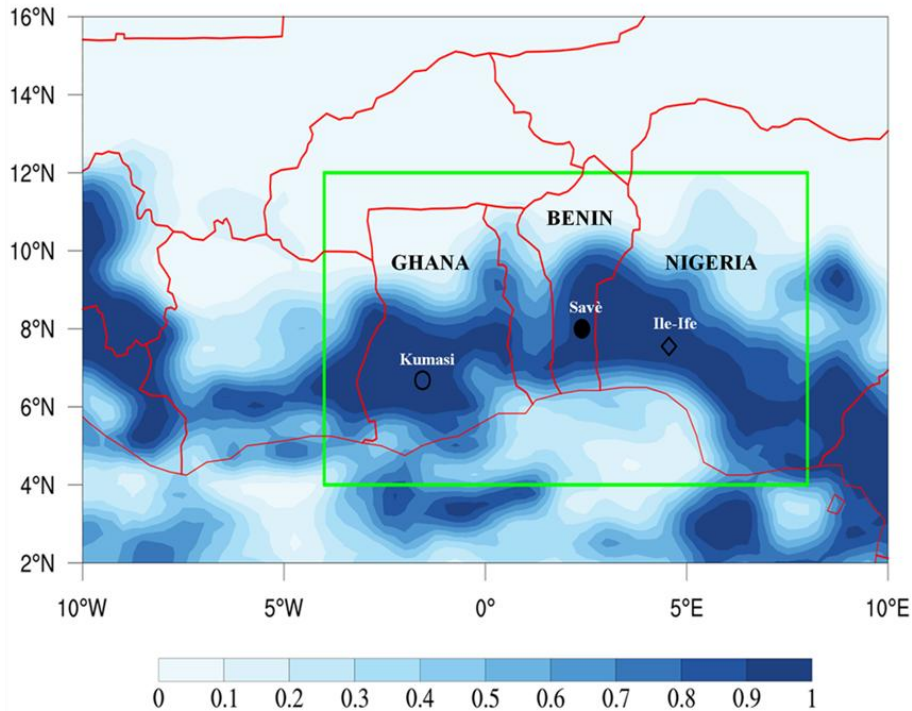


Figure 1. Low-cloud coverage fraction over southern West Africa from ERA5 Re-analyses, averaged between 05:00 and 07:00 UTC on 8 July 2016. The fraction varies from 0 (clear sky) to 1 (totally covered sky). The red lines represent the geopolitical boundaries. The green box delimits the area of interest during DACCIWA field campaign. The black markers indicate the geographical locations of DACCIWA supersites, Kumasi in Ghana (unfilled circle), Savè in Benin (filled circle) and Ile-Ife in Nigeria (unfilled diamond).

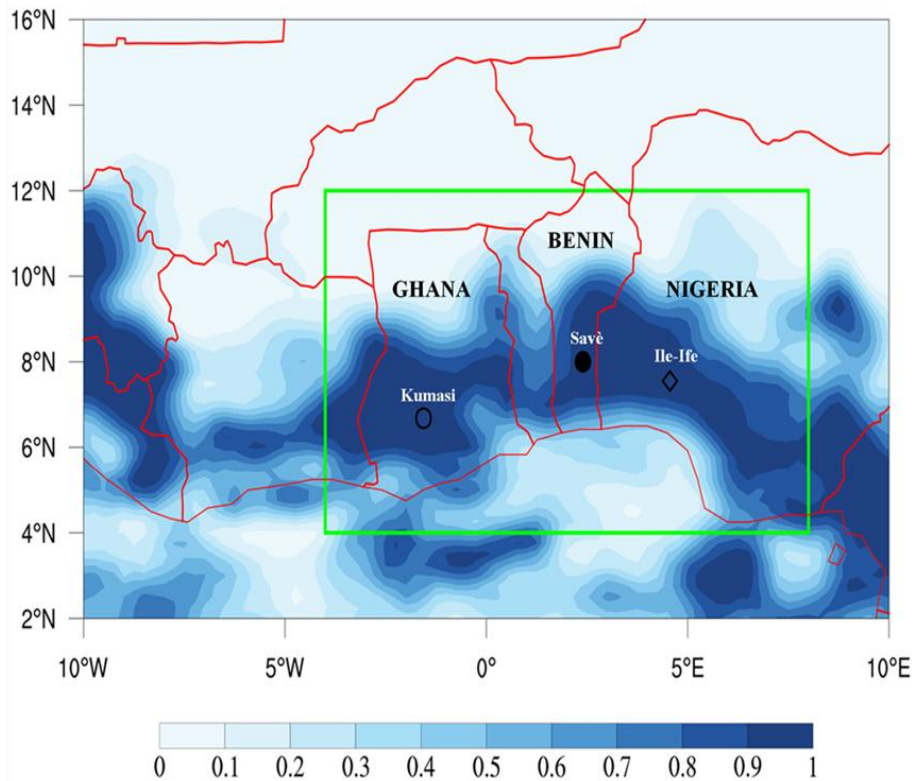


Figure 1. Low-level cloud fraction over West Africa from ECMWF (European Centre for Medium range Weather Forecast) ERA5 re-analyses (Copernicus Climate Change Service, 2019), averaged between 05:00 and 07:00 UTC on 8 July 2016. The fraction varies from 0 (clear sky) to 1 (totally covered sky). The red lines represent the geopolitical boundaries. The green box delimits the area of interest during DACCWA field campaign. The black markers indicate the geographical locations of DACCWA ground supersites Savè in Benin (filled circle), Kumasi in Ghana (unfilled circle) and Ile-Ife in Nigeria (unfilled diamond).

During the boreal summer 2016, a field campaign was conducted over SWA within the framework of the European project Dynamics-Aerosol-Chemistry-Cloud Interaction in West Africa (DACCWA) (Knippertz et al., 2015). The project was developed to study the impact of increasing air pollution on SWA weather and climate. A joint measurement, including aircraft and ground-based campaigns (Flamant et al., 2017; Kalthoff et al., 2018), was performed. The area of interest during this field experiment is indicated in Fig. 1-, which gives an overview of the LLSC horizontal extent between 05:00 and 07:00 UTC on 8 July 2016. One of the primary goals of this project was to provide the first high quality and comprehensive dataset in order to conduct a detailed observational study of the LLSC. To this end, several three so-called “supersites”, which gather a large set of complementary instruments reporting the evolution of atmospheric conditions and low level cloud coverage, were deployed installed at three supersites, Kumasi (6.68° N, 1.56° E) in Ghana, Savè (8.00° N, 2.40° W) in

Benin, and Ile-Ife (7.55° N, 4.56° W) in Nigeria (Fig. 1). The comprehensive dataset acquired at the Savè supersite allowed the first research studies of LLSC over SWA based on high temporal resolution observations. Adler et al. (2019) and Babić et al. (2019a,b) studied the physical processes which govern the LLSC formation and its maintenance up to the next day. Dione et al. (2019) performed a statistical analysis on the LLSC characteristics and low troposphere dynamic features during the DACCIWA field campaign. The findings of these studies have been generalized and synthesized by Lohou et al. (2020) who also quantified for the first time the impact of the LLSC on the surface energy budget terms. These observational-based studies focused ~~essentially~~mainly on the ~~mechanism~~mechanisms involved in the formation of LLSC ~~induring~~ the WAM context in order ~~West Africa monsoon season~~, to evaluate the ~~hypothesis~~hypotheses proposed by earlier research works. They confirmed the role played by the horizontal advection and ~~the~~ vertical wind shear driven by a nocturnal low-level jet (NLLJ) which is among the main features of the ~~WAM~~West African monsoon (Parker et al., 2005; Lothon et al., 2008). The breakup of the LLSC deck after the sunrise which leads to the transition towards shallow convective clouds has not been well documented yet with the unique DACCIWA dataset. Only Pedruzo-Bagazgoitia et al. (2019) analyzed this transition by the mean of idealized Large Eddy Simulations (LES), inspired by the data collected during the LLSC occurrence on 25-26 June 2016 at the Savè supersite. This was the first LES of stratocumulus to shallow cumulus (Sc-Cu) transition over land in SWA.

Our study aims at analyzing the transition from the LLSC to ~~the~~shallow convective ~~shallow cumulus~~ clouds of twenty-two ~~(22)~~ cases observed at Savè supersite during DACCIWA experiment, addressing the possible scenarios and the involved processes, as far as enabled by the available measurements. This should provide a complementary guidance for numerical model evaluation of this Sc-Cu transition over SWA. The rest of this paper is organized as follow. ~~The~~ Section 1 presents a brief state of our knowledge on the diurnal cycle of, the LLSC covering the SWA, and, stratocumulus at other places around the world with a focus on the Sc-Cu transition. ~~The~~ Section 3 describes the observational data and the deduced diagnostics used to monitor the LLSC evolution. It also overviews how the contributions of some processes involved in the LLSC diurnal cycle are derived from the measurements. ~~The~~ Section 4 presents the LLSC characteristics just before the sunrise, at the initial stage of the transition. The relative contributions of the physical processes governing the LLSC are estimated. In section 5, the evolution of LLSC on daylight hours is analyzed. Finally, a summary and conclusion are given in section 6.

~~2 State of art~~

2 Review

The diurnal cycle of the LLSC over SWA consists of four main stages: the *stable phase*, the *jet phase*, the *stratus phase* and the *convective phase* (Babić et al., 2019a; Lohou et al., 2020). **The increase of relative humidity (Rh) within the ABL leading to saturation and ~~the~~LLSC formation is due to the cooling which mainly occurs during the stable and the jet phases: in the monsoon layer, up to around 1.5 km above ground level (a.g.l.). The main process behind this cooling is**

the horizontal advection of cooler air from Guinea coast, due to the combination of a maritime inflow (MI) (Adler et al., 2017; Deetz et al., 2018) and the NLLJ (Schrage and Fink, 2012; Dione et al., 2019). The onset time and the strength of the NLLJ, as well as the level of background humidity in the ABL, are crucial for the LLSC formation (Babić et al., 2019b). Indeed, from two ~~eases-study~~case studies, Babić et al. (2019b) showed that weaker and later NLLJ onset leads to a reduced cooling, so that the saturation within the ABL may not be reached. The formation of the LLSC marks the end of the jet phase and the beginning of the *stratus phase*. The LLSC base is firstly located around the NLLJ core where the cooling is maximum (Adler et al., 2019; Babić et al., 2019a; Dione et al., 2019; Lohou et al., 2020). During the *stratus phase*, the maximum ~~of~~ wind speed in the NLLJ is reduced and shifted upward by the turbulent mixing induced by the longwave radiative cooling at the cloud-top, typical characteristic of stratocumulus clouds. In addition, the dynamical turbulence underneath the NLLJ and the convective turbulence due to the cloud top cooling are potential drivers of the coupling between the LLSC and the surface (Adler et al., 2019; Lohou et al., 2020). This dynamical turbulence could also be an important factor for additional cooling below the LLSC base (Babić et al., 2019a). When the LLSC is coupled to the surface, its base coincides quite well with the surface-based lifting condensation level (LCL) (Adler et al., 2019; Lohou et al., 2020). The final *convective phase* of the LLSC diurnal cycle starts after sunrise, when the sensible heat flux becomes larger than 10 W m⁻², and ends at the cloud layer breakup (Dione et al., 2019; Lohou et al., 2020).

A comprehensive overview on the current state of research on the stratocumulus dynamic is presented by Garratt (1994) and Wood (2012). Such a cloud is regulated through feedbacks between several processes: radiation, precipitation, turbulence fluxes of moisture and heat at cloud base, entrainment and large-scale subsidence at the cloud top. The cloud Liquid Water Path (LWP) budget is considered to disentangle the respective contribution of each process. **During nighttime, the longwave radiative cooling at the ~~cloud~~-stratocumulus top is the leading process governing theits maintenance-of. This cooling occurs because the cloud droplets emit more infrared radiation towards the ~~cloud~~-free troposphere than they receive from the drier air above. It is modulated by cloud-top temperature, cloud optical thickness, thermodynamic and cloudy conditions in the free-troposphere (Siems et al., 1993; Wood, 2012; Christensen et al., 2013; Zheng et al., 2019).** After the sunrise, the solar radiation comes into play, warming the cloud, and penetrating more and more down to the surface as the Secloud layer breaking occurs. The LES performed by Ghonima et al. (2016) revealed that the effect of turbulent fluxes at cloud base depends upon Bowen ratio (B) at the surface, where B is the ratio of surface sensible flux to latent flux. Low values of B contribute to cloud layer humidification, favouring cloud persistence. In contrast, the predominance of surface sensible heat over latent heat flux ($B > 1$) warms the cloud, leading to its evaporation. The precipitation formation, the large-scale subsidence and entrainment have generally drying and warming effects on the cloud layer (Wood, 2012; van der Dussen et al., 2016; Wood, 2012).

The Sc-Cu transition in other climatologic regions was the subject of several studies, most of them made over the ocean (e.g. Bretherton et al., 1999; Duynkerke et al., 2004; Sandu and Stevens, 2011; Duynkerke et al., 2004; van der Dussen et al., 2016; de Roode et al., 2016; Mohrmann et al., 2019; Sarkar et al., 2019), and a few over land (e.g. Price, 1999; Ghonima et al., 2016; Price, 1999). In these studies ~~essentially based on numerical simulations,~~ the stratocumulus is initially coupled to

the surface with the convective turbulence produced by ~~the cloud-top radiative cooling at the cloud top. They. The processes-analyzed studies, essentially based on numerical simulations,~~ proposed specific mechanisms for the ~~Se~~cloud layer breakup, but still based on an enhancement of entrainment warming and drying effect. Over land especially, the main driver is the intensification of the convection within the ABL by the solar heating.

5 The LES made by Pedruzo-Bagazgoitia et al. (2020) provide an insight on the evolution of a coupled LLSC to surface in terms of involved processes in the SWA monsoon conditions. Before the sunrise, the cloud-top radiative cooling is the unique positive contribution ~~into the~~ LWP budget and is the factor which maintains the cloud layer. The breakup of the cloud deck five hours after the sunrise is mainly due to the progressive decrease of cloud-top cooling, and ~~to the~~ increase of cloud-top entrainment negative contribution ~~into~~ LWP budget. About thirty minutes before the stratiform cloud deck breakup, a
10 negative buoyancy flux at ~~the cloudits~~ base decouples it from the surface. Later on, a shallow cumulus cloud fully coupled to the surface appears at the ~~top of the~~ convective ABL ~~top. These. Since the LES also showed that wind shear at the stratiform cloud top accelerates the Se-Cu transition~~ made by enhancing the impact of entrainment Pedruzo-Bagazgoitia et al. (2020) are set with atmospheric and surface conditions measured at Savè during the DACCIWA campaign, some simplifying assumptions used in our study are based on their results, and the simulated and observational results are compared.

15

3 Data and Methodology

The period in which the DACCIWA field experiment took place from 14 (June to 31 July 2016) was divided in four synoptic phases by Knippertz et al. (2017) divided this period in four synoptic phases, based on the precipitation north-south precipitation difference between the coastal (south) and Sudanian-Sahelian areas (north). The ~~second~~ first phase ~~(from 22 June to 20 July), so-called post, the pre-onset phase, started ends on 16 June 2016 with a northward shift of the rainfall. It is characterized by an increase, indicating the settlement of low-level cloudiness over SWA. The period from 27 June to 8 July 2016 was characterized by undisturbed monsoon flow over the West Africa, especially over DACCIWA investigated area monsoon season (KnippertzFitzpatrick et al., 20172015).~~

20 The ground sites were located at roughly the same distance from the Guinean coast (200 km in land) but with different topography. The second synoptic phase, the post-onset phase, characterized by higher rainfall over the Sudanian-Sahelian zone, lasted from 22 June to 20 July 2016. During the first days of this phase, namely from 27 June to 8 July 2016, undisturbed monsoon flow and an increase of low-level cloudiness were observed over SWA, especially over DACCIWA investigated area. Between 9 and 16 July 2016, the formation of the nocturnal LLSC over SWA was inhibited by drier conditions in the low troposphere due to an unusual anticyclonic vortex which had its center in the Southern Hemisphere (KalthoffKnippertz et al., 20182017; Babić et al., 2019b). By using the ground-based data, Kalthoff et al. (2018) give an overview of the diurnal cycle of the low troposphere at the three supersites. The DACCIWA field campaign includes 15 intensive observation periods (IOPs), during which the temporal resolution of the radiosoundings performed at the

30

supersites, especially at Savè supersite, was improved. Each IOP lasted from 17:00 UTC on one day (Day-D) to 11:00 UTC on the following day (Day-D+1).

. During the third phase, from 21 to 26 July 2016, the rainfall maximum shifts back to the coastal zone and a strong westerly flow was observed in the low-troposphere over the Sudanian-Sahelian zone. At last, during the final synoptic phase named the recovery phase, meteorological conditions return to a more typical behaviour for the monsoon season, with a precipitation maximum in the Sahel and low-troposphere dynamic similar to the beginning of the post-onset phase.

The DACCIWA supersites were located at roughly the same distance from the Guinean coast (200 km in land, Fig. 1), between the coastal and the Sudanian areas, but with a different topography (Kalthoff et al., 2018). The supersites are part of the savannah ecosystem, where grassland is intercut with crops and degraded forest. By using the ground-based data, Kalthoff et al. (2018) give an overview of the low-troposphere diurnal cycle at these three ground sites. The DACCIWA field campaign includes fifteen intensive observation periods (IOPs) during which the temporal resolution of the radiosondes performed at the supersites, especially at Savè, was improved. Each IOP lasted from 17:00 UTC on one given day (day-D) to 11:00 UTC on the following day (day-D+1).

The ground-based data acquired at Savè supersite on which our investigation is based offer ~~the most complete~~ nearly continuous information on ~~both the cloudy and~~ atmospheric conditions. The instrumentation and the data collected correspond to four published DOI (Derrien et al., 2016; Handwerker et al., 2016; Kohler et al., 2016; Wieser et al., 2016). We analyzed a set of twenty-two LLSC occurrences for which the cloud forms during night and persists at least until sunrise the next day. These cases have been selected over the period from 20 June to 31 July 2016, because of ~~a~~ good data coverage (Dione et al., 2019). Only cases for which the stratus phase, determined by the methodology of Adler et al. (2019), started before 04:00 UTC on day-D+1 have been selected. ~~In addition~~ Additionally, for each ~~of the~~ selected cases, no or light precipitation, i.e. less than 1 mm, was recorded at ~~the~~ surface from 21:00 UTC on day-D to 16:00 UTC on day-D+1. Among these ~~22~~ twenty-two cases, ~~9~~ nine are IOPs, including the 07-08 July 2016 (IOP8) case (Babić et al., 2019a) and the 25-26 June 2016 case (IOP3) (Pedruzo-Bagazgoitia et al., 2020). About 60% of the selected cases occurred between the 26 June and 11 July 2016, a period ~~with pronounced LLSC occurrence over West Africa due to favourable synoptic conditions (Knippertz et al., 2017). Note that we hereafter consider UTC time rather than Benin local time (UTC+1 which roughly fits within the first three weeks of the post-onset phase, and is characterized by a low-troposphere dynamic typical for West Africa monsoon season. Note that we hereafter consider UTC time rather than Benin local time (UTC + 1 hour).~~

3.1 Observational data used

3.1 Instrumentation

Two complementary and co-located instruments installed at Savè supersite were used to provide information on the LLSC macrophysical characteristics: a ceilometer for the cloud base height (CBH), and a cloud radar for the cloud top height (CTH).

Through ~~the~~ backscatter vertical profiles measured by the ceilometer, from the surface to 15 km a.g.l with a vertical resolution of 15 m, manufacturer software automatically provides each minute three estimates of CBH allowing the detection of several cloudy layers. As we focus on the LLSC (the lowest cloudy layer), we use only the lowest value (~~hereafter~~hereafter CBHs). The LLSC top height (CTHs) are derived from 5-min averaged radar reflectivity vertical profiles from 150 m to 15 km a.g.l at a vertical resolution of 30 m, by a methodology described in Babić et al. (2019) and Adler et al. (2019). According to Dione et al. (2019) ~~the top of~~, the LLSC top evolves overall under 1200 m a.g.l. To be consistent with this outcome, an upper limit of 1200 m a.g.l was applied to the CTHs. **Unfortunately, several values of CTHs are missing, particularly during daytime for many selected cases, due to the retrieval technique limitation.**

~~The meteorological conditions at the surface (temperature, relative humidity, and, pressure of the air at 2 m height), and, the different terms of the surface energy budget were continuously acquired. In this study, the net radiative flux (R_n), the surface sensible (SHF) and the latent heat (LHF) fluxes measured at 4 meters above ground level (m a.g.l) are used. SHF and LHF are deduced from high frequency (20 Hz) measurements processed with Eddy covariance methods with the TK3.11 software~~ The thermodynamical and dynamical characteristics of the low troposphere are retrieved from the radiosondes of the MODEM radiosounding system. The MODEM radiosonde collects every second (which corresponds to a vertical resolution of 4-5 m) the air temperature and relative humidity, and the probe GPS localization from which horizontal wind speed components, altitude and pressure are deduced (MauderDerrien et al., 20132016). The thermodynamical sensors accuracy is 0.2 °C, 2 % and dynamical characteristics of the low troposphere are retrieved from the radiosoundings. 0.01 m for temperature, relative humidity and GPS localization respectively. A standard radiosonde was launched every day at 05:00 UTC and usually rose up to ~~2014~~ km a.g.l. On IOP days, ~~3~~three additional radiosondes were performed at 23:00 UTC on day-D, and at 11:00 and 17:00 UTC on day-D+1. In between these soundings, so-called re-usable radiosondes were more frequently launched, at regular time interval in order to provide higher temporal resolution of the conditions within the ABL. The re-usable radiosondes reached a maximum height of around 1500 m a.g.l. During the ~~six~~ first six IOPs of DACCIIWA, the frequent soundings were performed hourly and each 1.5 h during the ~~others~~other IOPs. The radiosondes data were ~~smoothed by averaging with~~averaged at a final vertical resolution of ~~10~~50 m. Additionally, measurements of an ultra-high frequency (UHF) wind profiler are used to derive the NLLJ core height at 15 min time interval (Dione et al., 2019).

The meteorological conditions at the surface (temperature, relative humidity and pressure of the air at 2 m a.g.l), and some terms of the surface energy budget (net radiative flux (R_{n0}) sensible heat (SHF_0) and latent heat (LHF_0) fluxes at 4 m a.g.l) were continuously acquired. SHF_0 and LHF_0 are deduced from high-frequency (20 Hz) measurements processed with Eddy-covariance methods by using the TK3.11 software (Mauder et al., 2013).

3.2 Derived diagnostics to monitor the LLSC

We define some diagnostics to monitor the evolution of the LLSC layer: *the fraction of the low cloud coverage*, the *LLSC base height* and *the homogeneity of the cloud layer*, the *link between the LLSC and the surface*, as well as two characteristic

times of the LLSC *evolution*. The LLSC depth would also be a key diagnostic, but the low availability of CTHs cloud radar-based estimates during daytime limits *the cloud depth* monitoring. In addition to that, the humidity and temperature sensors onboard the radiosonde were affected by the water deposition during the crossing of the LLSC layer, so neither these are *alwaysfully* reliable for the CTH estimate (Adler et al., 2019; Babić et al., 2019a).

5

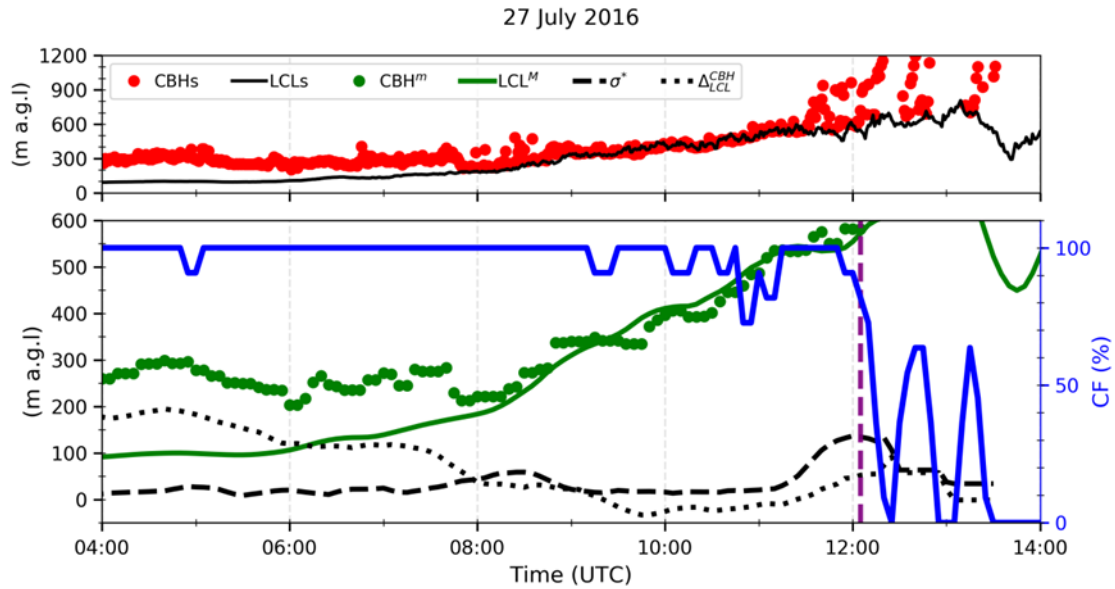


Figure 2 : Time series of, 1-min ceilometer derived CBHs and surface based lifting condensation level (LCLs) (upper panel), and derived 5-min diagnostics (lower panel), minimum of CBHs (CBH^m), mean LCLs (LCL^M, full green line), standard deviation of the difference between CBHs and CBH^m (σ*, dashed black line), The difference between CBH^m et LCL^M (Δ_{LCL}^{CBH}, dotted black line) and LLSC coverage fraction (CF, full blue line), between 04:00 and 14:00 UTC on 27 July 2016. The vertical dashed purple line marks the breakup time of the LLSC layer (T_b).

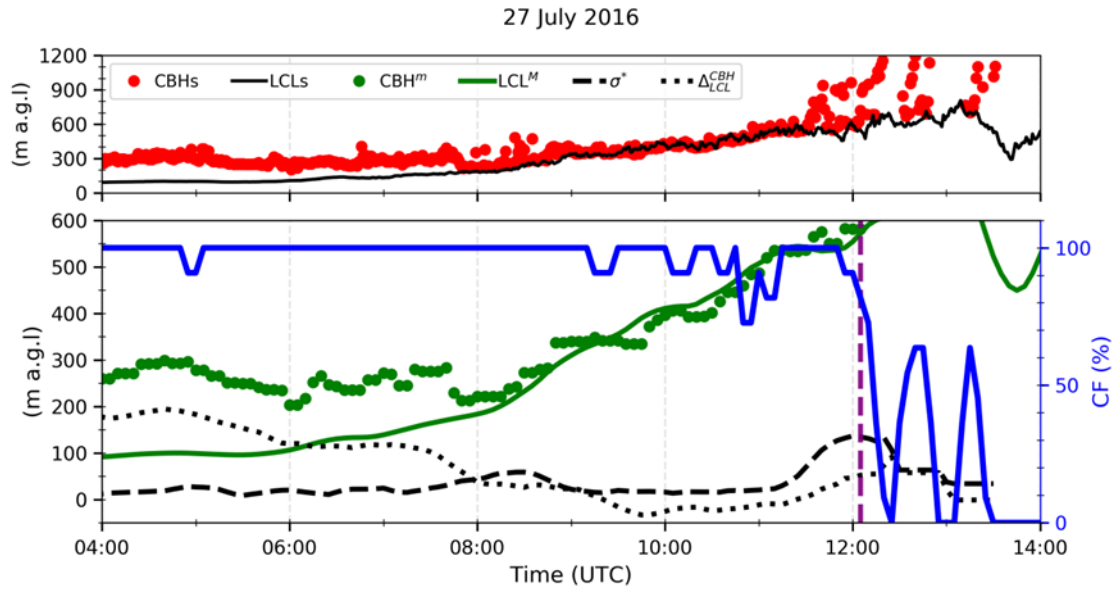


Figure 2 : Time series of, 1-min ceilometer-derived CBHs and surface-based lifting condensation level (LCLs) (upper panel), and derived 5-min diagnostics (lower panel), minimum of CBHs (CBH^m), mean LCLs (LCL^M, full green line), standard deviation of the difference between CBHs and CBH^m (σ*, dashed black line), the difference between CBH^m et LCL^M (Δ_{LCL}^{CBH}, dotted black line) and cloud coverage fraction (CF, full blue line), between 04:00 and 14:00 UTC on 27 July 2016. The vertical dashed purple line marks the breakup time of the LLSC layer (T_b). The Local time at Savè (in Benin) is UTC +1 hour.

The diagnostics are calculated over a time interval of 10 minutes with a moving window of 5 minutes, which roughly corresponds to the convective time scale. Figure 2 illustrates our methodology, with an example of the measurements and the derived diagnostics for the case of 26-27 July 2016.

- Fraction of the low cloud coverage: The low-cloud fraction (*CF*) is defined as the percentage of 1-min ceilometer CBHs lower than or equal to 1000 m a.g.l. Thus, *CF* greater or equal to 90% corresponds to the presence of LLSC. A similar methodology was used by Adler et al. (2019), but with a threshold of 600 m a.g.l. We extend the upper limit to 1000 m a.g.l to take into account of the rising of the LLSC base during the *convective phase* (Lohou et al., 2020). On 27 July 2016 (Fig. 2), the few periods between 04:00 UTC and 11:30 UTC with *CF* < 90% indicate intermittent break within the LLSC deck. This feature is common to many other cases.
- 5 - LLSC base height and homogeneity of the cloud layer: As seen in Fig. 2, the cloud “base height” may be more or less homogeneous in time and space, from a compact level cloud deck (like from 06:00 UTC to 06:30 UTC in Fig. 2) to a fragmented Secloud layer or even separated Acumulus clouds (like from 12:30 UTC to 13:00 UTC in Fig. 2). In the latter case, the ceilometer beam often hits Acumulus cloud base or higher edges introducing a large variability of the so-called and measured “CBH” (which is here more rigorously the first height above ground, with detected clouds). In order to take

this aspect into account in the definition of the LLSC base, and to quantify the LLSC base homogeneity, we define two other diagnostics based on the 1-min ceilometer-derived CBHs. The first one is a characteristic LLSC ~~cloud~~-base height, defined as the minimum of CBHs over the 10-min intervals (CBH^m). The second, is the standard deviation of CBHs (≤ 1000 m a.g.l.) minus CBH^m within the 10-min intervals (σ^*), which gives an insight on the LLSC layer heterogeneity by deleting the effect of CBH morning increase. ~~Small values of σ^* indicate nearly constant CBHs, that is horizontally homogenous base in the cloud layer (like from 04:00 UTC to 06:30 UTC on 27 July). High values of σ^* indicate irregular bases of the stratus layer or a mix of cloud base and edges after the stratus breakup (like from 12:30 UTC to 13:00 UTC on 27 July). (Lohou et al., 2020). Small values of σ^* indicate nearly constant CBHs, that is horizontally homogenous base of the cloud layer (like from 04:00 UTC to 07:00 UTC on 27 July). High values of σ^* indicate irregular bases of the LLSC layer or a mix of cloud base and edges after the LLSC breakup (like around 12:00 UTC on 27 July).~~ The increase of σ^* from 21 to 135 m after 11:00 UTC on 27 July (Fig. 2), typically indicates an evolution towards a more heterogeneous LLSC layer.

- Link between the LLSC and the surface: When a stratiform cloud is coupled to the surface, its base coincides rather well with the LCL (Wood, 2012; Zhu et al., 2001; Wood, 2012). So that, the coupling between the LLSC and the surface may be assessed by the distance between the ~~LCL and the~~ cloud base height and the LCL. We define LCL^M as the mean value of LCL calculated on 10-min time interval by the use of Roms (2017) formulation with near surface meteorological measurements. The coupling is estimated by $\Delta_{LCL}^{CBH} = CBH^m - LCL^M$. On 27 July 2016 (Fig. 2), Δ_{LCL}^{CBH} is initially around 190 m, from 04:00 to 06:00 UTC, indicating that the LLSC is decoupled from the surface. The progressive increase of the LCL starting around 06:00 UTC leads to the LLSC coupling of the LLSC with the surface slightly before 08:00 UTC.

Finally, the diagnostics LCL^M , Δ_{LCL}^{CBH} and σ^* defined before are smoothed with a moving average over 30 minutes every 5 min (Fig. 2).

- Characteristic times of the LLSC evolution: From the above diagnostics, two specific times characterizing the LLSC lifetime are determined.

- The surface-convection influence time (T_i) corresponding to the time from which the low-level cloud coverage reacts to solar heating at the surface. The method to determine T_i depends on the evolution of LLSC during the convective phase. Thus, it will be precisely defined later in the text, after the presentation of the different observed scenarios.

- The LLSC breakup time of the LLSC (T_b) which corresponds to the end of the LLSC occurrence. It is the time (after 06:30 UTC) from which CF is lower than 90% during at least one hour. [Figure 2](#) (lower panel) shows several periods, between 09:00 UTC and 11:00 UTC, with CF lower than 90%, but for less than one hour, so that they are included in the LLSC lifetime. For this case, T_b is at 12:05 UTC.

3.3 LWP budget

The equation of LWP tendency is based on the assumption of ~~an~~ horizontally-homogeneous stratocumulus, ~~and~~ vertically well-mixed, by the convective ~~turbulenee~~ turbulent mixing which is driven by the cloud-top radiative cooling. Following (van der Dussen et al., (2014, 2016; Wood, 2012). Following van der Dussen et al. (2014) the LWP tendency can be split into five relevant processes:

this equation can be split into five relevant processes:

$$\frac{\partial \text{LWP}}{\partial t} = \text{BASE} + \text{ENT} + \text{PREC} + \text{RAD} + \text{SUBS} \quad (1)$$

in which

$$\text{BASE} = \rho \eta (\overline{w'q_t^b} - \Pi \gamma \overline{w'\theta_1^b}) \quad (1.a)$$

$$\text{ENT} = \rho w_e (\eta \Delta q_t - \Pi \gamma \eta \Delta \theta_1 - \overline{Dh} \Gamma_{ql}) \quad (1.b)$$

$$\text{PREC} = \rho \Delta P \quad (1.c)$$

$$\text{RAD} = \rho \eta \gamma \Delta F_{\text{rad}} \quad (1.d)$$

$$\text{SUBS} = -\overline{\rho D} \rho h \Gamma_{ql} \overline{w_{s,H}} \overline{w_{s,CTH}} \quad (1.e)$$

representing the effects of turbulent moisture and heat fluxes at the cloud base (BASE), evaporation or condensation caused by entrainment of ambient air from aloft (ENT), precipitation formation (PREC), radiative cooling budget along the cloud layer (RAD) and large-scale subsidence (SUBS) at ~~the~~ heights cloud top.

In the above equations (1.a) to (1.e), ~~$\overline{w'q_t^b}$~~ $\overline{w'q_t^b}$ and $\overline{w'\theta_1^b}$ are respectively the total moisture specific humidity (q_t) and liquid-water potential temperature (θ_1) heat fluxes at the cloud base (superscript “b”), ρ is the mean air density over the cloud layer, ~~\overline{D} and \overline{h}~~ \overline{D} and \overline{h} is the cloud depth. ΔF_{rad} and ΔP are the differences, in net radiation and precipitation respectively, between the cloud top and base heights (van der Dussen et al., 2014). $\Delta \theta_1$ and Δq_t are the jumps of respectively θ_1 and q_t across the cloud ~~top~~ layer. w_e ~~is and~~ $w_{s,CTH}$ are the cloud top entrainment velocity and large scale subsidence velocities, respectively.

The equations also introduce the following parameters: the Exner function $\Pi = \left(\frac{P}{1000}\right)^{\frac{R_d}{C_p}}$; the adiabatic lapse rate of liquid water content $\Gamma_{ql} = g \eta \left(\frac{q_s}{R_d \bar{T}} - \frac{\gamma}{C_p}\right)$; $\gamma = \frac{L_v q_s}{R_v \bar{T}^2}$ and $\eta = \left(1 + \frac{L_v \gamma}{C_p}\right)^{-1}$. In those parameters, P and \bar{T} are respectively the pressure and temperature of the Secloud layer, q_s is the saturation water vapour specific humidity at P and \bar{T} . R_d and R_v are respectively the dry air and water vapour gas constant, L_v is the vaporization latent heat of water, C_p the specific heat of dry air at constant pressure, and g is the gravitational acceleration.

For our analysis of ~~a set of~~ DACCIIWA cases, we consider the LWP budget in early morning, and use the 05:00 UTC radiosounding, the ceilometer and the cloud radar measurements to estimate some ~~of the~~ terms of equation (1). In fact, this is the optimized time for the assumption of horizontally homogeneous cloud and vertically well-mixed LLSC layer. The term PREC is supposed to be close to zero because no significant rain was measured at surface for the selected cases. The BASE

term is not estimated because the turbulent fluxes at ~~the~~ the LLSC base cannot be deduced from the available data set at Savè supersite. According to Pedruzo-Bagazgoitia et al. (2020), ~~this~~ the term BASE is small at this time relatively to the radiation, entrainment and subsidence ~~three~~ terms RAD, ENT and SUBS. The latter are the most significant contributions in early morning that we attempt to estimate, ~~based on further hypotheses.~~

5 ~~For the estimate of RAD (Eq. 1.d), shortwave radiation is zero at that time, and ΔF_{rad} estimation is only based on the longwave radiation. Typically, the longwave radiative cooling is overall confined over about ten meters in the upper part of the well mixed stratocumulus layer. The term RAD (Eq. 1.d) is retrieved from the vertical profiles of upwelling and downwelling radiative fluxes which are computed by using the Santa Barbara DISORT Atmospheric Radiative Transfer (SBDART) model (Pedruzo-Bagazgoitia~~ Ricchiuzzi et al., 2020; Wood, 2012 ~~1998). This cooling occurs because the cloud top droplets emit more infrared radiation towards the free troposphere than they receive from the drier air above. In nighttime conditions, the longwave cooling at cloud top is thus related to the difference in temperature across the cloud top, and to the difference of emissivity between cloudy and dry air (resp. ϵ_c and ϵ_a) aloft. ϵ_a depends on the air temperature and moisture, whereas ϵ_c is strongly influenced by the cloud LWP. On this basis, we deduce ΔF_{rad} from the cloud top radiative cooling (RadF), approximated with use of the Stephan Boltzmann's law:~~

15 . This software tool, which solves the radiative transfer equation for a plane-parallel atmosphere in clear and cloudy conditions, was used in the studies of Babić et al. (2019a) and Adler et al. (2019) to estimate the temperature tendency due to radiative interactions during the LLSC diurnal cycle. For our simulations, the model configuration was very similar to that used in these studies. We prescribed 65 vertical input levels with a vertical resolution of 50 m below 2 km a.g.l, 200 m between 2 and 5 km a.g.l, and, 1 km above 5 km a.g.l. The vertical profiles of air pressure, temperature and water vapour density as well as the integrated water vapour are based on 05:00 UTC standard radiosounding data. The cloud optical thickness, which varies with its water and ice content, is required to describe a cloud layer in the SBDART model. Yet, the LWP provided by the microwave radiometer deployed at Savè supersite (Wieser et al., 2016) includes all the existing cloudy layers, and also is not available for five of our selected cases. Therefore, the LLSC optical thickness is determined from a parameterized LWP (Eq. 2), by assuming an adiabatic
25 cloudy layer in which the liquid water mixing ratio (q_l) increases linearly (van der Dussen et al., 2014; Pedruzo-Bagazgoitia et al., 2020). The downwelling longwave radiations from potential mid-level and high-level clouds may reduce the radiative cooling at the stratocumulus top (e.g. Christensen et al., 2013). However, the cloud layers above the LLSC (base, top and water content) cannot be precisely described in the SBDART model from the available data set. Thus, the higher clouds radiative effect is not directly included in our estimate of downwelling radiative fluxes,
30 but it is partially taken into account through vertical profiles of temperature and relative humidity given by the radiosonde. As the shortwave radiations are zero before the sunrise, only the longwave range, 4.5-42 μm with spectral resolution of 0.1 μm (Babić et al., 2019a), was selected for radiative fluxes calculations. For all the cases, the vertical optical depth of ABL aerosol is fixed to 0.38, which corresponds to the average value of the measurements performed with a sun photometer in June and July 2016 at Savè.

$$\rho C_p \Delta F_{\text{rad}} = \text{RadF} \approx \sigma (c_e (T^+ - \Pi \Delta \theta_1)^4 - c_a (T^+)^4) \text{LWP} = -\frac{1}{2} \rho \Gamma_{\text{ql}} h^2 \quad (2)$$

For the term ENT (Eq. 1.b), where $\sigma = 5.67 \times 10^{-8} \text{ W m}^{-2}$ is the Stephan Boltzmann's constant, T^+ is the state temperature of clear air just above the cloud top and $\Pi \Delta \theta_1$ represents the state temperature difference along the inversion layer. Note that RadF is positive for a cooling. This formulation assumes that the above ambient air absorbs completely the radiation from potential mid-level and high level cloud layers and irradiates at temperature T^+ . In the infrared band, the stratocumulus behaves nearly like an ideal blackbody. 1.b), we use the parameterization of (Liu, Stevens et al., 2018, (2005), therefore, we consider $c_e = 1$ in this study. While, c_a is retrieved by using the formulation of Prata (1996):

to estimate w_e :

$$c_a = 1 - (1 + c_1 \text{IWW}) * e^{-\sqrt{c_2 + c_3 \text{IWW}}} w_e = A * \frac{\Delta F_{\text{rad}}}{\Delta \theta_1} \quad (3)$$

with $c_1 = 0.1 \text{ m}^2 \text{ kg}^{-1}$, $c_2 = 1.2$, $c_3 = 0.3 \text{ m}^2 \text{ kg}^{-1}$ and IWW, the Integrated Water Vapour above the cloud layer. IWW is calculated by using the sounding measurements with CTH as lower limit of the atmosphere.

in which A is a non-dimensional quantity representing the efficiency of the warming caused by the input of warmer free tropospheric air into the stratocumulus cloud layer by the buoyancy-driven eddies generated by cloud-top radiative cooling. **A varies with $\Delta \theta_1$, Δq_1 , wind shear at the cloud top, surface turbulent fluxes and cloud microphysical processes via the buoyancy flux vertical profile** For the term ENT (Eq. 1.b), we use the parameterization of (Stevens et al., 2005; Stevens, 2006) to estimate the entrainment rate (w_e):

$$w_e = A * \frac{\Delta F_{\text{rad}}}{\Delta \theta_1} \quad (4)$$

in which A is a non dimensional quantity representing the efficiency of the warming caused by the input of warmer ambient air from aloft into the cloud layer by the convective eddies generated by cloud top radiative cooling. A depends on Δq_1 , wind shear through the inversion, surface turbulent fluxes and cloud microphysical processes via the buoyancy flux vertical profile. **Despite the spatial and temporal variability of A , its value is generally fixed and treated as a constant parameter in several research studies (e.g. van Zanten et al., 1999; (van der Dussen et al., 2014; Stevens et al., 2005)).** The used value of A found in the literature varies from one study to another. By considering the results of the LES made by Pedruzo-Bagazgoitia et al. (2020). Nevertheless, its value is generally fixed and treated as a constant parameter in several research studies (e.g. van der Dussen et al., 2014; vanZanten et al., 1999 on a DACCIWA case, just before sunrise, with $w_e \approx 4.5 \text{ mm. s}^{-1}$, $\Delta \theta_1 \approx 4 \text{ K}$, a cloud-top longwave radiative cooling of around 43 W m^{-2} , and, $\rho \approx 1.13 \text{ kg.m}^{-3}$ as the average value from the surface to 1000 m a.g.l (from 26 June 05:00 UTC sounding), we obtain $A \approx 0.5$. This means that the contribution of entrainment driven by convective turbulence to the heat budget at the cloud top is around two times smaller than that driven by the cloud-top radiative cooling. For simplicity and due to a lack of precise estimate, we assume here the same behaviour for all the DACCIWA cases, and consider $A = 0.5$ in our analysis.

The used value of A found in the literature varies from one study to another. By considering the results of the LES made by Pedruzo Bagazgoitia et al. (2020) on a DACCIWA case, just before sunrise, with $w_e \approx 4.5 \text{ mm. s}^{-1}$, $\Delta \theta_1 \approx 4 \text{ K}$ and

RadF $\approx 43 \text{ W} \cdot \text{m}^{-2}$, and considering $\rho \approx 1.13 \text{ kg} \cdot \text{m}^{-3}$ as the average value from the surface to 1000 m above (from 26 June 05:00 UTC sounding), we obtain $A \approx 0.5$. This means that the contribution of entrainment driven by convective turbulence in the heat budget at the cloud top is around 2 times smaller than that driven by the cloud top radiative cooling. For simplicity, and in lack of more precised estimates, we assume here the same behaviour for all the DACCIWA cases, and consider $A = 0.5$ in our analysis.

The jumps in temperature $\Delta\theta_1$ and in total water content Δq_t are estimated ~~based on~~ from the ~~radiosoundings~~ soundings. We write $\theta_1 = \theta - \frac{1}{\pi} \left(\frac{L_v}{c_p} \right) q_1$, with θ as the potential temperature, whereas $q_t = q + q_1$. We define:

$$\Delta\varphi \approx \varphi^+ - \varphi^- \quad (5)(4)$$

where φ can be either θ_1 or q_t . φ^+ and φ^- are in theory the values of the variable φ just above and just below the cloud top respectively. Under the assumption of a well-mixed cloud layer, θ_1 (q_t) is conserved ~~from the surface up to~~ through the cloud ~~top layer~~ and increases (decreases) abruptly in the warmer (drier) ambient air right above (vanZanten et al., 1999). Thus, $\Delta\theta_1$ and Δq_t can be estimated from the vertical profiles of θ and q derived ~~from~~ to the ~~morning~~ 05:00 UTC standard sounding ~~measurements~~. For θ_1^+ and q_t^+ , we consider the mean over the ~~50~~ 100 m above CTH. For θ_1^- and q_t^- , we consider the ~~mean over the 50 m sounding level just below~~ the CBH. ~~This is based on the conservation of those variables through the cloud, and the fact that we have no measurement of liquid water content with the radiosoundings.~~ In ~~summary~~ brief, we use

$$\begin{aligned} \varphi_t^- &= \varphi_{t \{ \text{below cloud top} \}} = \varphi_{t \{ \text{below cloud base} \}} = \varphi_{t \{ \text{below cloud base} \}} \quad \text{and} \quad \theta_1^- = \theta_{1 \{ \text{below cloud top} \}} = \theta_{1 \{ \text{below cloud base} \}} = \\ & \theta_{1 \{ \text{below cloud base} \}}; \\ \left\{ \begin{aligned} q_t^- &= q_{t \{ \text{below cloud top} \}} = q_{t \{ \text{below cloud base} \}} = q_{t \{ \text{below cloud base} \}} \\ \theta_1^- &= \theta_{1 \{ \text{below cloud top} \}} = \theta_{1 \{ \text{below cloud base} \}} = \theta_{1 \{ \text{below cloud base} \}} \end{aligned} \right. \quad (5) \end{aligned}$$

For the term SUBS (Eq. 1.e), we have ~~no possibility of estimating precisely the large scale subsidence at the cloud~~ LLSC top. But in order One possibility is ~~to have an approximation~~ consider evaluations from models or re-analyses. However, we decided to discard this approach, because the subsidence profiles from regional simulations with Consortium for Small-Scale Modelling (COSMO) or from ERA-interim and ERA-5 reanalyses showed a very high temporal variability and a strong lack of its magnitude ~~coherence among the different cases. According to the cloud-radar CTH estimates, the LLSC top is often stationary at the end of the stratus phase, we may consider that the cloud top is stationary, like in~~ phases during DACCIWA. This feature has been observed ~~Pedruzo-Bagazgoitia et al. (2020)~~ (Adler et al., 2019; Babić et al., 2019a; Dione et al., 2019). ~~According to the cloud radar CTH estimates, this hypothesis is often met during DACCIWA cases at this time of the day, as also observed by previous analyses of the DACCIWA dataset~~ but also simulated by ~~(Adler et al., 2019; Babić et al., 2019a; Dione et al., 2019)~~ Pedruzo-Bagazgoitia et al. (2020). ~~But the availability of CTH estimates is not large enough to assess the cloud top evolution for all cases. Based on the LLSC top stationarity of the cloud top at the time of our LWP budget analysis, the term~~ SUBS $w_{s,CTH}$ is estimated with the assumption that $\frac{\partial h}{\partial t} = w_{s,h} + w_e \approx 0$ following ~~(Lilly,~~ (1968):

$$\frac{\partial CTH}{\partial t} = w_{s,CTH} + w_e \approx 0 \quad (6)$$

4 LLSC during the stratus phase

In this section, we ~~start by documenting/document~~ the *stratus* phase, ~~especially its end of the LLSC diurnal cycle~~. The aim is to ~~analyse/analyze~~ the way the ~~LLSC/cloud layer~~ is coupled to the surface ~~processes~~, and ~~if that implies different/the possible impacts the coupling has on the~~ cloud characteristics (macrophysical properties and LWP terms) ~~just before the convective phase~~. During the DACCIWA ~~field~~ campaign ~~field~~, the sunrise occurred at Savè between 05:33 and 05:42 UTC (Kalthoff et al., 2018). According to Lohou et al. (2020), the ~~final-convective phase~~ starts between 07:30 and 09:00 UTC. ~~Moreover~~, the last radiosonde ~~launched/released~~ before the *convective phase* is performed at 06:30 UTC, consequently, the analysis in this section concerns the period from the ~~LLSC formation~~ (beginning of the *stratus phase*) to 06:30 UTC on day-D+1.

4.1 Coupled and decoupled LLSC

~~We first consider the start of the stratus phase and define the CBH of the LLSC by the median value of 1-min CBHs over the firsts 15 minutes. When the LLSC forms, its base is located around the NLLJ core height, where the cooling driven by the horizontal advection is optimal (Adler et al., 2019; Dione et al., 2019; Lohou et al., 2020). This is visible in Fig. We first analyze the evolution of LLSC base height (CBH) and its link with the NLLJ core height and surface-based LCL along the stratus phase (Fig. 3). The CBH and LCL at the beginning of the stratus phase (Fig. 3a, which shows CBH as a function of the 15-min NLLJ heights median value over one hour centered on and b) are given by the diagnostic parameters CBH^m and LCL^M respectively when the stratus phase start. The averaged-LLSC base ranges from 50 to 500 m a.g.l, similarly to forms, and the averaged-NLLJ core height is the hourly-averaged value at that time. For the end of the stratus phase (Fig. 3b shows that meanwhile, c and except for one case among the 22 selected cases, d), CBH, LCL and NLLJ are averaged between 04:00 and 06:30 UTC on day-D+1.~~

~~When the LLSC forms, its base is located within the NLLJ core, where the cooling driven by the horizontal advection is maximum (Adler et al., 2019; Dione et al., 2019; Lohou et al., 2020). Both the CBH and NLLJ core height range between 50 and 500 m a.g.l (Fig. 3a) and are a hundred meters above the mean-surface-based LCL over the corresponding time interval, except for one case (Fig. 3b). This means that the LLSC is decoupled from the surface when it forms.~~

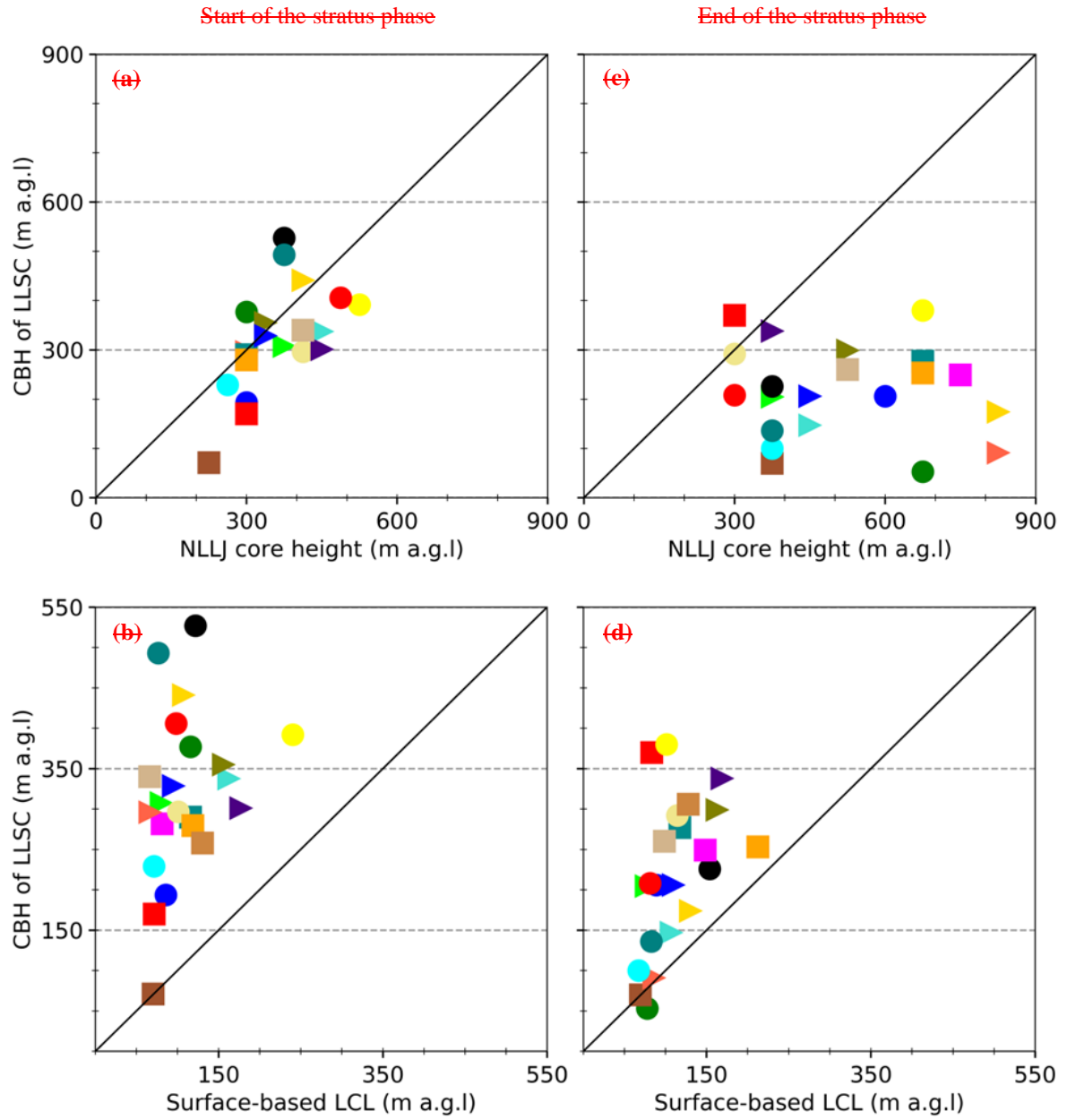


Figure 3 : CBH of LLSC against the NLLJ core height (top panels), the surface-based LCL (bottom panels), at the start (a, b) and at the end of stratus phase (c, d). Each of the 22 selected cases is represented by a different marker. (See the text for precise definition)

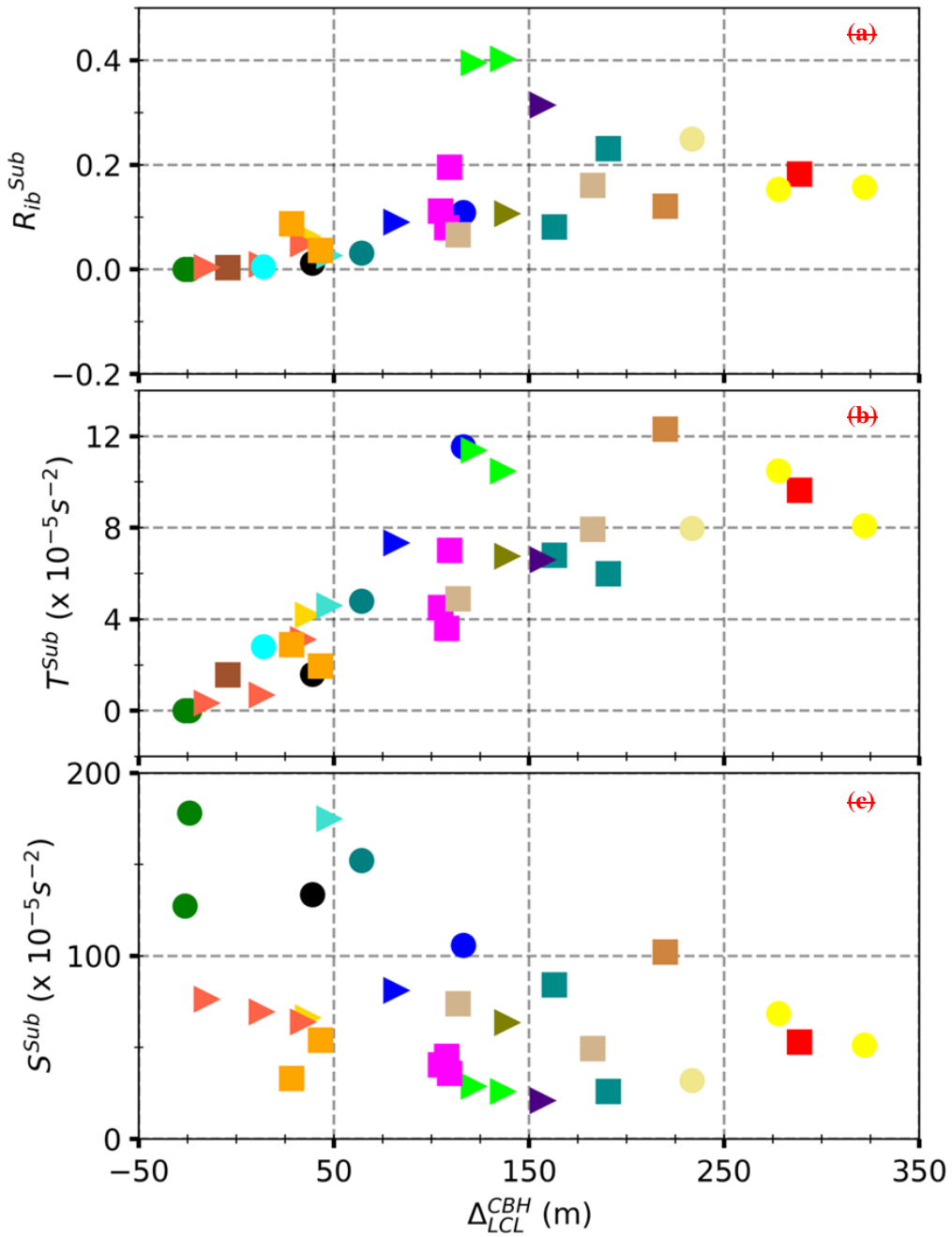


Figure 4: (a) R_{ib}^{Sub} , (b) T^{Sub} and (c) S^{Sub} as a function of Δ_{LCL}^{CBH} , performed by using all radiosoundings available from 04:00 to 06:30 UTC on each studied case. Each marker corresponds to one case.

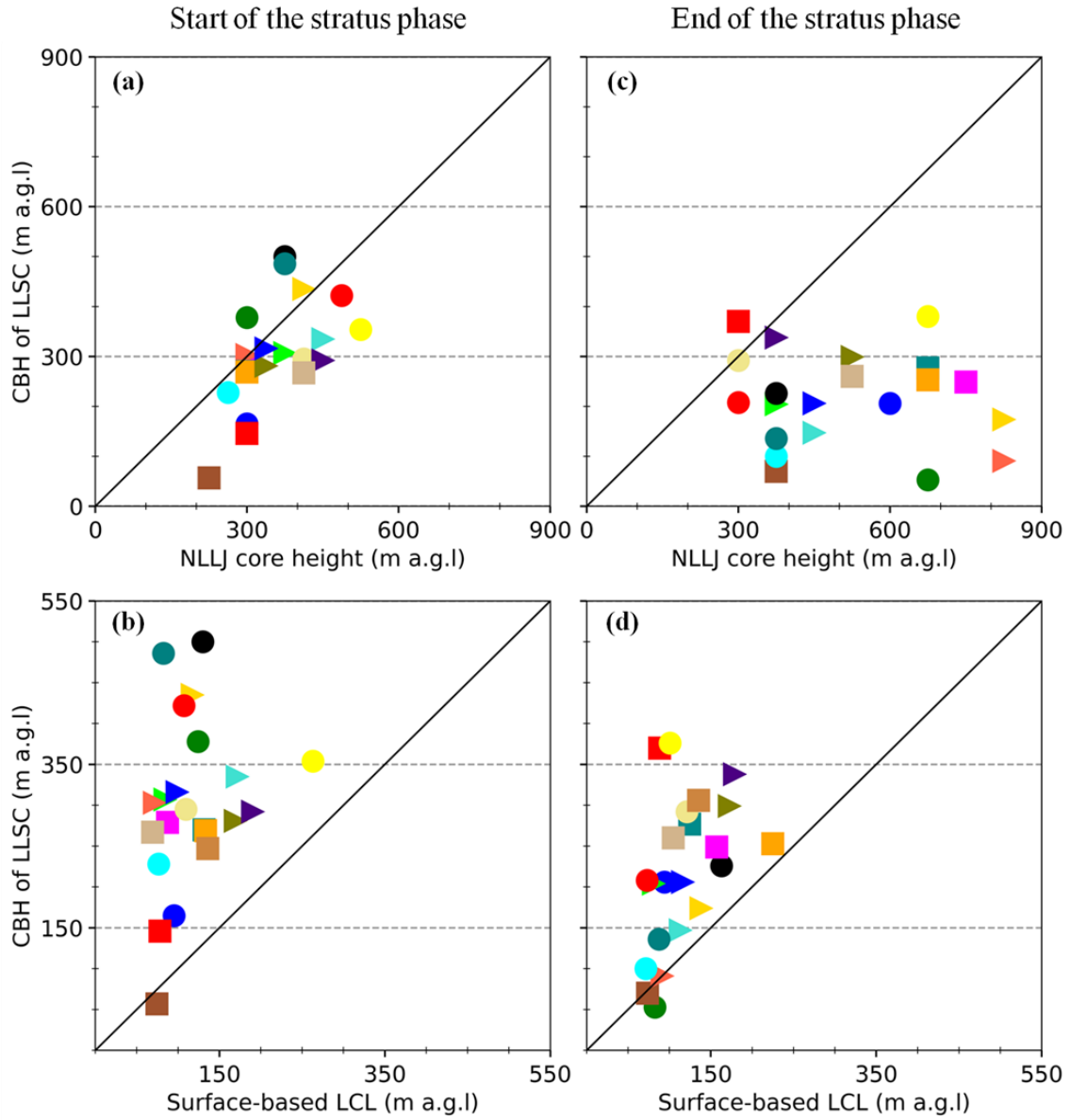


Figure 3 : LLSC base height (CBH) against the nocturnal low-level jet (NLLJ) core height (top panels), the surface-based lifting condensation level (LCL) (bottom panels), at the start (a, b) and at the end of stratus phase (c, d). Each of the twenty-two selected cases is represented by a different marker.

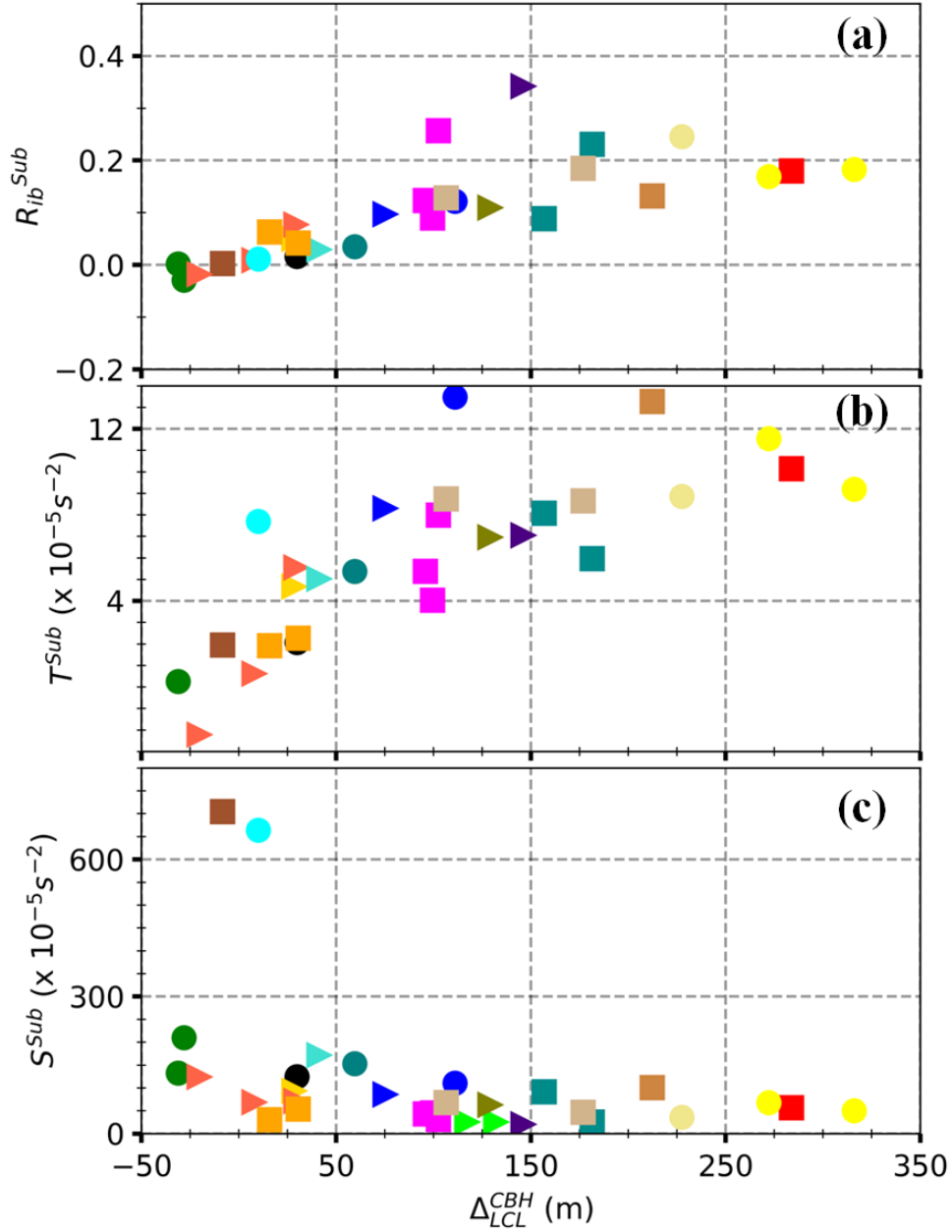


Figure 4: Bulk Richardson number (R_{ib}^{Sub} , a), and its thermal (T^{Sub} , b) and vertical wind-shear (S^{Sub} , c) composing terms, as a function of the diagnostic parameter Δ_{LCL}^{CBH} , which corresponds to the mean distance between the LLSC base height (CBH) and surface-based lifting condensation level (LCL), performed by using all radiosoundings available from 04:00 to 06:30 UTC on day-D+1 for each studied case. Each marker corresponds to one case.

At the end of the *stratus phase*, ~~and, CBH of LLSC and surface-based LCL are the medians of respectively CBH^m and LCL^m between 04:00 and 06:30 UTC, the same for the NLLJ core height.~~ one can see that the relationship between CBH and the NLLJ core height has totally changed (Fig. 3c). There is no clear linear link between both, and CBH remains mostly lower than or equal to 300 m a.g.l, while the NLLJ core height is above 600 m a.g.l in average several cases. This is most likely because, during the *stratus phase*, the jet axis is shifted upward by the convective turbulence within the LLSC layer (Adler et al., 2019; Dione et al., 2019; Lohou et al., 2020). ~~For most of~~ In addition to the ease jet axis rising, the averaged CBH ~~has decreased~~ decreases by the end of the *stratus phase* (Fig. 3b and d). ~~In some cases, CBH coincides pretty well with LCL (Fig. 3a and c) for most of the cases. In some cases, CBH coincides pretty well with LCL (Fig. 3d), indicating which indicates~~ a coupling ~~between of~~ the LLSC ~~and with~~ the surface, at the end of the *stratus phase*. But, in others, CBH is still at least 100 m higher than LCL, meaning that the LLSC remains decoupled from the surface.

~~This different nature of~~ We further analyze the coupling between the ~~cloud~~LLSC and the surface ~~is further analyzed by the~~ end of the *stratus phase* by using the bulk Richardson number (Stull, 1988) of the subcloud layer (R_{ib}^{Sub}). It reads:

$$R_{ib}^{Sub} = \frac{T^{Sub}}{S^{Sub}} \text{ with } T^{Sub} = \frac{g}{\theta} * \frac{\partial\theta}{\partial z} \frac{\Delta\theta}{CBH} \text{ and } S^{Sub} = \frac{(\partial U / \partial z)^2}{(CBH)} \left(\frac{\Delta U}{CBH} \right)^2. \quad (6)(7)$$

T^{Sub} and S^{Sub} are respectively the thermal and ~~vertical~~horizontal wind shear contributions to the Richardson number. $\frac{\partial\theta}{\partial z} \frac{\Delta\theta}{CBH}$ and $\frac{\partial U}{\partial z} \frac{\Delta U}{CBH}$ are the bulk vertical gradient of θ and horizontal wind speed (U) respectively, within the subcloud layer (between the cloud base and the surface), with the assumption that U is null at the surface. R_{ib}^{Sub} is estimated with all radiosoundings available from 04:00 to 06:30 UTC on day-D+1, for each studied case. ~~For this, the~~ The subcloud layer height is estimated with the half-hourly median of CBH^m ~~over the 30 minutes centered on~~ at the radiosounding ~~radiosonde released~~ time is used (in Eq. 67).

Figure 4 shows R_{ib}^{Sub} (Fig. 4a), T^{Sub} (Fig. 4b) and S^{Sub} (Fig. 4c) as a function of the half-hourly median value of Δ_{LCL}^{CBH} (the median over 30 minutes centered on ~~at the radiosounding~~ radiosonde released ~~time for this plot).~~ Smaller. The smaller Δ_{LCL}^{CBH} are associated with, the lower R_{ib}^{Sub} . Interestingly, for when Δ_{LCL}^{CBH} is smaller than or equal to 75 m, R_{ib}^{Sub} are about of is less than or equal to 0.1, and vice versa (Fig. 4a). This ~~supposes~~ evidence suggests that, the potential early morning coupling between the LLSC and the surface during the *stratus phase* is driven by the underlying ~~shear driven~~ turbulent mixing. A similar tendency was found by Adler et al. (2019) ~~when analyzing who analyzed~~ the soundings performed along the *stratus phase* of 11 eleven IOPs, ~~and explained by the role of shear related processes in the formation of the LLSC when the LCL is close to the CBH, that is when the surface is coupled to the cloud.~~

~~However, while T^{Sub} has a quite similar relationship than~~ As R_{ib}^{Sub} , the term T^{Sub} increases with Δ_{LCL}^{CBH} , it is not ~~whereas~~ the ease for term S^{Sub} . ~~For~~ is nearly constant. This means that, when the CBH is close to the LCL, although the subcloud layer is well mixed, although the shear-driven turbulence ~~in the subcloud layer~~ is not necessarily larger particularly significant. Thus, the ~~nature of~~ coupling between the LLSC and the surface at the end of the *stratus phase* seems to be mostly linked to the

thermal stratification in the subcloud layer, rather than to the shear. ~~This outlines the relative importance of the cloud-top cooling in the production of turbulent mixing in the subcloud layer which couples the LLSC to the surface-driven turbulence.~~

5 Finally, based on ~~the~~ Fig. 4 (a and b), the value of 75 m is used thereafter as a threshold for Δ_{LCL}^{CBH} to distinguish the ~~coupling nature coupled and decoupled LLSC~~ at the end of the *stratus phase*. Through this classification, our set of ~~22~~twenty-two studied cases includes ~~9 cases in which the~~nine LLSC ~~layer is~~ coupled to the surface (case C) and ~~the~~thirteen LLSC decoupled from the surface (case D) ~~for the 13 others cases~~ (Table A-1). Among the ~~eases C, 3 are~~nine selected IOPs, three (N° 5, 6 and 8) ~~and six (N° 3, 4, 7, 9, 11 and 14) are cases C and D respectively.~~

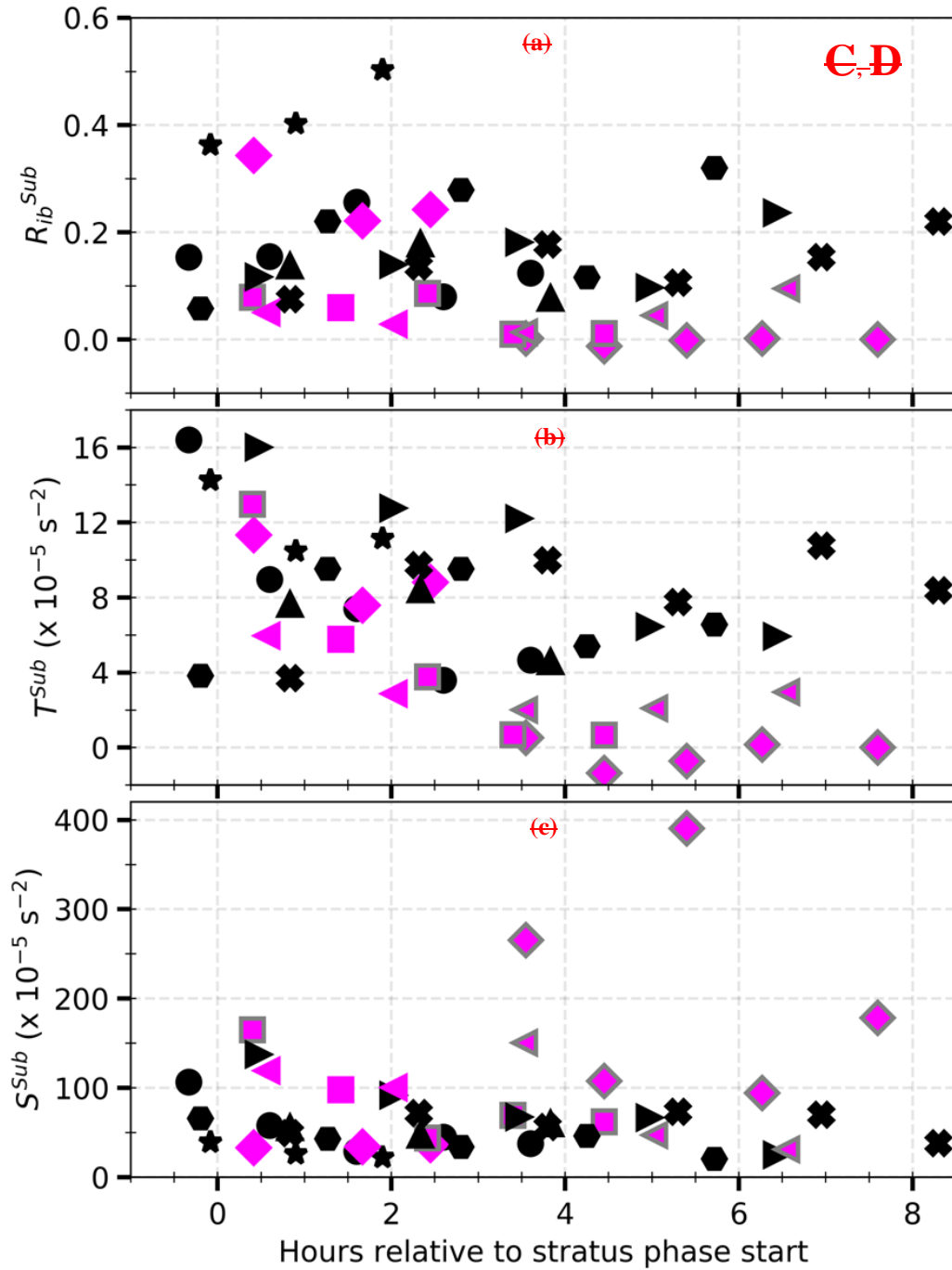


Figure 5: (a) R_{ib}^{Sub} , (b) T^{Sub} and (c) S^{Sub} , performed by using all the soundings available during the stratus phase on the 9 IOPs (Table A-1). The quantities are presented against the sounding time which is expressed in hours relative to the start of the stratus phase. Each IOP is represented by a marker. C and D stand for the coupled and decoupled cases respectively. The grey edge indicates that $\Delta LCL^{CBH} \leq 75 \text{ m}$ at the sounding time.

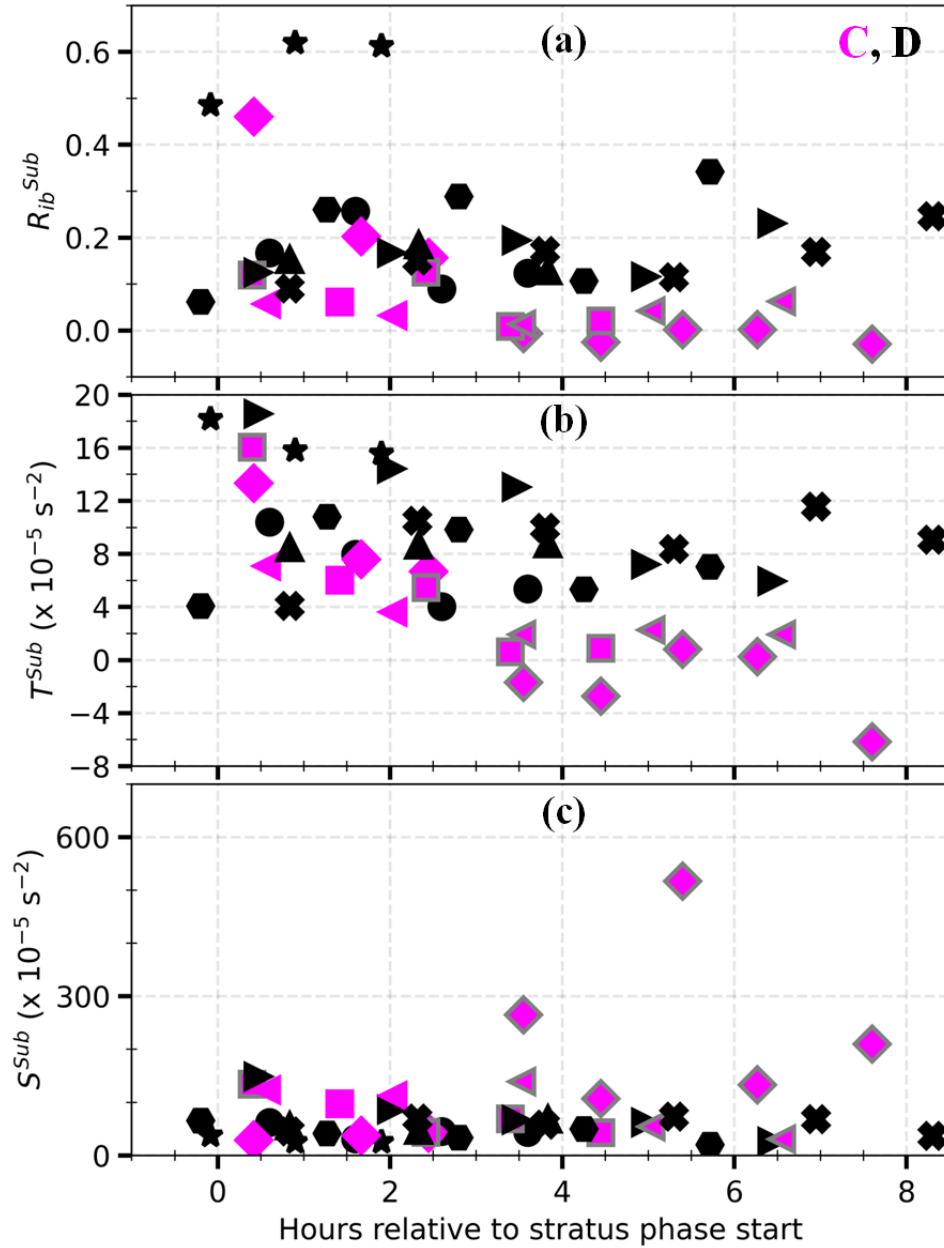


Figure 5 : Evolutions of the bulk Richardson number (R_{ib}^{Sub} , **a**) and its thermal (T^{Sub} , **b**) and vertical wind-shear (S^{Sub} , **c**) composing terms during the stratus phase, based on all the soundings available until 06:00 UTC on day-D+1 during the nine selected IOPs (Table A-1). The quantities are presented against the radiosonde released time which is expressed in hours relative to the start of the stratus phase. Each IOP is represented by a marker. C and D stand for the coupled and decoupled LLSC at the end of the stratus phase respectively. The grey edge indicates that the mean distance between the LLSC base height and the surface-based lifting condensation level (LCL) (Δ_{LCL}^{CBH}) is of less than 75 m at the sounding time, meaning that the cloud is coupled to the surface.

We have seen before that, for almost all the cases, the LLSC is decoupled from the surface at the start of the stratus phase. The lowering of the LLSC base was first pointed out by Babić et al. (2019a) for the 07-08 July study case. We now try to understand why the LLSC may couple to the surface by the end of the stratus phase only in some cases.

Based on the re-usable radiosoundings available for the nine selected IOPs, the temporal evolution of R_{ib}^{Sub} and its composing terms have been calculated from the start of the *stratus phase* up to 06:30 UTC on day-D+1 (Figure 5). R_{ib}^{Sub} , T^{Sub} and S^{Sub} in cases C and D are similar when the stratus phase begins LLSC forms. For cases C, T^{Sub} decreases down to zero (neutral stratification) within the three following hours while S^{Sub} remains almost constant, which causes a decrease of R_{ib}^{Sub} (Fig. 5a and b). A few cases D show a slightly similar pattern, but only for a much shorter time. In the cases C presented in Fig. 5, the steady definitive coupling with the surface occurs within 2-4 the four hours after the beginning of the *stratus phase*. The same behaviour is observed for the cases C which are not IOP and therefore not included in Fig. 5 (not shown). Furthermore, for two out of three For cases C in Fig. 5, one can note an increase of S^{Sub} but only after D, the coupling-subcloud layer remains thermally stable along the stratus phase and the shear-driven turbulence is of the same order than for cases C. Considering these results, it appears that the shear-driven turbulence below in the LLSC base, either dynamic or thermal, may subcloud layer is not be the main driver of process which causes the LLSC coupling with the surface during the stratus phase in the cases C.

In conclusion, the LLSC forms typically decoupled from the surface. Subsequently, its base lowers during the first hours of the stratus phase. The numerical experiments performed by In the cases C, this decrease is more important and leads to the coupling between the cloud and the surface before the sunrise. The lowering of the LLSC base was first pointed out by Dearden Babić et al. (2018 2019a), based on the LLSC occurrence of 04-05 July at Savè supersite (case D, IOP 7), showed that the lowering of the LLSC may be due to cloud droplets sedimentation. Furthermore, the occurrence of the cases C and D over the DACCIWA field campaign (for the 07-08 July case. They explained this feature by an additional cooling in the subcloud layer mainly due to a shear-driven turbulent mixing caused by the NLLJ. Yet, no substantial differences in wind shear below the LLSC are observed between the cases C and D, indicating that the processes related to the mechanical turbulence underneath the LLSC cannot fully explain the coupling observed by the end of the stratus phase. The other relevant processes which may couple the LLSC to the surface in night-time conditions are discussed in section 4.3) suggests that the coupling between the LLSC and the surface is sensitive to the synoptic scale atmospheric circulation within the low-troposphere. Indeed, all the cases C, except one, occurred between the 26 June and 8 July 2016, the first days of the post-onset phase characterized by a well established and undisturbed monsoon flow over studied area (Knippertz et al., 2017).

The turbulent mixing below the LLSC is not the principal driver of the coupling between the cloud and the surface. But this turbulence has a crucial role for the maintenance of this coupling during the remaining time of the stratus phase, as indicated by the reduction of thermal stability in the subcloud layer (Fig. 5b). Indeed, the contributions of shear driven turbulence below the NLLJ and turbulence due to the cooling at the cloud top are important for mixing potential temperature in the subcloud layer (Dione et al., 2019; Lohou et al., 2020). In the LES experiment under windless conditions carried out

by Pedruzo-Bagazgoitia et al. (2020), the radiative cooling at cloud top was the unique source of turbulence in the ABL until sunrise, and the coupling between the cloud and the surface was maintained.

. In the next paragraph, we analyze the LLSC macrophysical characteristics in the C and D cases at the end of the *stratus phase*, i.e. just before the *convective phase*.

5 ~~In conclusion, the LLSC forms typically decoupled from the surface. Subsequently, its base lowers during the first hours of the *stratus phase*. In the cases C (9 cases out of 22), this decrease is more important, leading to the coupling between the cloud and the surface before the sunrise. In the following, we analyze the LLSC characteristics in the C and D cases at the end of the *stratus phase*.~~

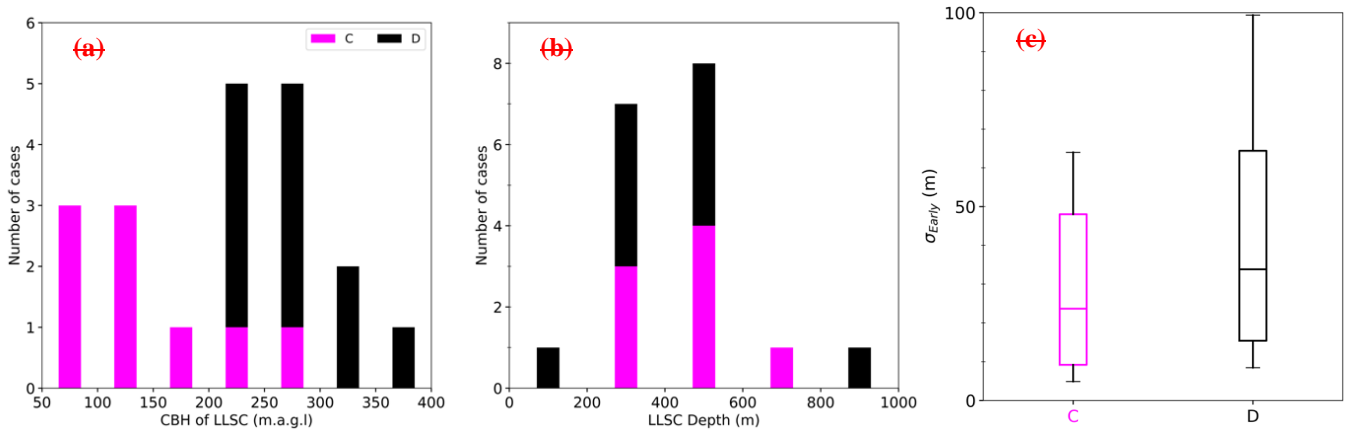


Figure 6 : Statistic on the LLSC macrophysical characteristics at the end of the stratus phase, performed on the 20 cases (the 9 C and 11 D out of 13), for which the LLSC is present ($CF \geq 90\%$) over at least 70% of the time. (a) Distribution of LLSC CBH, the same than on Figure 3. (b) Distribution of the LLSC depth calculated by using the median value of CTHs between 04:00 and 06:30 UTC as the LLSC summit. The depth was not estimated for 2 cases (1 C and 1 D) among the 20 due to CTHs missing data. (c) Statistical information on σ_{Early}^* , which is the median value of σ^* between 04:00 and 06:30 UTC. The edges of each box represent the 25th (bottom) and 75th (top) percentiles and the whiskers the minimum, the median and maximum values from the bottom to the top respectively. C and D stand for the coupled and decoupled cases respectively.

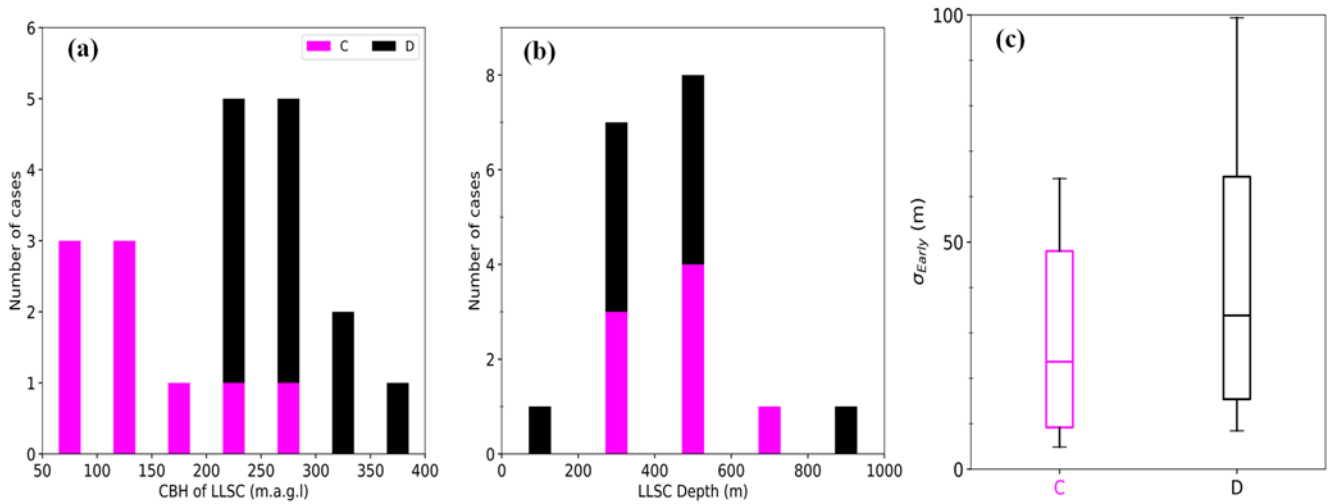


Figure 6 : Statistic on the LLSC macrophysical characteristics at the end of the stratus phase, performed on the twenty cases (the nine cases C and eleven cases D out of thirteen), for which the LLSC is present ($CF \geq 90\%$) over at least 70% of the time between 04:00 and 06:30 UTC on day-D+1. Distributions of, LLSC base height (CBH, a), the same than on Figure 3, and depth (b), calculated by using the median value between 04:00 and 06:30 UTC of cloud-radar estimated CTHs as the LLSC summit. The depth was not estimated for two cases (one C and one D) among the twenty due to CTHs missing data. Statistical information on σ_{Early}^* (c), which is the median value between 04:00 and 06:30 UTC of the diagnostic parameter σ^* , measuring the homogeneity at the LLSC base. The edges of the boxes represent the 25th, the median and 75th percentiles, and the whiskers, the minimum and the maximum values. C and D stand for the coupled and decoupled LLSC respectively.

The distributions of averaged LLSC base height, CBH, and depth at the end of the *stratus phase* are ~~shown on~~ summarized in Fig. 6a and b respectively. Only the ~~20~~ twenty cases for which the cloud is persistent ($CF \geq 90\%$) ~~over at least 70% of the time between 04:00 and 06:30 UTC on day-D+1~~ are considered (including ~~9~~ nine cases C and ~~4~~ eleven cases D). Note that, the depth could not be estimated for ~~2~~ two of these cases because of CTH missing data. The CBH ranges within 50-200 m a.g.l for cases C, and within 200-400 m a.g.l for cases D. This clear difference between coupled and decoupled LLSC explains the bimodal distribution of morning CBH ~~found~~ observed by Kalthoff et al. (2018). ~~It is explained by the fact that the base of the cloud descends during the stratus phase in cases C.~~ In contrast, the morning LLSC depth does not depend on the state of ~~the~~ coupling with the surface.

Figure 6c presents helps to study the LLSC base homogeneity at the end of the *stratus phase* by presenting the statistical information of σ_{Early} , which is the median value of the diagnostic parameter σ^* between 04:00 and 06:30 UTC on day-D+1 for ~~the each~~ considered ~~cases~~ case. The median of σ_{Early} is 24 m for cases C and 34 m for the cases D. Their 25th percentiles and minimums are close, but, the 75th percentile for cases D is more than ~~40~~ 15 meters higher than that of cases C, and the maximum is significantly larger, close to 100 m. This reveals the larger LLSC base heterogeneity found for several cases D. Likely, the coupling with the surface limits the fragmentation of the LLSC layer, and helps maintaining the homogeneity of the cloud in cases C.

In brief, the mechanism of coupling favours lower CBH and slightly more homogeneous cloud base in the cases C. But the LLSC depth is similar in cases C and D, so that the LLSC vertical extension ~~is~~ does not seem to be influenced by the coupling with the surface. This may be related to the negligible contribution of surface fluxes during the night.

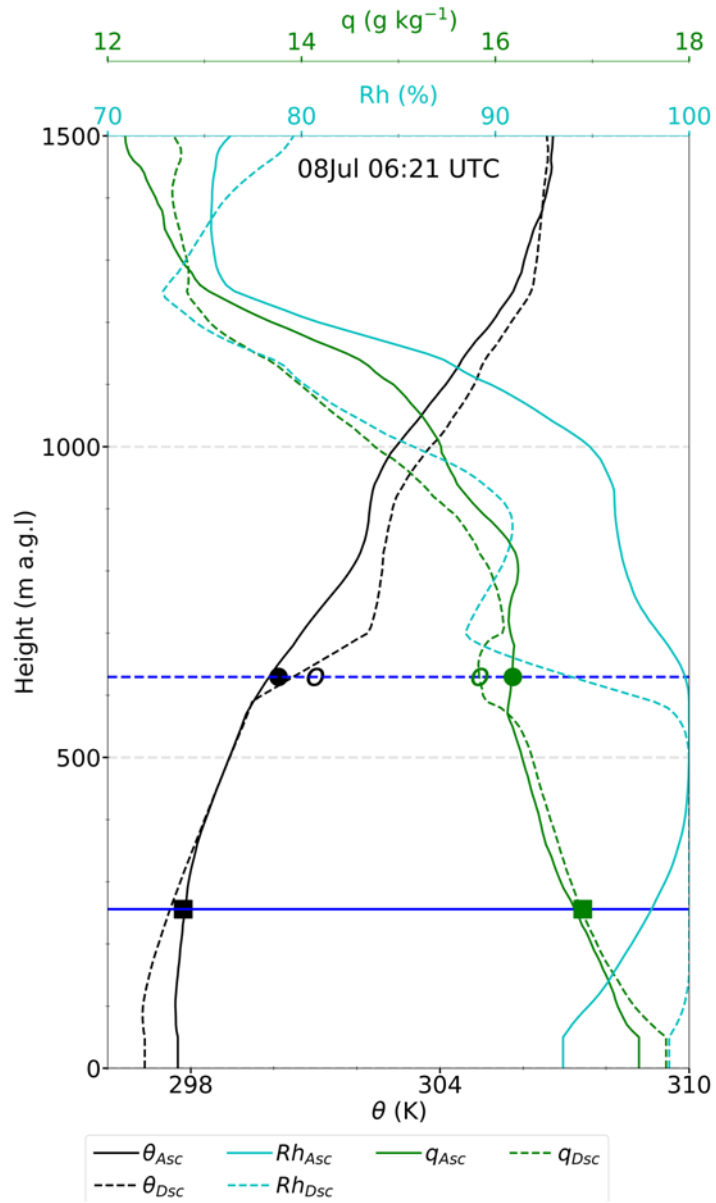


Figure 7: Vertical profiles of the low troposphere acquired by the re-usable radiosonde of 08 July 2016 at 06:21 UTC, when the probe ascends ('Asc', filled line) and descends ('Dsc', dashed line). The variables shown are the relative humidity (Rh), the potential temperature (θ) and the water vapour specific humidity (q). The horizontal blue lines mark the CBH (filled line) from the ceilometer, and the CTH (dashed line) from the cloud radar. The values of ϕ^+ (ϕ^-) (section 3.1) for θ and q are marked with dot (square). The filled symbols correspond to the ascent, whereas the unfilled symbols correspond to the descent.

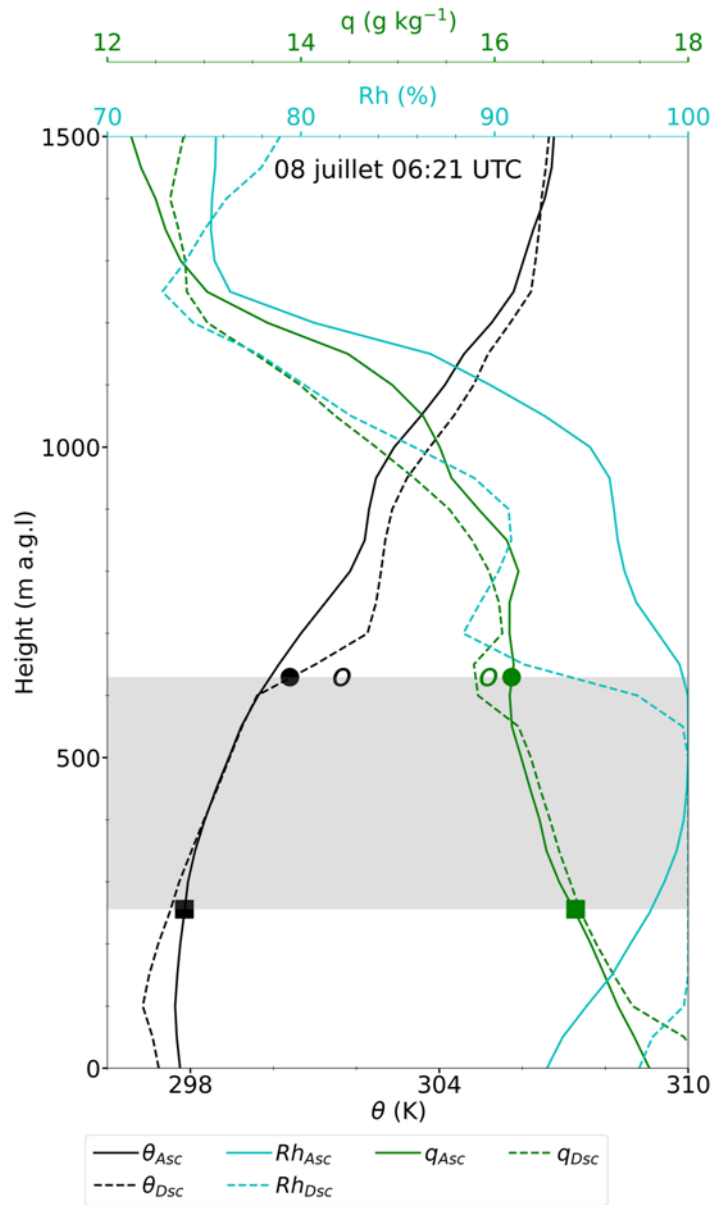


Figure 7 : Vertical profiles of the low-troposphere acquired by the re-usable radiosonde of 08 July 2016 at 06:21 UTC, when the probe ascends ('Asc', filled line) and descends ('Dsc', dashed line). The variables shown are the relative humidity (Rh), the potential temperature (θ) and the water vapour specific humidity (q). The shaded grey delimits the LLSC layer, based on the ceilometer and cloud-radar measurements. The values of φ^+ (φ^-) (Eq. 4) for θ and q are marked with dot (square). The filled symbols correspond to the ascent, whereas the unfilled symbols correspond to the descent.

4.2 LWP terms

In order to deepen the analysis, we make an attempt to estimate the LWP terms at the end of the *stratus phase*, ~~i.e. just before the convective phase.~~ Several questions motivate this attempt:

1) Do we find similar results with observations ~~as~~ and with previous numerical simulations, particularly that of Pedruzo-Bagazgoitia et al. (2020)?

2) Does the LWP budget analysis help us to ~~depart~~ differentiate the cases C and D?

As ~~seen~~ previously seen, the most important contributions in the LWP budget are that of radiation, entrainment and subsidence. Based on the available observations and by using the SBDART model, we estimate ENT and RAD (Eq. 1.b and ENT,d respectively), and also give a rough ~~order of~~ magnitude order of SUBS. ~~We first discuss the jumps Δq_t and $\Delta \theta_1$ across (Eq. 1.e). The LLSC layer here is defined by the cloud top, which are involved in ENT and RAD terms. They are estimated by use of averaged CBH and CTH at the radiosoundings, although end of the crossing of the wet cloud makes it delicate.~~ stratus phase (Fig. 6a and b).

~~Indeed, the crossing of the cloud wets the probe, such that the measurements get possibly erroneous.~~ We first discuss the jumps Δq_t and $\Delta \theta_1$ across the cloud top (Eq. 4 and 5), which are involved in ENT and RAD terms. They are estimated by the use of the 05:00 UTC (day-D+1) standard radiosoundings. **The liquid water buildup on the probe sensors possibly renders some measurements suspect, especially at the exit of the cloud.** In order to evaluate the impact of this issue on

our jump estimations from the 05:00 UTC standard radiosonde, we first consider a re-usable sounding at a different time, for which the probe has crossed the ~~cloud~~ LLSC layer both at ascent and descent. At ascent, the sensor is reliable at cloud base, but may get wrong data when it reaches cloud top. At descent, it is the reverse: correct at cloud top but possibly erroneous measurements when it reaches cloud base. This is shown in Fig. 7, which displays the vertical profiles of θ , q and relative humidity (Rh) measured by the re-usable sounding of 08 July 2016 at 06:21 UTC, during both the probe ascent and the descent of the probe. By analyzing the Rh vertical profiles, one can see that the upper limit of the saturated layer ($Rh \approx 98.5$), i.e. LLSC layer top, obtained by the descent measurements is more consistent with the cloud-radar-estimated CTH than that obtained during the ascent. Further, the descent ~~measurement indicates~~ measurements indicate warmer and drier atmospheric conditions from the CTH to around ~~500~~ 800 meters above, with θ^+ (q^+) around 1 K (0.3 g kg^{-1}) higher (smaller).

By analysing all re-usable soundings of that kind during daytime, we find that the maximum underestimation (overestimation) of θ^+ (q^+) during the ascent due to the wetting of the sensors is ~~of~~ about 1.2 K (0.3 g kg^{-1}). The overestimation of q^+ by the ascending sounding is within the measurement accuracy. While, compared to the 0.2° C measurement accuracy, the underestimation of θ^+ is significant. Consequently, we only consider a systematic error of 1.2 K on the estimates of θ^+ from the 05:00 UTC standard radiosounding, for which we can only rely on the ascent (the descent is too far away from the ~~area~~ supersite).

Figure 8 displays Δq_t and $\Delta \theta_l$ against q^- and θ^- respectively, as estimated for the ~~14~~fourteen cases (~~8~~eight cases C and ~~6~~six cases D) among the ~~20~~twenty cases of Figure 6, for which there is evidence that the radiosonde flew throughout the LLSC layer. It first reveals that the thermodynamical conditions of the subcloud layer are quite steady during this summer period, with only 1.5 g kg^{-1} and 2 K variation range for humidity and temperature, respectively, over all the cases. Similar conclusion was found by Adler et al. (2019). This may be due to the fact that the considered cases occurred in nearly similar synoptic conditions over SWA (Table A-1).

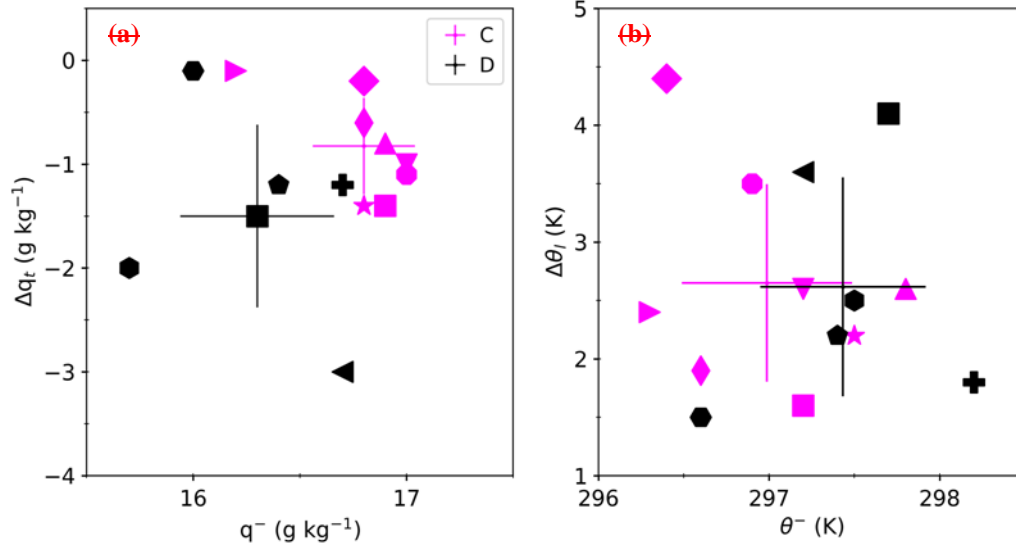


Figure 8: Δq_t against q^- (a), $\Delta \theta_l$ against θ^- (b), derived from the 14 standard morning soundings for which the probe flew within the LLSC layer (Table A-1). In each panel, the error bars correspond to the standard deviation, and cross at the mean over all C (magenta) or D (black) cases. Each symbol represents a single LLSC case.

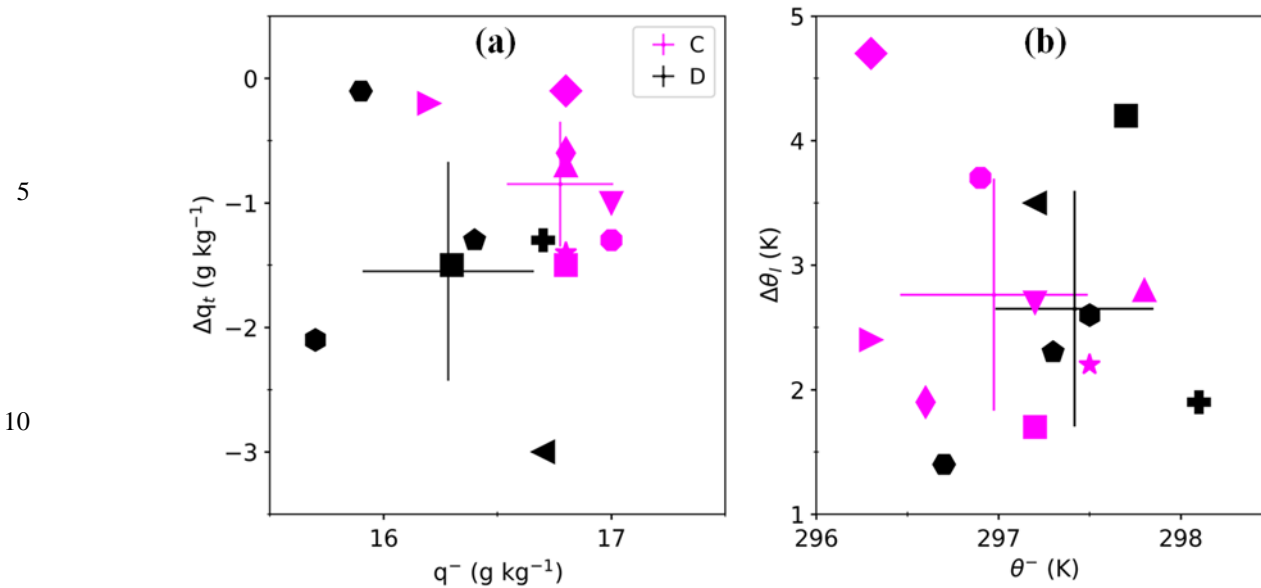


Figure 8 : Humidity jump at the LLSC top (Δq_t) against specific humidity at the LLSC base q^- (a), temperature jump at the LLSC top $\Delta\theta_1$ (possible underestimation of around 1.2 K) against potential temperature at the LLSC base θ^- (b), derived from the fourteen 05:00 UTC standard morning soundings for which the probe flew within the LLSC layer (Table A-1). In each panel, the error bars correspond to the standard deviation, and cross at the mean over all C (magenta) or D (black) cases. Each symbol represents a single case.

In the cases C, q^- ranges within the interval 16-17 g kg⁻¹, with a mean of 16.8 g kg⁻¹ and a standard deviation of 0.5 g kg⁻¹. It is lower in the cases D, with an average of 16.3 g kg⁻¹ and a standard deviation of 0.9 g kg⁻¹. Thus, in early morning, the air just below the LLSC is in average 0.5 g kg⁻¹ moister in the cases C. This is qualitatively true for the entire *stratus phase*, when analyzing the re-usable soundings of the [9nine](#) IOPs (not shown). Δq_t is overall in absolute lower than 3.0 g kg⁻¹. It is smaller than [or equal to](#) 1.5 g kg⁻¹ for 85% of [all](#) the cases. This indicates a generally weak moisture jump across the LLSC top. This is still more pronounced in the cases C, for which Δq_t remains lower than 1.5 g kg⁻¹ in absolute.

The parameter θ^- ranges within 296-299 K. Beyond the same variability found in cases C and D, θ^- is in average around 0.5 K cooler in the cases C, probably because of [the cloud closer LLSC base lowering to the surface](#). $\Delta\theta_1$, which varies within the interval 1-5 K, does not exhibit a clear difference between the cases C and D. Thus, the fact that the LLSC base gets closer to the surface in the cases C does not impact the temperature jump across the LLSC top.

The magnitude of $\Delta\theta_1$ and Δq_t observed [here](#) in SWA conditions are much smaller than those typically found for the mid-latitude stratocumulus, which can be as strong as 10 K and -10 g kg⁻¹ ([Duynderke et al., 2004](#); [Wood, 2012](#); [van der Dussen et al., 2016](#); [Duynderke et al., 2004](#); [Ghonima et al., 2016](#); [Wood, 2012](#)), especially over the ocean. The vertical profile used by [Pedruzo-Bagazgoitia et al. \(2019\)](#) to initialize their LES had a $\Delta\theta_1$ of 4.5 K and no humidity jump across the LLSC layer.

This representation is consistent with what we find for the moisture jump, but is on the sidelines for the temperature jump.

Table 1 : Median and standard deviation of some of the parameters in the RAD, ENT and SUBS formulation estimated from the 14 soundings fourteen 05:00 UTC radiosoundings presented in Figure 8. The standard deviation (in brackets) over the cases is not indicated when it is negligible. Our results are compared with the values used in van der Dussen et al. (2014).

Parameters	Order of magnitude	
	DACCIWA cases	Study case of van der Dussen et al. (2014)
\bar{T}	294 (0.7) K	283 K
\bar{q}	16.2 (0.65) g kg ⁻¹	8.2 g kg ⁻¹
$\text{RadF} \rho C_p \Delta F_{\text{rad}}$	4055 (5) W m ⁻²	48 W m ⁻²
γ	~1.012 g kg ⁻¹ K ⁻¹	0.55 g kg ⁻¹ K ⁻¹
η	~ 0.28	0.42
Γ_{qt}	~ -2.2829 g kg ⁻¹ km ⁻¹	-1.86 g kg ⁻¹ km ⁻¹
w_e	7.6810.12 (2.853) mm s ⁻¹	--

Table 1 compares our estimates of some parameters involved in the formulation of the RAD, ENT and SUBS terms with those of van der Dussen et al. (2014) study case, study case, which are based on the DYCOMS-II (Second Dynamics and Chemistry of Marine Stratocumulus field study) case setup. The quantities γ , η , and Γ_{qt} differ from the typical values used by these authors because the cloud layer is in average 11 K warmer and 8 g kg⁻¹ wetter in our case. For these three parameters, the standard deviation over the 14 cases is lower than 3% of the median. The median and the standard deviation of RadF are respectively about of 40 and 5 W m⁻². Our estimate of RadF, of 40 W m⁻², is in good agreement with the value of 43 W m⁻² given by the Pedruzo-Bagazgoitia (Stevens et al. (2020., 2005)). The quantities γ , η , and Γ_{qt} differ from the typical values used by these authors because the cloud layer is in average 11 K warmer and 8 g kg⁻¹ wetter in our case. simulations just before the sunrise. This is much smaller than the values of 50-90 W m⁻², typically found in the subtropical stratocumulus (van der Dussen et al., 2014; Wood, 2012). Given that the LLSC is warmer, we attribute this difference to the weaker temperature and nearly absent moisture jumps at its top.

We find only 5 W m⁻² standard deviation for RadF, showing again that the conditions during this period remain surprisingly steady from one day to the other. Note that uncertainties of 0.2 K on T^+ and 0.4 K on $\Delta\theta_1$ give a systematic error of around 2.2 W m⁻² on RadF. Increasing systematically θ^+ by 1.2 K for the temperature correction decreases RadF by about 6 W m⁻², which remains small.

The entrainment velocity, w_e , deduced from the parameterization of Eq. (4) has a median of 7.68 mm s⁻¹ and its variability is around 40% of the median. This is around 40% higher than the velocity obtained by. For these three parameters, the

standard deviation over the fourteen cases is lower than 3% of the median. After the analysis of the SBDART model output, ΔF_{rad} is determined from the difference of the net radiative fluxes between the model levels just above and below the LLSC layer respectively. The median and the standard deviation of cloud-top longwave radiative cooling are respectively about of 55 and 5 W m^{-2} . Our estimate of the radiative cooling at the LLSC top for the 25-26 June 2016 case is 44.6 W m^{-2} (Table A-1), which is in good agreement with the value of 43 W m^{-2} estimated in Pedruzo-Bagazgoitia et al. (2020) with LES and among the highest values found by other authors (LES for the same day just before the sunrise. Despite weaker temperature and nearly absent moisture jumps at the LLSC top, the median value of our estimated cloud-top radiative cooling is around 10 W m^{-2} greater than the one of Duynkerke et al., 2004; Faloona et al., 2005; Ghonima et al., 2016; Mechem et al., 2010)van der Dussen et al. (2014). Finally, this discussion shows that our estimates of RAD and ENT should be suitable, beyond the potential errors on entrainment efficiency (A). As mentioned in section 3.1, we only roughly approximate SUBS with the assumption that $w_{s,\text{H}} = -w_e$ (stationary cloud top at the time of the sounding). This term has to be taken with more caution than the two other terms, due to this hypothesis.

and fits within 50-90 W m^{-2} which is the typical interval range found for the subtropical stratocumulus (Wood, 2012). This is most likely because our LLSC is significantly warmer.

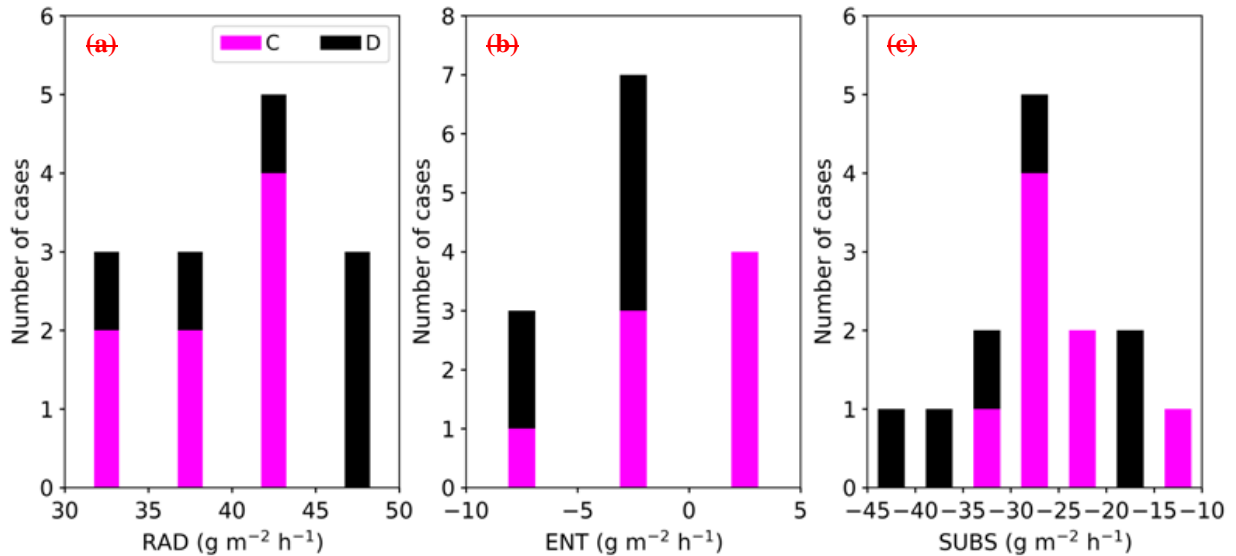


Figure 9: Distributions of LWP budget terms RAD (a), ENT (b) and SUBS (c), derived from the 14 standard morning radiosoundings (Table A-1).

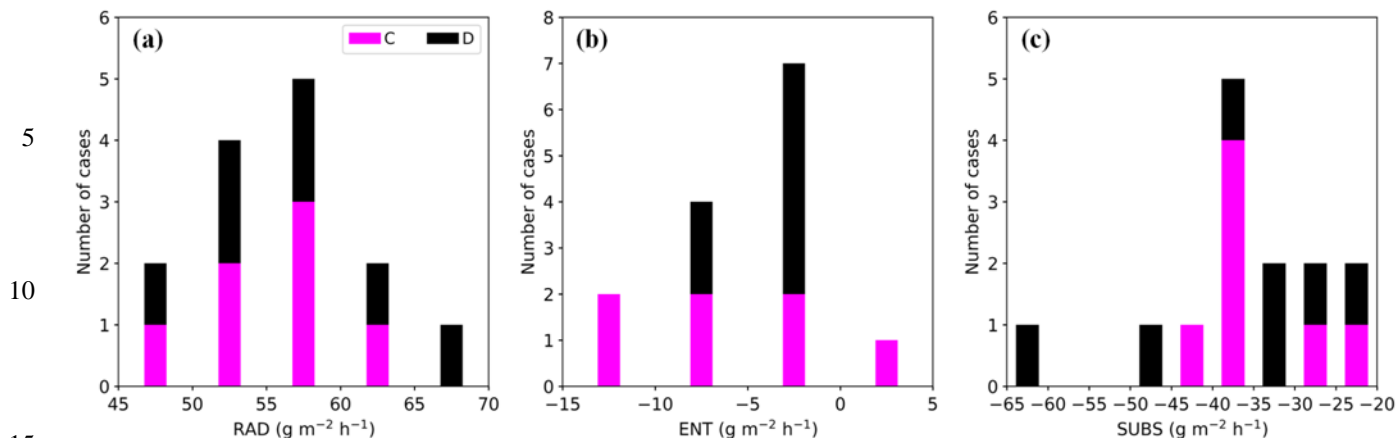


Figure 9 : Distributions of radiative (RAD, a), entrainment (ENT, b) and large scale subsidence (SUBS c) LWP budget terms (Eq. 1), derived from the fourteen 05:00 UTC standard soundings at Savè supersite for which the probe crossed into the LLSC layer (Fig. 8 and Table A-1). The methodology is described in section 3.3.

We find only a 5 W m^{-2} standard deviation for the radiative cooling at the LLSC top and no particular difference between cases C and D. This very low standard deviation may be due to the conditions which remained very steady from one case to the other, but may also be underestimated because the impact of higher clouds are not fully included in the radiative fluxes estimate. In order to evaluate the error due to the temperature underestimation above the LLSC top, SBDART is run with the measured and a corrected temperature profile, while the other inputs remain unchanged. The correction of the potential temperature vertical profile consists in a linear tendency between the measured θ plus a 1.2K correction right above the CTH and the measured θ at 800 m, where we consider that the radiosonde sensor is no more affected by the LLSC crossing. The cloud-top radiative cooling estimated by SBDART with this corrected temperature vertical profile is larger by less than 2 W m^{-2} .

The cloud-top entrainment velocity, w_e (Eq. 3), has a median value of 10.12 mm s^{-1} and its variability is around 25% of the median. This median is around 2.5 times higher than the velocity obtained by Pedruzo-Bagazgoitia et al. (2020) with LES and among the highest values found by other authors (Duynderke et al., 2004; Faloon et al., 2005; Mechem et al., 2010; Ghonima et al., 2016). Finally, this discussion shows that our estimates of RAD and ENT are suitable, beyond the potential errors on the entrainment efficiency, A , and the simplified settings in SBDART. As mentioned in section 3.3, we approximate SUBS with the assumption of stationary LLSC top at the sounding time (Eq. 6). This term has to be taken with more caution than the two other terms, due to this hypothesis.

Figure 9 presents the distributions of RAD (Fig. 9a, Eq. 1.d), ENT (Fig. 9b, Eq. 1.b) and SUBS (Fig. 9c, Eq. 1.e) derived from the 14 fourteen radiosoundings considered in Fig. 8 by the methodology described in section 3.3. The RAD term ranges within 30-5045-70 $\text{g m}^{-2} \text{h}^{-1}$, with a median of 4257 $\text{g m}^{-2} \text{h}^{-1}$. ENT varies between -1015 and 5 $\text{g m}^{-2} \text{h}^{-1}$, indicating a smaller contribution to the LWP budget compared to RAD. The negative value of about -10 is consistent with the study of Pedruzo-Bagazgoitia et al. (2020), with a predominant role of cloud-top temperature and humidity jumps at the cloud top, and a drying and warming effect of the entrainment. Among the 14 fourteen cases, several have a smaller contribution of ENT than this, some of them having. One case even has a positive value for ENT, which means that the LLSC depth has more impact than the temperature and humidity jumps, so that the entrainment in those cases that case favours the LLSC deepening of the cloud. The term SUBS ranges between -4565 and -1020 $\text{g m}^{-2} \text{h}^{-1}$, with a median of around -2736 $\text{g m}^{-2} \text{h}^{-1}$. It corresponds to as much as -0.4 to -0.9 times the RAD term, that which is very significant. This is also consistent with Pedruzo-Bagazgoitia et al. (2020), (who found the ratio SUBS/RAD) approximately equals to -0.4 before sunrise. The Our answers to the two questions raised at the start of this section are:

1) We found similar results compared to Pedruzo-Bagazgoitia et al. (2020). However, the West African inland LLSC layer which develops within the monsoon flow is characterized by weaker temperature and humidity jumps, and smaller radiative cooling at its top as However, the West African inland LLSC layer, which develops within the monsoon flow (Dione et al., 2019), is characterized by weaker temperature and humidity jumps, but with similar radiative cooling at its top compared to marine stratiform clouds.

2) The three cloud-top radiative cooling and the three LWP terms RAD, ENT and SUBS do not exhibit significant differences between the cases C and D (Fig. 9), because of similar cloud depth and thermodynamic characteristics. The slight differences in CBH and moisture jump across the cloud top between the two types of cases do not impact the cloud-top radiative cooling and the LWP budget analysis at the end of the stratus phase.

By a series of sensitivity tests based on horizontal wind speed profiles, Pedruzo-Bagazgoitia et al. (2020) found that a wind shear at the cloud top before the sunrise, as such observed for the LLSC during DACCIWA (Lohou et al., 2020), accelerates may accelerate the cloud deck breakup during the convective phase, by generating dynamical turbulence which enhances the term ENT. However, they did not investigate the effect of wind shear underneath the LLSC.

From the 14 fourteen morning soundings considered in Fig. 8, we quantified the contribution of vertical shear to the production of turbulence at the LLSC top (Table A-1). We find it to be generally smaller than $20 \cdot 10^{-5} \text{ s}^{-2}$, that is considerably smaller than the one imposed at the initialization of the LES experiments performed by Pedruzo-Bagazgoitia et al. (2020). However, this contribution in the subcloud layer is mostly higher than $50 \cdot 10^{-5} \text{ s}^{-2}$ (Fig. 4c). Thus, the dynamical instability induced by the NLLJ is more important below the LLSC than above. This should imply that the mechanical turbulence driven by the NLLJ impacts much more the turbulent fluxes below at the LLSC base than the entrainment of ambient air from above.

4.3 Factors controlling the coupling

5 From previous studies, several processes may lower the LLSC base and couple it with the surface during the stratus phase: (i) the shear-driven turbulence in the subcloud layer (Adler et al., 2019; Babić et al., 2019a), (ii) the cloud droplet sedimentation at the cloud base (Dearden et al., 2018), (iii) the light precipitation formation, i.e. drizzle (Wood, 2012), (iv) the convective overturning driven by the cloud-top radiative cooling (Wood, 2012), and, (v) large scale advection (Zheng and Li, 2019). Sections 4.1 and 4.2 allowed us to test several of these hypotheses to understand why the LLSC couples to the surface in some cases during DACCIWA.

10 As discussed in section 4.1, there is no difference in shear-driven turbulence between cases C and cases D which could explain the thermally neutral stratification of the subcloud layer in cases C and the stable stratification in cases D. So, the NLLJ does not seem responsible for the coupling in the cases C.

15 With LES experiments based on the 04-05 July case (case D, IOP7), Dearden et al. (2018) hypothesized that the LLSC base descent during the night is due to the cloud droplets sedimentation at the cloud base. However, the cloud base decrease is of less than 50 m before the sunrise in this numerical experiment, whereas the observed LLSC base descent is larger than 100 m by the end of the stratus phase in most of our studied cases, either C or D. Thus, the cloud droplets sedimentation should not explain by its own the coupling in cases C.

20 For all the studied cases, no precipitation was recorded at the surface during the stratus phase. However, drizzle formation below the LLSC base can hardly be measured by rain-gauge sensors. So, this hypothesis cannot be fully verified and remains a possibility. Concerning the radiative cooling at the LLSC top, section 4.2 shows that this positive contribution to the LWP budget at the end of the stratus phase is similar in cases C and D.

25 The large scale effects must be considered in the LLSC formation (Babić et al., 2019b), but also in its diurnal cycle. Indeed, eight of the nine cases C are observed between the 26 June and 8 July 2016 (Table A-1). This period corresponds to the first days of the post-onset phase characterized by a well-established and undisturbed monsoon flow over SWA (Knippertz et al., 2017). Warmer advection was observed to decouple stratiform cloud from the surface (Zheng and Li, 2019). Therefore, the reverse process, i.e. cooler advection, may produce the opposite effect. This hypothesis is all the more likely since the LLSC formation during the West African monsoon season is mainly due to a cooler air horizontal advection. The res-usable soundings performed during the stratus phase of the nine IOPs revealed that, at 50 m a.g.l (sounding level below the lowest CBH at the end of the stratus phase), the relative humidity remains larger than 90% for all the cases (not shown). For cases C, a decrease of the specific humidity (by around 1 g kg^{-1}) and a slight decrease of temperature (by around $0.2 \text{ }^\circ\text{C}$) are observed between the LLSC formation and its coupling, which maintains Rh constant. However, no clear tendency was observed in the cases D. The very small temporal tendency of the temperature and humidity and the small number of studied cases do not allow us to definitively conclude on the effect of cooling and drying due to horizontal advection of the maritime inflow. However, this advection seems to persist in cases C and could have some impacts. If not on the LLSC base lowering (because Rh

30

is constant at 50 m a.g.l), the dry advection can have an effect on the LCL evolution. Indeed, a 1 g kg^{-1} decrease of near-surface specific humidity implies an elevation of surface-based LCL by a hundred meters, which facilitates the coupling.

It emerges from the above discussion that none of the processes listed at the beginning of this section is solely responsible for the coupling. We can hypothesize that it is the combination of several of those processes, each with a small impact, which leads to the LLSC coupling with the surface. After the coupling, the turbulence underneath has a crucial role for its maintenance during the rest of the *stratus phase*, as indicated by the reduction of thermal stability in the subcloud layer for the cases C (Fig. 5b). Indeed, the contributions of the shear-driven turbulence below the NLLJ and the turbulence due to the radiative cooling at the cloud top are important for mixing potential temperature in the subcloud layer (Dione et al., 2019; Lohou et al., 2020). In the LES experiments under windless conditions carried out by Pedruzo-Bagazgoitia et al. (2020), the cloud-top radiative cooling was the unique source of turbulence in the ABL until sunrise, and the coupling between the cloud and the surface was maintained.

5 Evolution of the LLSC layer under daytime conditions

In this section, the evolution of the LLSC during the *convective phase* until its breakup is analyzed.

5.1 The three scenarios of evolution

The evolution of LLSC during the *convective phase* is first analyzed according to the ceilometer-derived CBHs temporal change relatively to the surface-based LCLs. From this point of view, all the cases C evolve quite similarly during ~~the~~ convective phase, while two distinct scenarios are observed among the cases D (hereafter named DC for “decoupled-coupled” and DD for “decoupled-decoupled”). Each of the three scenarios is illustrated by one typical example; the LLSC occurrence on 07-08 July (Fig. 10a) for scenario C, 25-26 June (Fig. 10b) and 04-05 July (Fig. 10c) for scenarios DC and DD respectively.

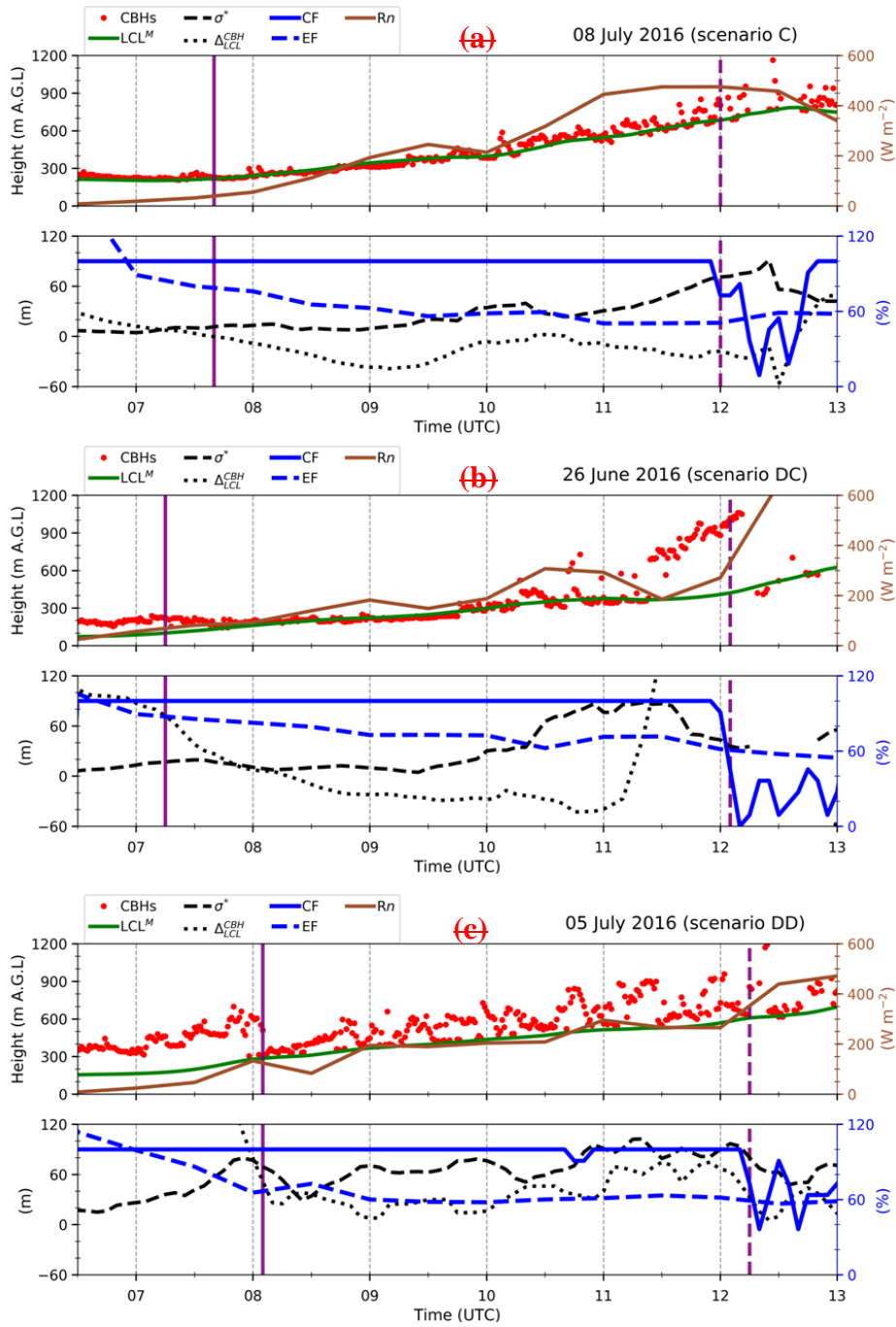


Figure 10 : Illustration of the three scenarios of LLSC evolution during the convective phase: (a) 8 July for scenario C, (b) 26 June for scenario DC and (e) 5 July for scenario DD. The top panels present the ceilometer-derived CBHs, the lifting- condensation level (LCL^M) and the net radiation (R_n) measured at surface. The bottom panels gather the cloud fraction (CF), the evaporative fraction (EF in %), the standard deviation of the cloud base height (σ^*) and the distance between the cloud base and the LCL (Δ_{LCL}^{CBH}). The vertical solid and dashed lines indicate T_c and T_b , respectively.

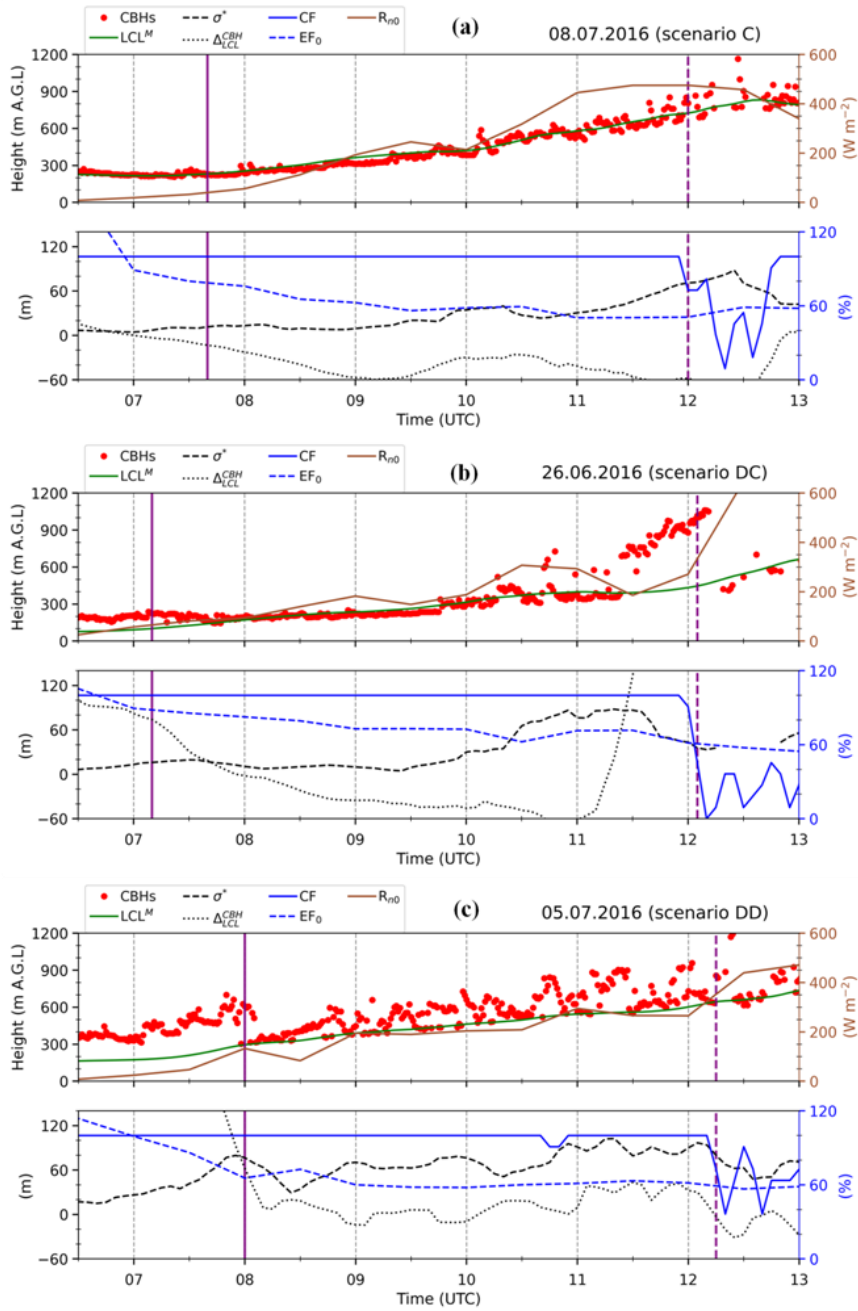


Figure 10 : Illustration of the three scenarios of LLSC evolution after the sunrise observed at Savè supersite during DACCIWA field campaign: **(a)** 08 July 2016 for scenario C, **(b)** 26 June 2016 for scenario DC and **(c)** 05 July 2016 for scenario DD. The top panels present the ceilometer-derived CBHs, the lifting condensation level (LCL) and the net radiation measured at surface (R_{n0}). The bottom panels gather the cloud fraction (CF), the evaporative fraction at the surface (EF_0 in %), the standard deviation of the cloud base height in the LLSC layer (σ^*) and the mean distance between cloud base height and surface-based LCL (Δ_{LCL}^{CBH}). The vertical solid and dashed lines indicate the surface-convection influence time (T_i) and the cloud deck breakup time (T_b), respectively. The Local time at Savè (Benin) is UTC +1 hour.

Whether the CBHs is close to the LCL (Fig. 10a) or not (Fig. 10b and c), it has a low variability before 07:00 UTC in these three illustrative cases, indicating a quite horizontally homogenous base of the LLSC layer before the start of the *convective phase* (as already seen in the previous section). The CBHs and the LCL in scenario C lift together after 07:30 UTC, due to thermal convective conditions in the subcloud layer. After 09:00 UTC, σ^* increases gradually, but the lower bases always fit with the LCL, with Δ_{LCL}^{CBH} ranging between 0 and -40 m (Fig. 10a, lower panel). This can be interpreted as a progressive change in the LLSC base structure which is more and more heterogeneous in height but the cloud layer remains coupled with the surface all along. The evolution from stratus to stratocumulus and eventually to cumulus can hardly be established with the use of CBHs only, but CBHs already show a clear evolution ~~off from~~ the homogeneous ~~low-stratus~~LLSC towards a more heterogeneous low cloud structure until the ~~LLSC~~cloud deck breakup time, established when CF decreases to less than 90%, which happens at 12:00 UTC on the 08 July.

The LLSC in the scenario DC (Fig. 10b) is decoupled from the surface at the end of the *stratus phase*. The LCL starts to rise at 07:00 UTC and joins the LLSC base about 1 hour later, indicated by a decrease of the Δ_{LCL}^{CBH} down to zero (Fig. 10b, lower panel). After the coupling, the scenario DC is very similar to the scenario C and will be further commented in ~~the last~~ section ~~5.3~~.

The evolution of the LLSC in the scenario DD (Fig. 10c) is quite different compared to the two others. The LLSC layer remains decoupled from the surface until 08:00 UTC as shown by the significant departure between LCL and CBHs ($\Delta_{LCL}^{CBH} > 120$ m, Fig. 10c, lower panel) due to a similar lifting rate of both levels. After 08:00 UTC, a new cloud layer with a base very close to the LCL ($\Delta_{LCL}^{CBH} < 40$ m), is detected 200 m below the LLSC ~~deck~~. The values of σ^{**} , much larger than 60 m after 08:30 UTC, indicate that, this new cloud layer rapidly turns to shallow cumulus clouds. Unfortunately, ~~the~~ ~~ceilometer~~it is not ~~able~~possible to ~~monitor~~distinguish both cloud layers ~~separately with the ceilometer-derived CBHs, because they remain too close to each other, with variable cloud bases and edges~~. But, one can suppose that the LLSC formed during the night remained above the cumulus clouds layer ~~after sunrise~~during part of the *convective phase*. The higher CBHs detected by the ceilometer after 09:00 UTC are the overlying ~~stratus-layer~~LLSC base (about 200 m higher). The cumulus and ~~stratus~~LLSC layers ~~above~~ can ~~however~~ clearly be seen on the visible and infra-red full sky cameras (not shown). **In the case where the two cloud layers are superimposed, two possibilities may occur: (i) the underlying surface-convection driven cumulus cloud do not interact with the LLSC which remains decoupled from the surface, (ii) the underlying cumulus clouds develop vertically, reach the LLSC layer, and act to intermittently and locally couple it with the surface (Wood, 2012).**

Among the ~~13~~thirteen cases D observed at the end of the *stratus phase*, ~~8~~eight follow the scenario DD and ~~5~~five follow the scenario DC during the *convective phase* (Table A-1). The main difference between the three scenarios is that the first shallow convective clouds form when the LLSC breaks up in ~~the~~ scenarios C and DC, whereas in the scenario DD, shallow cumulus clouds form below the LLSC layer before it breaks up. Similar transitions were reported by previous observational and modelling studies on the stratiform low clouds (Price, 1999; Xiao et al., 2011; Ghonima et al., 2016; Mohrmann et al.,

2019; Sarkar et al., 2019; Zheng and Li, 2019; Pedruzo-Bagazgoitia et al., 2020; Price, 1999; Xiao et al., 2011). Especially, the transition of scenario DD is part of the conceptual model for marine stratocumulus (Wood, 2012; Xiao et al., 2011; Wood, 2012). ~~In such conditions, the underlying cumulus clouds act to intermittently and locally couple the stratocumulus layer with the surface (Wood, 2012).~~

5
-
One can wonder what conditions lead the LLSC to either be coupled to the surface in the scenario DC, or ~~remain~~**remains possibly** decoupled with the formation of an underlying cumulus layer in the scenario DD. No relevant differences in macrophysical characteristics of LLSC (base and depth) were found between the two scenarios at the end of the *stratus phase* and beginning of the *convective phase* (not shown). ~~One could argue that the low number of cases does not allow a robust statistic, but the LLSCs~~ The LLSC with low bases are not systematically those which will be coupled to the surface at the beginning of the *convective phase*. ~~Eventually,~~ The four parameters presented in Fig. 8, ~~and summarizing which summarise~~ the thermodynamical conditions in the subcloud layer and above the LLSC, are not fundamentally different either between DC and DD scenarios. The relative humidity in the subcloud layer ~~at~~by the ~~beginning~~end of the *stratus phase* is larger than 95 % ~~whatever~~in all the ~~ease~~cases D, and the difference between the different scenarios DD and DC is smaller than 2 % which is about the ~~accuracy of the~~ measurement or lower accuracy.
15
Consequently, alternative approaches are needed to identify the processes involved in the coupling of LLSC during the *convective phase*.

In conclusion, the ~~nature of~~ coupling between the LLSC and the surface during the *convective phase* appears to be the key factor determining the way by which the transition towards shallow convective clouds takes place. When the LLSC is coupled to the surface (cases C and DC), it is the breakup of the cloud deck which leads to the formation of different low-level clouds type (stratocumulus or cumulus). When the LLSC is decoupled from the surface (cases ~~DDD~~), the convective clouds ~~firstly~~ form below it. In the next paragraphs, we deeply analyze the different scenarios of the LLSC evolution.
20

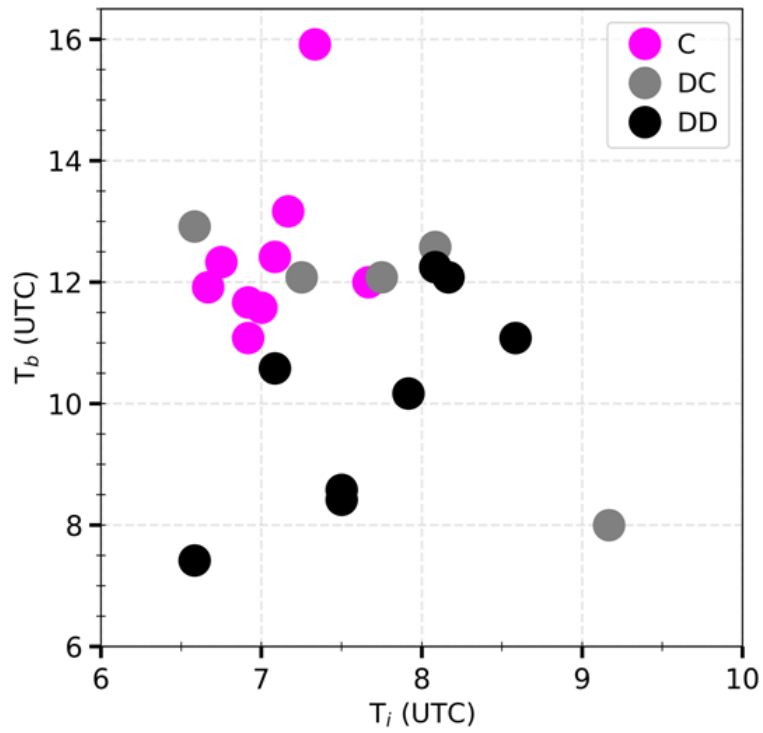


Figure 11 : LLSC breakup time (T_b) against the time at which the low cloud coverage is impacted by thermally driven turbulence (T_i) for the 22 selected cases (Table A 1). Colors stand for the three scenarios.

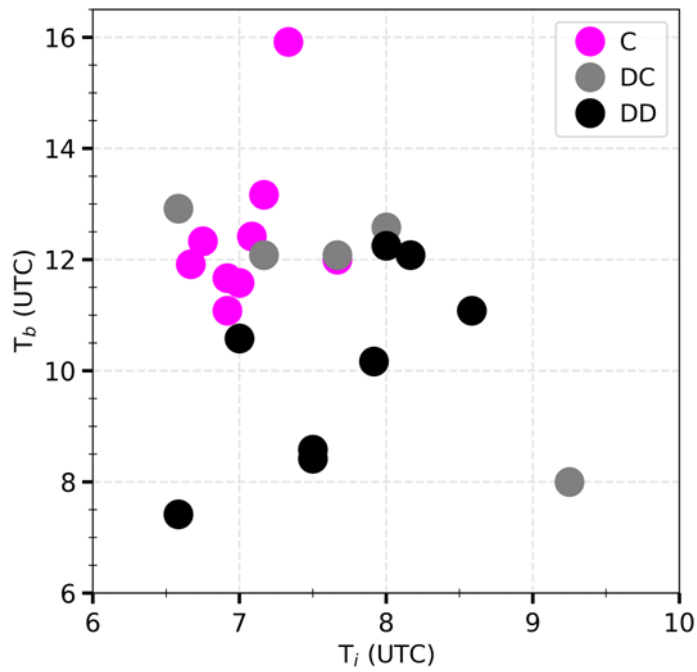


Figure 11 : LLSC breakup time (T_b) against surface-convection influence time (T_i) for the twenty-two selected cases (Table A-1). Colors stand for the three scenarios.

5.2 Surface-convection and breakup times

The ~~The~~ surface-convection influence time, T_i , indicates when the low cloud coverage is influenced by the surface-buoyancy-driven turbulence, and T_b when the low cloud breaks up. T_i is defined differently according to the scenario. For the scenario C, T_i corresponds to the time when the LLSC base starts to lift together with the LCL. After sensitivity tests, T_i is defined as the first time when LCL^M increases to at least 5 m above its value at 06:30 UTC. For the scenario DC, T_i corresponds to the time when the rising LCL reaches the LLSC base, that is when the LLSC is coupled to the surface ($\Delta_{LCL}^{CBH} < 75$ m, which is also the threshold used to ~~sort-out~~ differentiate C and D cases at the end of the *stratus phase* in section 4.1). For the scenario DD, T_i is the first time when new low clouds appear below the LLSC deck. As these clouds are coupled to the surface, T_i is also determined when Δ_{LCL}^{CBH} decreases to less than 75 m.

Figure 11 displays T_b and T_i for the ~~22~~twenty-two LLSC cases (Table A-1). T_i ranges between 06:30 and 09:15 UTC. T_b varies between 07:30 and 16:00 UTC, with breakup times occurring before 12:00 UTC for 72% of all the cases. The latter result is consistent with the findings of Dione et al. (2019) who used the infrared images from the cloud camera to define the LLSC lifetime. One can see that the LLSC breakup time is not linked to the time at which it starts to rise or at which the underlying clouds form.

For the scenario C, T_i hardly changes from one case to the other. It ranges between 06:40 and 08:00 UTC, ~~that~~which is not long after the sunrise (06:30 UTC). The LLSC persists at least 4.5 hours and breaks up between 11:00 and 16:00 UTC. **The latest breakup time occurring at 16:00 UTC corresponds to the 02-03 July 2016 case for which the hydrometeors radar reflectivity from the cloud collocated radar reveals light precipitations from higher clouds, above the LLSC layer, during the first hours of the convective phase (not shown), while nothing was recorded by the surface rain gauge.** This external forcing, able to enhance the liquid water content in the LLSC layer, is certainly responsible for this late breakup. Because this case is an exception and cannot easily be compared to the others, it is not considered ~~here~~afterhereafter.

For ~~4~~four DC cases out of ~~5~~five, T_i and T_b are very close to the values observed for C cases. This means that the stable stratification in the subcloud layer before the *convective phase* (which allowed the classification of this case as decoupled during the stratus phase) is rapidly eroded after sunrise and does not seem to impact the breakup time. The case for which T_b occurred at 08:00 UTC (16-17 July 2016) is removed in the following as well, because the LLSC breaks up before the LCL reaches its base.

The scenario DD presents the largest variation ranges of T_i (between 06:35 UTC and 09:00 UTC) and T_b (between 07:00 UTC and 13:00 UTC). The most striking result is that the LLSC in scenario DD often breaks up earlier than in scenarios C and DC.

Following the LES of Pedruzo-Bagazgoitia et al. (2020), the start of the *convective phase* leads to three main changes in LWP equation. First, the radiative cooling (RAD term) decreases due to the solar heating at the cloud top. Second, the ENT term also strongly decreases because the thermally-driven convection enhances the entrainment of dry and warm air from

aloft in the LLSC. Third, the BASE term, which was close to zero during the *stratus phase*, comes into play during the convective phase and contributes positively to $\frac{\partial LWP}{\partial t}$. Despite the BASE term, the strong decrease of both ENT and RAD makes $\frac{\partial LWP}{\partial t}$ negative one hour after the sunrise. The RAD and ENT terms cannot be estimated during the *convective phase* with the dataset acquired at Savè because several data are missing, and, among them, the CTH.

5 The scenarios C and DC during the convective phase are very close to the case simulated in Pedruzo-Bagazgoitia et al. (2020) and one can expect a quite similar evolution of the terms involved in the LWP prognostic equation. Conversely, the scenario DD might be very different. The LLSC breaks up earlier, mostly before or around 10:30 UTC, when it is decoupled from the surface layer, likely due to a weaker BASE term. This hypothesis is supported by the findings of van der Dussen et al. (2014) ~~who found~~ suggesting that stratiform low clouds coupled to the surface moisture are more resistant to cloud-
10 thinning related processes such as the entrainment of dry and warm air into the cloudy layer. The stronger variability of the breakup time for DD cases may come from the fact that the LLSC thinning depends on its interaction with the underlying cloud layer. If the latter penetrates the LLSC, local coupling can happen which induces a homogeneous layer from surface to the ~~cloud~~ LLSC top, but, at the same time, the entrainment at the cloud top is enhanced by the cumulus vertical development (Wang and Lenschow, 1995).

15 **The LLSC breakup time impacts the radiative budget at surface over the day, then the surface fluxes, and consequently, the vertical development of the ABL, as shown by (Lohou et al., (2020). The later develops up to). They estimated that the ABL height is about 900 m when the LLSC breaks up at 09:00 UTC and is 30% lower when the LLSC breaks up at 12:00 UTC. Consequently, one can expect a quite different vertical development of the ABL in C/DC cases than in DD cases.**

20

5.3 Evolution of the LLSC horizontal structure for C and DC cases

The changes in the LLSC horizontal structure for C and DC scenarios is now further analyzed based on the evolution of the LLSC base and its standard deviation, σ^* . The cases DD are excluded from this analysis because the macrophysical characteristics of the associated LLSC cannot be determined after the underlying cloud formation. As illustrated in Fig. 10a
25 and b, the elevation rate of the LCL, and consequently of the LLSC base, may change a lot from one case to the other. It is about 108 m h^{-1} and 67 m h^{-1} for 8 July and 26 June, respectively. One could expect that the higher this rate, the higher $R_n R_{n0}$, and the more intense is the thermally-driven convection in the subcloud layer as well as the corresponding BASE term. However, no clear link is pointed out between T_b and this elevation rate of the LLSC base (not shown).

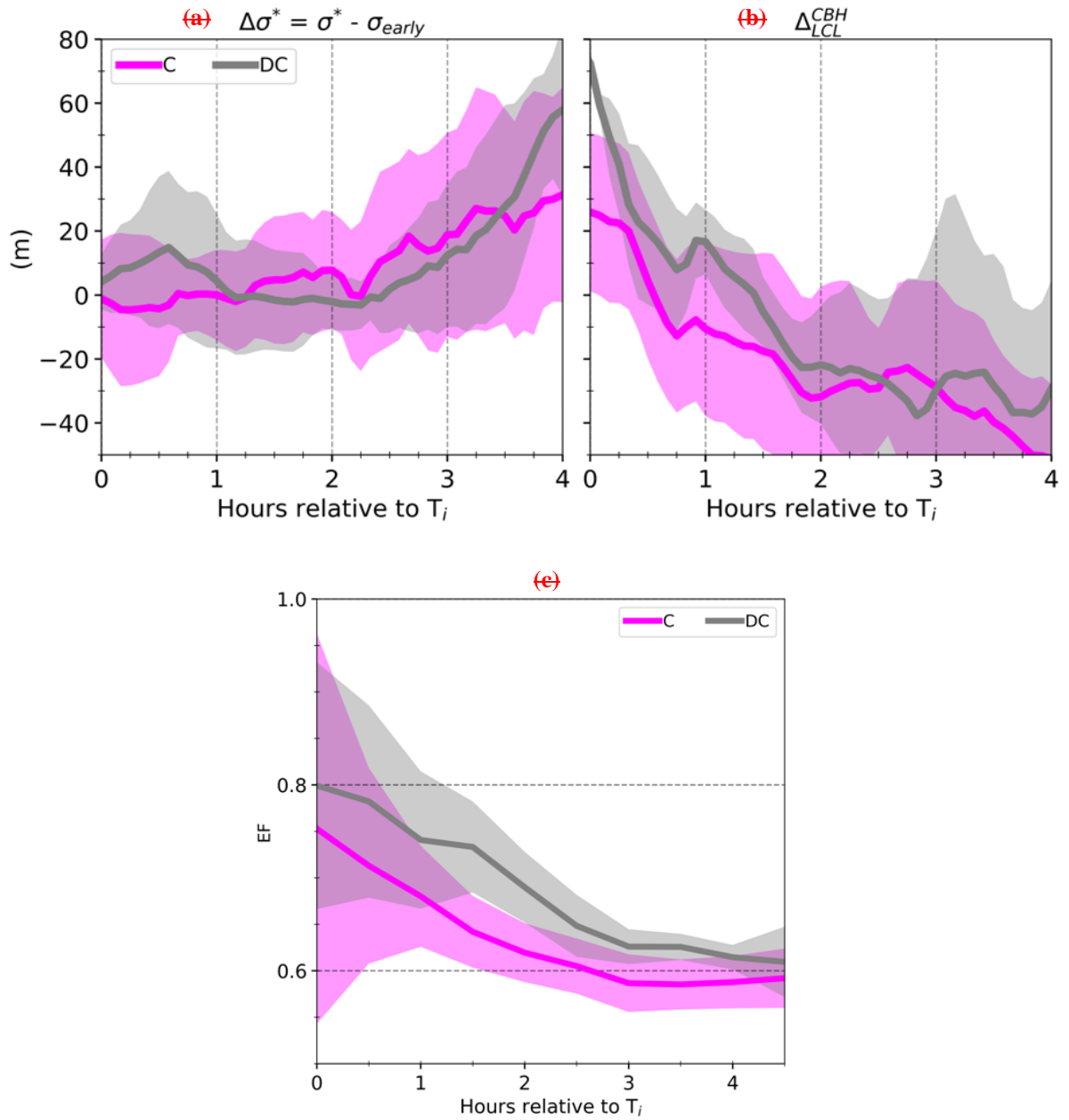


Figure 12 : Evolution of, (a) $\Delta\sigma^*$, which is the difference between σ^* and its median over the period from 04:00 to 06:30 UTC (σ_{early}), and, (b) Δ_{LCL}^{CBH} , (c) the evaporative fraction (EF) at surface, for C (coupled) and DC (decoupled-coupled) scenarios. The solid lines indicate the median and shaded areas represent the standard deviation. The time is expressed in hours relative to T_i .

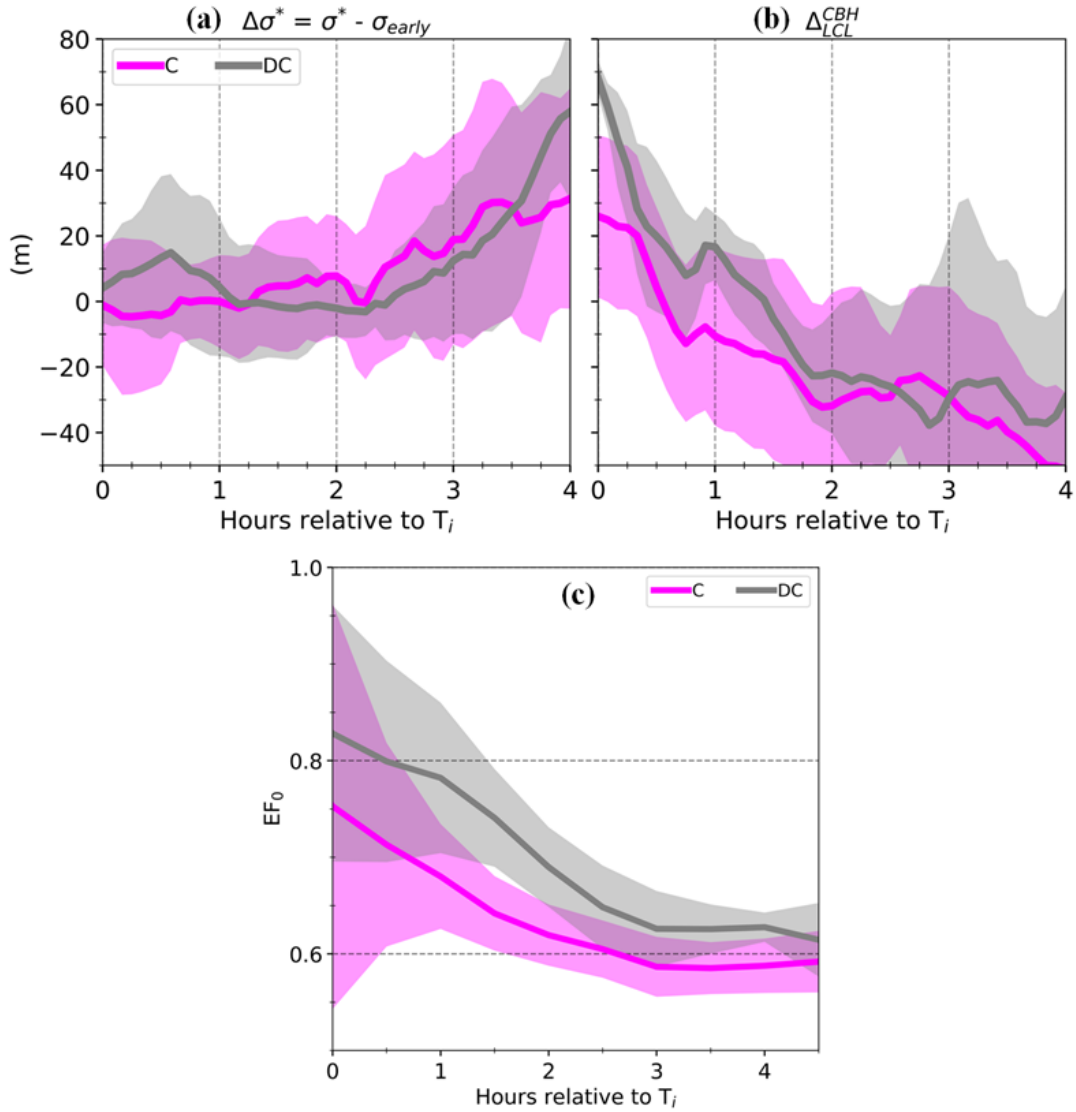


Figure 12 : Evolutions of, **(a)** $\Delta\sigma^*$, which is the difference between the diagnostic parameter σ^* and its median over the period from 04:00 to 06:30 UTC on day-D+1 (σ_{early}), **(b)** the mean distance between the LLSC base height and surface-based LCL (Δ_{LCL}^{CBH}), **(c)** the evaporative fraction at surface (EF_0), for C (coupled) and DC (decoupled-coupled) scenarios. The solid lines indicate the median and shaded areas represent the standard deviation. The time is expressed in hours relative to surface-convection influence time (T_i).

Contrary to the LLSC base height, σ^* has a common tendency among all the C and DC cases. The evolution of σ^* with time compared to its value at T_i , σ_{Early} , is presented in Fig. 12a. A four-hour-period is considered here because it is the smallest duration between T_i and T_b (Fig. 11) for the ~~12~~twelve C and DC cases included in this statistic. As also illustrated in Fig. 10a and Fig. 10b, σ^* remains close to σ_{Early} during at least two hours after T_i (until 09:00 UTC for 8 July and 09:30 UTC for 26 July). Consequently, during this period, the structure of the LLSC bases remains quasi-unchanged ~~in time~~. Afterwards, σ^* progressively increases during at least 2 hours until the LLSC deck breakup. From T_i to the breakup, $\Delta_{\text{LCL}}^{\text{CBH}}$ remains lower than 70 m, with even a slight decrease in the first two hours (Fig. 12b), suggesting an enhancement of the coupling due to an increase of the thermally-driven turbulence in the subcloud layer. The combination of (1) very heterogeneous LLSC base and (2) the fact that the lowest ones remain close to the LCL during the few hours before T_b , indicates that some of the bases are coupled to the surface but some tend to be decoupled from the surface.

Eventually, the evolution of σ^* and $\Delta_{\text{LCL}}^{\text{CBH}}$ (Fig. 12) allows to define two periods between T_i and T_b : (1) the two first hours after T_i during which the LLSC is fully coupled to the surface and the homogeneity of its base is not affected yet, and, (2) the few hours before T_b during which the base of the LLSC layer becomes more and more heterogeneous and intermittently decoupled from the surface. This latter tendency can be seen in Fig. 10a upper panel after 11:00 UTC and in Fig. 10b lower panel after 10:15 UTC. A decoupling of the stratiform cloud from the surface is also observed about half an hour before the cloud deck breakup in Pedruzo-Bagazgoitia et al. (2020) simulations.

The bottom panels of Fig. 10 present the evolution of the evaporative fraction (~~EF~~) at the surface (EF₀) for the illustrative cases. ~~The Figure~~ 12c displays the medians of this parameter over all C and DC cases. Defined as the ratio of LHF/LHF₀ to (LHF + SHF), EFLHF₀ + SHF₀, EF₀ larger than 0.5 means that the evapo-transpiration dominates over the warming. This is in average the case ~~in~~at Savè during the DACCIWA campaign (Kalthoff et al., 2018). Figure 12c shows that the median of EF₀ decreases from around 0.75 at T_i to 0.6 at the LLSC breakup. The predominance of the evapo-transpiration over the sensible heat flux, particularly during the two first hours after T_i , and the full coupling of the LLSC to the surface, might contribute to maintain the LLSC through the BASE term. The LLSC base is indeed strongly homogeneous. The decrease of EF₀ and its stabilisation/levelling at 0.6 implies a faster increase of SHF/SHF₀ than LHF-at surface/LHF₀. One can then expect a larger contribution of $\overline{w'\theta_1^b}$ and a smaller one from $\overline{w'q_1^b}$ in BASE term with time. **This could favour/favours the convection in the cloud/LLSC which enhances the entrainment, at the expense of the cloud moistening by the underlying turbulent mixing.** In addition to this, the final intermittent decoupling of the LLSC from the surface likely contribute, together with the decrease of RAD and ENT terms (Pedruzo-Bagazgoitia et al., 2020), to the LLSC breakup.

It appears that, the LLSC and the timing of its evolution in the scenarios C and DC are very similar during the *convective phase*. In these scenarios, the LLSC keeps the same characteristics in terms of coupling and base ~~height and~~ homogeneity during two hours after T_i . Afterwards and until its breakup, the LLSC becomes more and more heterogeneous and intermittently decoupled from the surface. These two steps are in phase with the evolution of the EF₀ which likely impacts the BASE term ~~which that~~ is the only positive contribution into LWP budget during the ~~LWP equation~~convective phase.

6 Summary and conclusion

The breakup of the almost daily LLSC during monsoon season in southern West Africa is the object of this study. It is based on the analysis of a set of twenty-two precipitation-free LLSC occurrences observed during the DACCIWA field experiment at Savè supersite. The diurnal cycle of the LLSC consists of ~~4~~four main stages and this study addresses the two latest, the *stratus* and *convective* phases. We used the ground-based observational data collected by (i) ceilometer and cloud radar for macrophysical properties of the cloud layer, (ii) energy balance and weather stations for the atmospheric conditions near the surface, and ~~finally, (iii)~~ (iii) radiosoundings and UHF wind profiler for the thermodynamical and dynamical conditions within the low-troposphere. From these measurements, some diagnostics of the LLSC layer are estimated, including: the cloud-base height, the cloud coverage fraction, the cloud base homogeneity and the cloud coupling with the surface. The ~~latter aspect~~coupling was assessed by the distance between the LLSC base height and the lifting condensation level; the cloud layer is coupled to the surface when these two levels coincide. Our main results are summarized in Fig. 13 by a schematic illustration.

At the beginning of the *stratus phase* (after 22:00 UTC), the LLSC is decoupled from the surface in all the studied cases, ~~except~~except in one ~~(dashed blue lines in Fig. 13)~~. Within the following four hours, in nine among the ~~22~~twenty-two cases, the LLSC base lowers in such way that the cloud layer gets coupled to the surface (referenced as cases C ~~with magenta dashed line in, Fig. 13)~~c). In the thirteen other cases (referenced as cases D ~~with dark dashed line in, Fig. 13)~~a and b), the LLSC remains decoupled from the surface. The weak thermodynamical differences observed between C and D cases at Savè can hardly explain the coupling which occurs in C cases. However, the cases C occurred preferentially between 27 June and 8 July 2016, a period with a well-established monsoon flow over West-Africa, especially over DACCIWA investigated area. Most of the cases D are observed during the monsoon onset period or during disturbed sub-periods after ~~the~~ 08 July 2016. If the synoptic conditions of the monsoon flow play a role on the LLSC coupling ~~of stratus to~~with the surface, it could be through the thermodynamical conditions, which were ~~not~~hardly highlighted with Savè data set. It could also be through large scale dynamical parameters like large scale subsidence, which is an important factor ~~into~~ LWP budget and could not be determined precisely for every day with Savè data set. The analyses of the stable and jet phase by Adler et al. (2019) and Babić et al. (2019a,b) outline a complex imbrications of different processes in LLSC formation. Similarly, we conclude that the LLSC coupling ~~of the LLSC~~ to the surface during the *stratus phase* is also based on different processes for which a slight intensity change may have an important impact.

The Savè data set allowed us to estimate ~~some of the~~ most important terms of the LWP ~~budget~~tendency equation at the end of the *stratus phase*, ~~notably~~ the radiative ~~cooling and the~~ entrainment and subsidence terms, ~~which are among the most important terms at that time of the LLSC cycle. Our values~~ are very close to those found by Pedruzo-Bagazgoitia et al. (2020) in ~~the~~ numerical study of a DACCIWA case. Since the LLSC layer develops in the monsoon flow, ~~the LWP budget terms are quite different from those described in previous studies, it is warmer~~ and especially those characterizing marine stratocumulus. ~~This is due to drastically~~ characterised by weaker ~~inversion jumps in~~ temperature and humidity jumps at its

~~top, but with same magnitude order of cloud-top during DACCIWA field campaign which impacts the-top radiative cooling and the entrainment terms, compared to marine stratocumulus over subtropical region.~~

During the *convective phase* of the LLSC diurnal cycle, a new separation occurs among the D cases. In some of them, the LLSC couples to the surface while the lifting condensation level rises with the thermally-driven convection at the surface- (Fig. 13b). Therefore, the LLSC deck may follow three scenarios until its breakup: (1) the scenario ~~EDD~~ for “decoupled-
5 ~~decoupled”~~ (followed by ~~all the C-most of D~~ cases ~~of the stratus phase, Fig. 13a~~), (2) the scenario DC for “decoupled-
~~coupled”~~ (followed by ~~some of the other~~ D cases ~~in dashed grey lines in, Fig. 13;b~~), and; (3) the scenario ~~DD~~ for
~~“decoupled decoupled”~~C (followed by ~~all the other DC~~ cases ~~of the stratus phase, Fig. 13c~~). The scenarios C and DD are the
most frequent among the ~~22~~²² studied cases with ~~9~~⁹ and ~~8~~⁸ occurrences respectively. The reason why the
10 cases D follow DC or DD was not clearly identified.

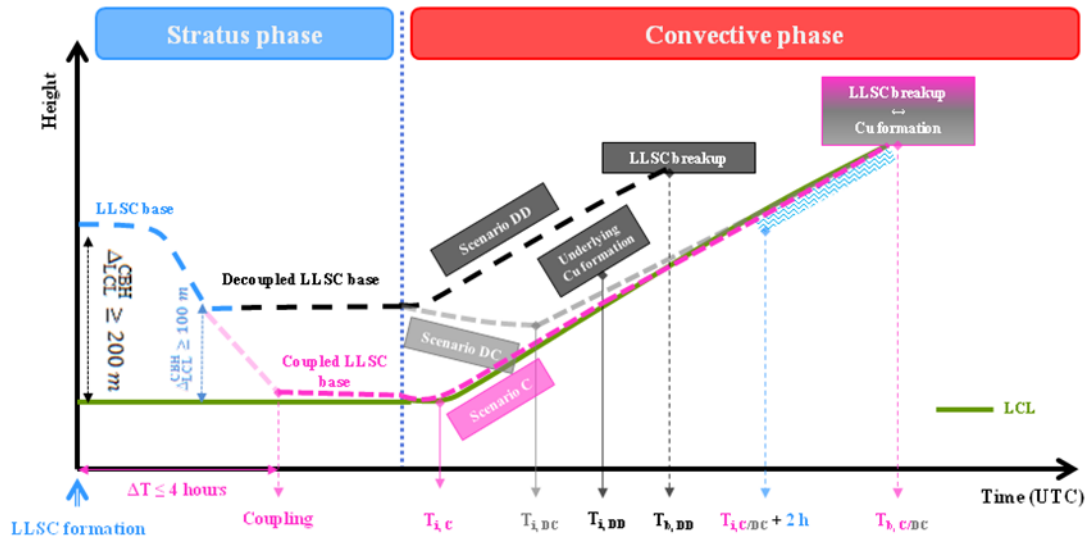
Typically, the scenarios C and DC are quite similar and consist of two steps: (i) the first two hours during which the LLSC layer lifts but remains fully coupled to the surface and the homogeneity of its base is not affected yet, (ii) the few hours preceding the breakup time during which the cloud layer is sometime decoupled from the surface as its base becomes more and more heterogeneous. In these two scenarios, the breakup of the LLSC deck leads to a transition towards shallow
15 cumulus clouds. ~~That~~^{This} occurs at around 11:00 UTC or later, approximately more than 4.5 hours after the LLSC starts to lift. In the scenario DD, cumulus clouds, triggered by convectively mixed layer, form below the LLSC deck before its breakup. The breakup time in this scenario varies strongly between 07:30 UTC and noon. But in most of the cases, it occurs before 11:00 UTC. The earlier breakup occurring in the scenario DD outlines the importance of the coupling with surface for the LLSC maintenance after the sunrise. Thus, we conclude that, in SWA conditions, the coupling between the LLSC and
20 the surface is a key factor for its evolution during daylight hours. **It determines the LLSC lifetime and the way by which the transition towards shallow cumulus occurs. The coupled LLSC last longer and can therefore more significantly impact the surface energy budget over the day convective clouds occurs. The coupled LLSC last longer (breakup time at 12:00 UTC in average) than decoupled cases (breakup time at 10:00 UTC in average). According to Lohou et al. (2020), such a difference in breakup time leads to a reduction of about 15% of net radiation at surface and of ABL vertical development during the day for coupled cases compared to decoupled one.**

~~These results can help to identify the weaknesses in global climate and weather model simulations for a better representation of WAM features. The influence of middle level clouds on the LLSC remains also an opened question. It is not objectively addressed in this study.~~

Data availability. ~~The data used in this study are available in the BAOBAB (Base Afrique de l’Ouest Beyond AMMA Base) database (<https://baobab.sedoo.fr/DACCIWA/>)~~ From these results, it appears important to correctly simulate the coupling of the nocturnal LLSC layer for a better representation of West African monsoon features in global climate and weather model simulations. However, the processes responsible for the coupling at different stages of the LLSC diurnal cycle (during the

stratus phase for C cases (Fig. 13c) and during the *convective phase* for DC scenario (Fig. 13b)) are not easy to identify. The coupling rather results from a combination of several processes than a well distinct and predominant one. Thus, it seems very difficult to advise one improvement in the model. **The aerosol loading in the low-troposphere is a potential factor controlling the LLSC evolution and lifetime** (Derrien ~~Deetz~~ et al., 2016; Handwerker 2018; Mohrmann et al., 2016; Kohler et al., 2016; Wieser et al., 2016 **2019**).

. The airborne measurements of low-cloud properties over SWA during DACCWA (Flamant et al., 2017) could be used to assess the microphysical role for aerosol in the LLSC evolution scenario. This may help to differentiate the scenarios DC and DD. Furthermore, the potentially large influence of middle-level clouds on the LLSC remains also an opened question and was not objectively addressed in this study. It would be also interesting to study how the LLSC breakup over SWA might change in future climate.



Scenario C	$T_{i,C} \sim 07:00$ UTC	$T_{b,C} \geq 11:00$ UTC
Scenario DC	$T_{i,DC} \sim 07:30$ UTC	$T_{b,DC} \geq 11:00$ UTC
Scenario DD	$T_{i,DD} \sim 08:00$ UTC	$07:00 \leq T_{b,DD} \leq 12:00$ UTC

Figure 13: Schematic representation of the main findings of this study. It portrays the typical LLSC evolutions over the southern West Africa during the Monsoon season. The different scenarios and their characteristic times are illustrated. Their typical values are given in the table at the bottom. The different lines represent the evolution of the LLSC base (dashed line) and the surface-based LCL (solid green line). The shaded blue pattern marks the characteristic time interval for the scenario C and DC in which the LLSC base becomes more and more heterogeneous until the cloud deck breakup.

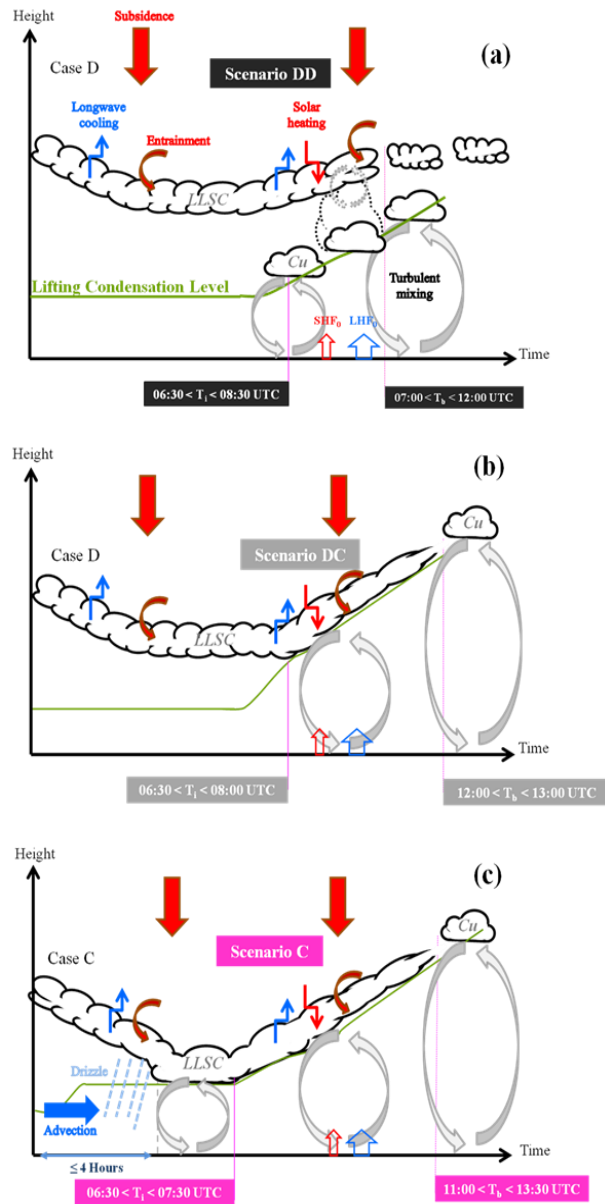


Figure 13 : Schematic illustration of the main findings of the present study. It portrays the typical evolutions of the LLSC sampled at Savé (Benin where local time equals UTC +1 hour), during DACCWA field experiment. The different scenarios and their characteristic times as well as the relevant physical processes are illustrated (the different arrows signification is indicated in **a**, and remains the same in **b** and **c**). The representation encompasses the stratus and convective phases of the LLSC diurnal cycle. The width of the arrows representing the near-surface latent and sensible heat fluxes (LHF₀ and SHF₀ resp.) correspond to their relative proportions. Typically, the LLSC forms decoupled from the surface (**a**, **b** and **c**). For the D cases (**a** and **b**), the LLSC remains uncoupled all along the stratus phase. For the C cases (**c**), the LLSC gets coupled to surface within the four hours after its formation as the cloud base descends significantly and the LCL increases potentially because of drier and cooler air horizontal advection (horizontal blue filled arrow in **c**), and drizzle formation in the subcloud layer (**c**). In all the C cases, the LLSC evolves by the scenario C, in which the cloud layer lifts with the growing convective boundary layer, the subsequent cloud deck breakup leads to shallow convective clouds formation. In the scenario DD (**a**), followed by most of the D cases, surface-convective driven cumulus forms below the LLSC deck before its breakup. The others cases D evolve by the scenario DC (**b**), in which the LLSC couples with the surface as the convective boundary layer top joins the LLSC base, and the subsequent LLSC evolution is similar to the scenario C.

Data availability. The data used in this study are available in the BAOBAB (Base Afrique de l'Ouest Beyond AMMA Base) database (<https://baobab.sedoo.fr/DACCIWA/>).

5 | *Author contributions.* FL, NK, ML, CD, BA and XPB performed the measurements at Savè supersite. MZ processed the data and carried out the analysis with contributions from FL and ML. MZ wrote the paper with contributions from all co-authors.

Competing interests. The authors declare that they have no conflict of interest.

10

Acknowledgements. The DACCIWA project has received funding from the European Union Seventh Framework Programme (FP7/2007-2013) under grant agreement no. 603502. The first author thanks Laboratoire d'Aérodynamique, Université de Toulouse, France for hosting the research activities. We would also like to thank two anonymous reviewers for their helpful comments and suggestions.

15

Financial support. This study received the financial support of the PASMU (Pollution de l'Air et Santé dans les Milieux Urbains de Côte d'Ivoire) project funded by the programme of Debt Reduction-Development Contracts (C2Ds) managed by the Institute of Research and Development (IRD, France).

Synoptic conditions	Onset												Post-Onset												Recovery			
	June 2016						July 2016						July 2016															
	20	22	26	27	29	30	01	02	03	04	05	06	07	08	09	10	11	17	18	19	27	28	29					
Day-D+1	-	-	03	--	04	--	05	--	06	--	07	--	08	--	09	--	09	--	10	--	14	--						
N° IOP	-	-	03	--	04	--	05	--	06	--	07	--	08	--	09	--	09	--	10	--	14	--						
LLSC at the end of the stratus phase (section 4)																												
CBH	206	370	204	226	249	174	53	70	91	100	277	147	292	253	299	380	306	338	136	260	206	208						
Depth	813	499	185	404	381	306	607	320	--	470	502	452	337	407	--	384	384	412	313	385	573	--						
Shear ⁺	6.47	2.42	0.81	76.0	4+0.8	0.24	0.65	4.549	--	3.3	5.85	4+2.1	2.3	46.41	9.67	--	--	--	4+0.2	--	--	--						
$\theta^- - 290$	7.2	7.5	6.67	7.5	7.43	7.2	6.9	6.6	--	6.43	7.7	7.2	8.31	7.8	--	--	--	--	6.3	--	--	--						
$\Delta\theta_l$	3.65	2.56	1.84	2.2	2.33	1.67	3.57	1.9	--	4.47	4.42	2.67	1.89	2.68	--	--	--	--	2.4	--	--	--						
q^-	16.7	15.7	44.61	16.8	16.4	16.98	17.0	16.8	--	16.8	16.3	17.0	16.7	16.98	--	--	--	--	16.2	--	--	--						
Δq_t	-3.0	-2.91	-0.21	-1.4	-1.23	-1.45	-1.43	-0.6	--	-0.21	-1.5	-1.0	-1.23	-0.87	--	--	--	--	-0.42	--	--	--						
RAD	44+46	47+66	3+2	39+53	43+35	43+41	32+65	42+53	--	32+45	33+46	37+45	46+95	44+75	--	--	--	--	42+75	--	--	--						
ENT	4+4	5+89	4+60	23.9	3+36	6+810	4+4	31.2	--	2+96	11.6	-0.64	3+47	9.82	--	--	--	--	1.0+3	--	--	--						
SUBS	44+46	38+04	202.3	26+63	20+73	32+73	22+43	20+93	--	13+62	4+42	25+83	34+24	25+93	--	--	--	--	22+42	--	--	--						
LLSC during the convective phase (section 5)																												
Scenarios	DD	DD	DC	C	DD	C	C	C	C	C	C	DD	C	DC	C	DD	DC	DD	C	DC	DD	DC						
T _i	0835	0730	0715	0700	0810	0705	0710	0655	0720	0655	0805	0640	0635	0740	0705	0755	0910	0730	0645	0745	0635	0805						
T _b	1105	0835	1205	1135	1205	1225	1310	1140	1555	1105	1215	1155	1255	1200	1035	1010	0800	0825	1220	1205	0725	1235						

Table A-1 : Summary of the LLSC features at the end of the stratus phase (section 4) and during the convective phase (section 5) for the 22 twenty-two occurrences at Savè supersite analyzed in this study. The Day-D+1 of the night-to-day transition and the eventual corresponding IOP number are indicated. The main synoptic conditions defined by Knippertz et al. (2017) in which they fall are mentioned at the top. The Cloud base height (CBH in m a.g.l) and depth (m) are estimated by from the ceilometer and cloud radar measurements. The contribution of wind shear in turbulence production at the cloud top (Shear⁺, in 10⁻⁵ s⁻²), the thermodynamical properties of the cloud, θ^- and $\Delta\theta_l$ in K, q^- , Δq_t and g kg⁻¹ as well as the LWP budget terms radiative (RAD⁻), entrainment (ENT) and subsidence (SUBS⁻), in g m⁻² h⁻¹ are derived from 05:00 UTC standard radiosoundings. They are only estimated only for the 14 fourteen cases for which the radiosonde flew into the LLSC layer. The scenario of evolution after the sunrise and its characteristic times, the surface-convection influence (T_i) and breakup (T_b) times are indicated in the format HHMM UTC. C, DC and DD stand for “coupled”, “decoupled-coupled” and “decoupled-decoupled” scenarios respectively. T_i and T_b are The local time at Savè in (Benin) is UTC in the format HHMM+1 hour.

References

- 5 Adler, B., Kalthoff, N. and Gantner, L.: Nocturnal low-level clouds over southern West Africa analysed using high-resolution simulations, *Atmospheric Chemistry and Physics*, 17(2), 899–910, doi:10.5194/acp-17-899-2017, 2017.
- Adler, B., Babić, K., Kalthoff, N., Lohou, F., Lothon, M., Dione, C., Pedruzo-Bagazgoitia, X. and Andersen, H.: Nocturnal low-level clouds in the atmospheric boundary layer over southern West Africa: an observation-based analysis of conditions and processes, *Atmospheric Chemistry and Physics*, 19(1), 663–681, doi:10.5194/acp-19-663-2019, 2019.
- 10 Babić, K., Adler, B., Kalthoff, N., Andersen, H., Dione, C., Lohou, F., Lothon, M. and Pedruzo-Bagazgoitia, X.: The observed diurnal cycle of low-level stratus clouds over southern West Africa: a case study, *Atmospheric Chemistry and Physics*, 19(2), 1281–1299, doi:10.5194/acp-19-1281-2019, 2019a.
- Babić, K., Kalthoff, N., Adler, B., Quinting, J. F., Lohou, F., Dione, C. and Lothon, M.: What controls the formation of nocturnal low-level stratus clouds over southern West Africa during the monsoon season?, *Atmos. Chem. Phys.*, 19(21), 13489–13506, doi:10.5194/acp-19-13489-2019, 2019b.
- 15 Bretherton, C. S., Krueger, S. K., Wyant, M. C., Bechtold, P., Van Meijgaard, E., Stevens, B. and Teixeira, J.: A GCSS Boundary-Layer Cloud Model Intercomparison Study Of The First Astex Lagrangian Experiment, *Boundary-Layer Meteorology*, 93(3), 341–380, doi:10.1023/A:1002005429969, 1999.
- 20 ~~Copernicus Climate Change Service: ERA5 Land hourly data from 2001 to present, , doi:10.24381/CDS.E2161BAC, 2019~~ Christensen, M. W., Carrió, G. G., Stephens, G. L. and Cotton, W. R.: Radiative Impacts of Free-Tropospheric Clouds on the Properties of Marine Stratocumulus, *Journal of the Atmospheric Sciences*, 70(10), 3102–3118, doi:10.1175/JAS-D-12-0287.1, 2013.
- Dearden, C., Hill, A., Coe, H. and Choulaton, T.: The role of droplet sedimentation in the evolution of low-level clouds over southern West Africa, *Atmos. Chem. Phys.*, 18(19), 14253–14269, doi:10.5194/acp-18-14253-2018, 2018.
- 25 Deetz, K., Vogel, H., Knippertz, P., Adler, B., Taylor, J., Coe, H., Bower, K., Haslett, S., Flynn, M., Dorsey, J., Crawford, I., Kottmeier, C. and Vogel, B.: Cloud and aerosol radiative effects as key players for anthropogenic changes in atmospheric dynamics over southern West Africa, *Atmos. Chem. Phys. Discuss.*, 1–36, doi:10.5194/acp-2018-186, 2018.
- Dione, C., Lohou, F., Lothon, M., Adler, B., Babić, K., Kalthoff, N., Pedruzo-Bagazgoitia, X., Bezombes, Y. and Gabella, O.: Low-level stratiform clouds and dynamical features observed within the southern West African monsoon, *Atmos. Chem. Phys.*, 19(13), 8979–8997, doi:10.5194/acp-19-8979-2019, 2019.
- 30 van der Dussen, J. J., de Roode, S. R. and Siebesma, A. P.: Factors Controlling Rapid Stratocumulus Cloud Thinning, *J. Atmos. Sci.*, 71(2), 655–664, doi:10.1175/JAS-D-13-0114.1, 2014.
- van der Dussen, J. J., de Roode, S. R. and Siebesma, A. P.: How large-scale subsidence affects stratocumulus transitions, *Atmos. Chem. Phys.*, 16(2), 691–701, doi:10.5194/acp-16-691-2016, 2016.
- 35 Duynkerke, P. G., de Roode, S. R., van Zanten, M. C., Calvo, J., Cuxart, J., Cheinet, S., Chlond, A., Grenier, H., Jonker, P. J., Köhler, M., Lenderink, G., Lewellen, D., Lappen, C.-L., Lock, A. P., Moeng, C.-H., Müller, F., Olmeda, D., Piriou, J.-M., Sánchez, E. and Sednev, I.: Observations and numerical simulations of the diurnal cycle of the EUROCS stratocumulus case, *Q. J. R. Meteorol. Soc.*, 130(604), 3269–3296, doi:10.1256/qj.03.139, 2004.

[Emetere, M. E.: Investigations on aerosols transport over micro- and macro-scale settings of West Africa, *Environmental Engineering Research*, 22\(1\), 75–86, doi:10.4491/eer.2016.080, 2016.](#)

- 5 Faloua, I., Lenschow, D. H., Campos, T., Stevens, B., van Zanten, M., Blomquist, B., Thornton, D., Bandy, A. and Gerber, H.: Observations of Entrainment in Eastern Pacific Marine Stratocumulus Using Three Conserved Scalars, *J. Atmos. Sci.*, 62(9), 3268–3285, doi:10.1175/JAS3541.1, 2005.

[Fitzpatrick, R. G. J., Bain, C. L., Knippertz, P., Marsham, J. H. and Parker, D. J.: The West African Monsoon Onset: A Concise Comparison of Definitions, *Journal of Climate*, 28\(22\), 8673–8694, doi:10.1175/JCLI-D-15-0265.1, 2015.](#)

- 10 Flamant, C., Knippertz, P., Fink, A. H., Akpo, A., Brooks, B., Chiu, C. J., Coe, H., Danour, S., Evans, M., Jegede, O., Kalthoff, N., Konaré, A., Lioussé, C., Lohou, F., Mari, C., Schlager, H., Schwarzenboeck, A., Adler, B., Amekudzi, L., Aryee, J., Ayoola, M., Batenburg, A. M., Bessardon, G., Borrmann, S., Brito, J., Bower, K., Burnet, F., Catoire, V., Colomb, A., Denjean, C., Fosu-Amankwah, K., Hill, P. G., Lee, J., Lathon, M., Maranan, M., Marsham, J., Meynadier, R., Ngamini, J.-B., Rosenberg, P., Sauer, D., Smith, V., Stratmann, G., Taylor, J. W., Voigt, C. and Yoboué, V.: The Dynamics–Aerosol–Chemistry–Cloud Interactions in West Africa field campaign: Overview and research highlights, *Bull. Amer. Meteor. Soc.*, doi:10.1175/BAMS-D-16-0256.1, 2017.

- 15 Garratt, J. R.: *The Atmospheric Boundary Layer*, Cambridge University Press., 1994.

Ghonima, M. S., Heus, T., Norris, J. R. and Kleissl, J.: Factors Controlling Stratocumulus Cloud Lifetime over Coastal Land, *J. Atmos. Sci.*, 73(8), 2961–2983, doi:10.1175/JAS-D-15-0228.1, 2016.

Handwerker, J., Scheer, S. and Gamer, T.: DACCIWA field campaign, Savè super-site, Cloud and precipitation, , doi:10.6096/dacchiwa.1686, 2016.

- 20 Hannak, L., Knippertz, P., Fink, A. H., Kniffka, A. and Pante, G.: Why Do Global Climate Models Struggle to Represent Low-Level Clouds in the West African Summer Monsoon?, *J. Climate*, 30(5), 1665–1687, doi:10.1175/JCLI-D-16-0451.1, 2017.

- 25 Kalthoff, N., Lohou, F., Brooks, B., Jegede, G., Adler, B., Babić, K., Dione, C., Ajao, A., Amekudzi, L. K., Aryee, J. N. A., Ayoola, M., Bessardon, G., Danour, S. K., Handwerker, J., Kohler, M., Lathon, M., Pedruzo-Bagazgoitia, X., Smith, V., Sunmonu, L., Wieser, A., Fink, A. H. and Knippertz, P.: An overview of the diurnal cycle of the atmospheric boundary layer during the West African monsoon season: results from the 2016 observational campaign, *Atmospheric Chemistry and Physics*, 18(4), 2913–2928, doi:10.5194/acp-18-2913-2018, 2018.

Knippertz, P., Fink, A. H., Schuster, R., Trentmann, J., Schrage, J. M. and Yorke, C.: Ultra-low clouds over the southern West African monsoon region, *Geophysical Research Letters*, 38(21), doi:10.1029/2011GL049278, 2011.

- 30 Knippertz, P., Coe, H., Chiu, J. C., Evans, M. J., Fink, A. H., Kalthoff, N., Lioussé, C., Mari, C., Allan, R. P., Brooks, B., Danour, S., Flamant, C., Jegede, O. O., Lohou, F. and Marsham, J. H.: The DACCIWA Project: Dynamics–Aerosol–Chemistry–Cloud Interactions in West Africa, *Bulletin of the American Meteorological Society*, 96(9), 1451–1460, doi:10.1175/BAMS-D-14-00108.1, 2015.

- 35 Knippertz, P., Fink, A. H., Deroubaix, A., Morris, E., Tocquer, F., Evans, M. J., Flamant, C., Gaetani, M., Lavaysse, C., Mari, C., Marsham, J. H., Meynadier, R., Affo-Dogo, A., Bahaga, T., Brosse, F., Deetz, K., Guebsi, R., Latifou, I., Maranan, M., Rosenberg, P. D. and Schlueter, A.: A meteorological and chemical overview of the DACCIWA field campaign in West Africa in June–July 2016, *Atmospheric Chemistry and Physics*, 17(17), 10893–10918, doi:10.5194/acp-17-10893-2017, 2017.

- Kohler, M., Kalthoff, N., Seringer, J. and Kraut, S.: DACCIWA field campaign, Savè super-site, Surface measurements, , doi:10.6096/dacchiwa.1690, 2016.
- Lilly, D. K.: Models of cloud-topped mixed layers under a strong inversion, Q.J.R. Meteorol. Soc., 94(401), 292–309, doi:10.1002/qj.49709440106, 1968.
- 5 van der Linden, R., Fink, A. H. and Redl, R.: Satellite-based climatology of low-level continental clouds in southern West Africa during the summer monsoon season: Low-level clouds in southern West Africa, Journal of Geophysical Research: Atmospheres, 120(3), 1186–1201, doi:10.1002/2014JD022614, 2015.
- 10 ~~Liu, L., Zhang, T., Wu, Y., Niu, Z. and Wang, Q.: Cloud Effective Emissivity Retrievals Using Combined Ground Based Infrared Cloud Measuring Instrument and Ceilometer Observations, Remote Sensing, 10(12), 2033, doi:10.3390/rs10122033, 2018.~~
- Lohou, F., Kalthoff, N., Adler, B., Babić, K., Dione, C., Lothon, M., Pedruzo-Bagazgoitia, X. and Zouzoua, M.: Conceptual model of diurnal cycle of low-level stratiform clouds over southern West Africa, Atmospheric Chemistry and Physics, 20(4), 2263–2275, doi:https://doi.org/10.5194/acp-20-2263-2020, 2020.
- 15 Lothon, M., Saïd, F., Lohou, F. and Campistron, B.: Observation of the Diurnal Cycle in the Low Troposphere of West Africa, Mon. Wea. Rev., 136(9), 3477–3500, doi:10.1175/2008MWR2427.1, 2008.
- Mauder, M., Cuntz, M., Drüe, C., Graf, A., Rebmann, C., Schmid, H. P., Schmidt, M. and Steinbrecher, R.: A strategy for quality and uncertainty assessment of long-term eddy-covariance measurements, Agricultural and Forest Meteorology, 169, 122–135, doi:10.1016/j.agrformet.2012.09.006, 2013.
- 20 Mechem, D. B., Kogan, Y. L. and Schultz, D. M.: Large-Eddy Simulation of Post-Cold-Frontal Continental Stratocumulus, J. Atmos. Sci., 67(12), 3835–3853, doi:10.1175/2010JAS3467.1, 2010.
- ~~Mohrmann, J., Bretherton, C. S., McCoy, I. L., McGibbon, J., Wood, R., Ghate, V., Albrecht, B., Sarkar, M., Zuidema, P. and Palikonda, R.: Lagrangian Evolution of the Northeast Pacific Marine Boundary Layer Structure and Cloud during CSET, Monthly Weather Review, 147(12), 4681–4700, doi:10.1175/MWR-D-19-0053.1, 2019.~~
- 25 Parker, D. J., Burton, R. R., Diongue-Niang, A., Ellis, R. J., Felton, M., Taylor, C. M., Thorncroft, C. D., Bessemoulin, P. and Tompkins, A. M.: The diurnal cycle of the West African monsoon circulation, Quarterly Journal of the Royal Meteorological Society, 131(611), 2839–2860, doi:10.1256/qj.04.52, 2005.
- Pedruzo-Bagazgoitia, X., de Roode, S. R., Adler, B., Babić, K., Dione, C., Kalthoff, N., Lohou, F., Lothon, M. and Vilà-Guerau de Arellano, J.: The diurnal stratocumulus-to-cumulus transition over land in southern West Africa, Atmos. Chem. Phys., 20(5), 2735–2754, doi:10.5194/acp-20-2735-2020, 2020.
- 30 ~~Prata, A. J.: A new long-wave formula for estimating downward clear-sky radiation at the surface, Q.J. Royal Met. Soc., 122(533), 1127–1151, doi:10.1002/qj.49712253306, 1996.~~
- Price, J. D.: Observations of stratocumulus cloud break-up over land, Q.J. Royal Met. Soc., 125(554), 441–468, doi:10.1002/qj.49712555404, 1999.
- 35 ~~Ricchiazzi, P., Yang, S., Gautier, C. and Sowle, D.: SBDART: A Research and Teaching Software Tool for Plane-Parallel Radiative Transfer in the Earth's Atmosphere, Bull. Amer. Meteor. Soc., 79(10), 2101–2114, doi:10.1175/1520-0477(1998)079<2101:SARATS>2.0.CO;2, 1998.~~

- Romps, D. M.: Exact Expression for the Lifting Condensation Level, *Journal of the Atmospheric Sciences*, 74(12), 3891–3900, doi:10.1175/JAS-D-17-0102.1, 2017.
- de Roode, S. R., Sandu, I., van der Dussen, J. J., Ackerman, A. S., Blossey, P., Jarecka, D., Lock, A., Siebesma, A. P. and Stevens, B.: Large-Eddy Simulations of EUCLIPSE–GASS Lagrangian Stratocumulus-to-Cumulus Transitions: Mean State, Turbulence, and Decoupling, *J. Atmos. Sci.*, 73(6), 2485–2508, doi:10.1175/JAS-D-15-0215.1, 2016.
- 5 S. Derrien, Y. Bezombes, G. Bret, O. Gabella, C. Jarnot, P. Medina, E. Piques, C. Delon, C. Dione, B. Campistron, P. Durand, C. Jambert, F. Lohou, M. Lothon, F. Pacifico and Y. Meyerfeld: DACCIWA field campaign, Savè super-site, UPS instrumentation, 2016.
- Sandu, I. and Stevens, B.: On the Factors Modulating the Stratocumulus to Cumulus Transitions, *J. Atmos. Sci.*, 68(9), 1865–1881, doi:10.1175/2011JAS3614.1, 2011.
- 10 [Sarkar, M., Zuidema, P., Albrecht, B., Ghate, V., Jensen, J., Mohrmann, J. and Wood, R.: Observations Pertaining to Precipitation within the Northeast Pacific Stratocumulus-to-Cumulus Transition, *Monthly Weather Review*, 148\(3\), 1251–1273, doi:10.1175/MWR-D-19-0235.1, 2019.](https://doi.org/10.1175/MWR-D-19-0235.1)
- Schrage, J. M. and Fink, A. H.: Nocturnal Continental Low-Level Stratus over Tropical West Africa: Observations and Possible Mechanisms Controlling Its Onset, *Monthly Weather Review*, 140(6), 1794–1809, doi:10.1175/MWR-D-11-00172.1, 2012.
- 15 Schuster, R., Fink, A. H. and Knippertz, P.: Formation and Maintenance of Nocturnal Low-Level Stratus over the Southern West African Monsoon Region during AMMA 2006, *Journal of the Atmospheric Sciences*, 70(8), 2337–2355, doi:10.1175/JAS-D-12-0241.1, 2013.
- 20 [Siems, S. T., Lenschow, D. H. and Bretherton, C. S.: A Numerical Study of the Interaction between Stratocumulus and the Air Overlying It, *J. Atmos. Sci.*, 50\(21\), 3663–3676, doi:10.1175/1520-0469\(1993\)050<3663:ANSOTI>2.0.CO;2, 1993.](https://doi.org/10.1175/1520-0469(1993)050<3663:ANSOTI>2.0.CO;2)
- Stevens, B.: Bulk boundary-layer concepts for simplified models of tropical dynamics, *Theor. Comput. Fluid Dyn.*, 20(5–6), 279–304, doi:10.1007/s00162-006-0032-z, 2006.
- Stevens, B., Moeng, C.-H., Ackerman, A. S., Bretherton, C. S., Chlond, A., de Roode, S., Edwards, J., Golaz, J.-C., Jiang, H., Khairoutdinov, M., Kirkpatrick, M. P., Lewellen, D. C., Lock, A., Müller, F., Stevens, D. E., Whelan, E. and Zhu, P.: Evaluation of Large-Eddy Simulations via Observations of Nocturnal Marine Stratocumulus, *Mon. Wea. Rev.*, 133(6), 1443–1462, doi:10.1175/MWR2930.1, 2005.
- 25 Stull, R. B., Ed.: *An Introduction to Boundary Layer Meteorology*, Springer Netherlands, Dordrecht. [online] Available from: <http://link.springer.com/10.1007/978-94-009-3027-8> (Accessed 10 October 2016), 1988.
- 30 vanZanten, M. C., Duynkerke, P. G. and Cuijpers, J. W. M.: Entrainment Parameterization in Convective Boundary Layers, *J. Atmos. Sci.*, 56(6), 813–828, doi:10.1175/1520-0469(1999)056<0813:EPICBL>2.0.CO;2, 1999.
- Wang, Q. and Lenschow, D.: An Observational Study of the Role of Penetrating Cumulus in a Marine Stratocumulus-Topped Boundary Layer, *Journal of The Atmospheric Sciences - J ATMOS SCI*, 52, 2778–2787, doi:10.1175/1520-0469(1995)052<2778:AOSOTR>2.0.CO;2, 1995.
- 35 Wieser, A., Adler, B. and Deny, B.: DACCIWA field campaign, Savè super-site, Thermodynamic data sets, , doi:10.6096/daccciwa.1659, 2016.

Wood, R.: Stratocumulus Clouds, *Mon. Wea. Rev.*, 140(8), 2373–2423, doi:10.1175/MWR-D-11-00121.1, 2012.

Xiao, H., Wu, C.-M. and Mechoso, C. R.: Buoyancy reversal, decoupling and the transition from stratocumulus to shallow cumulus topped marine boundary layers, *Clim Dyn*, 37(5–6), 971–984, doi:10.1007/s00382-010-0882-3, 2011.

5 | [Zheng, Y. and Li, Z.: Episodes of Warm-Air Advection Causing Cloud-Surface Decoupling During the MARCUS, J. Geophys. Res. Atmos., 124\(22\), 12227–12243, doi:10.1029/2019JD030835, 2019.](#)

[Zheng, Y., Rosenfeld, D., Zhu, Y. and Li, Z.: Satellite-Based Estimation of Cloud Top Radiative Cooling Rate for Marine Stratocumulus, Geophys. Res. Lett., 46\(8\), 4485–4494, doi:10.1029/2019GL082094, 2019.](#)

10 | Zhu, P., Albrecht, B. and Gottschalck, J.: Formation and Development of Nocturnal Boundary Layer Clouds over the Southern Great Plains, *Journal of the Atmospheric Sciences*, 58, doi:10.1175/1520-0469(2001)058<1409:FADONB>2.0.CO;2, 2001.